Disaggregation of SMOS soil moisture in southeastern Australia

Olivier Merlin, Christoph Rüdiger, Al Bitar Ahmad, Philippe Richaume, Jeffrey P. Walker, Yann H. Kerr

Disaggregation of SMOS Soil Moisture in Southeastern Australia

Olivier Merlin, Christoph Rüdiger, Ahmad Al Bitar, Philippe Richaume, Jeffrey P. Walker, and Yann H. Kerr

***Abstract*—Disaggregation based on Physical And Theoretical scale Change (DisPATCh) is an algorithm dedicated to the disaggregation of soil moisture observations using high-resolution soil temperature data. DisPATCh converts soil temperature fields into soil moisture fields given a semi-empirical soil evaporative efficiency model and a first-order Taylor series expansion around the field-mean soil moisture. In this study, the disaggregation approach is applied to soil moisture and ocean salinity (SMOS) data over the 500 km by 100 km AACES (Australian Airborne Calibration/validation Experiments for SMOS) area. The 40-km resolution SMOS surface soil moisture pixels are disaggregated at 1-km resolution using the soil skin temperature derived from moderate resolution imaging spectroradiometer (MODIS) data, and subsequently compared with the AACES intensive ground measurements aggregated at 1-km resolution. The objective is to test DisPATCh under various surface and atmospheric conditions. It is found that the accuracy of disaggregation products varies greatly according to season: while the correlation coefficient between disaggregated and *in situ* soil moisture is about 0.7 during the summer AACES, it is approximately zero during the winter AACES, consistent with a weaker coupling between evaporation and surface soil moisture in temperate than in semi-arid climate. Moreover, during the summer AACES, the correlation coefficient between disaggregated and *in situ* soil moisture is increased from 0.70 to 0.85, by separating the 1-km pixels where MODIS temperature is mainly controlled by soil evaporation, from those where MODIS temperature is controlled by both soil evaporation and vegetation transpiration. It is also found that the 5-km resolution atmospheric correction of the official MODIS temperature data has a significant impact on DisPATCh output. An alternative atmospheric correction at 40-km resolution increases the correlation coefficient between disaggregated and *in situ* soil moisture from 0.72 to 0.82 during the summer AACES. Results indicate that DisPATCh has a strong potential in low-vegetated semi-arid areas where it can be used as a tool to evaluate SMOS data (by reducing the mismatch in spatial extent between SMOS observations and localized *in situ* measurements), and as a further step, to derive a 1-km resolution soil moisture product adapted for large-scale hydrological studies.**

***Index Terms*—AACES, calibration/validation, disaggregation, Disaggregation based on Physical And Theoretical scale Change (DisPATCh), field campaign, moderate resolution imaging spectroradiometer (MODIS), soil moisture and ocean salinity (SMOS).**

I. Introduction

PASSIVE MICROWAVE remote sensing has the capability to provide key elements of the terrestrial hydrological cycle such as surface soil moisture [1], [2] and overland precipitation [3], [4]. Nevertheless, due to the large discrepancy between the observation scale (several tens of km) and the scale of physical interactions with the land surface (one wavelength or several cm), the radiative transfer models applied to passive microwave remote sensing data are only semiphysically based. Consequently, the retrieval process of land surface parameters from microwave brightness temperatures requires ancillary data for calibration and validation purposes [5]. It also requires a strategy to use such ancillary data since ground-based sampling is often made over a small area/point, which constrasts with the large integrated extent of spaceborne passive microwave observations.

The soil moisture and ocean salinity (SMOS), [6]) satellite was launched on November 2, 2009. Over land, the SMOS mission aims at providing $\sim$5 cm surface soil moisture data at a spatial resolution better than 50 km and a repeat cycle of less than 3 days. The payload is a 2-D interferometer equipped with 69 individual L-band antennas regularly spaced along Y-shaped arms. This new concept allows observing all pixels in the 1000 km wide field of view at a range of incidence angles. It also allows reconstructing brightness temperatures on a fixed sampling grid [7].

Since the SMOS launch, various field experiments (the HOBE site in Denmark [8], the Mali site in Western Africa [9], the SMOSMANIA site in Southwestern France [10] just to name a few) have been undertaken to validate SMOS reconstructed brightness temperatures and soil moisture retrievals. The AACES (Australian Airborne Calibration/validation Experiment for SMOS, [11]) is one of the most comprehensive campaigns worldwide dedicated to SMOS calibration/validation. A series of two experiments were undertaken in 2010, AACES-1 in January-February (Austral summer) and

Manuscript received March 31, 2011; revised September 1, 2011; accepted October 30, 2011. The AACES participants are gratefully acknowledged for their participation in collecting this extensive data set. The Australian Airborne Calibration/validation Experiments for SMOS have been made possible through infrastructure (LE0453434) and research (DP0879212) funding from the Australian Research Council, and the collaboration of a large number of scientists from throughout Australia, United States and Europe. Initial setup and maintenance of the study catchments was funded by two research Grants (DP0343778, DP0557543) from the Australian Research Council and by the CRC for Catchment Hydrology. This work was funded by the CNES TOSCA (Terre solide, Océan, Surfaces Continentales et Atmosphère) program and the Centre National de la Recherche Scientifique.

O. Merlin is with the Centre d'Etudes Spatiales de la Biosphère (CESBIO), 31401 Toulouse, France (e-mail: olivier.merlin@cesbio.cnes.fr).

C. Rüdiger (e-mail: chris.rudiger@monash.edu).

A. Al Bitar (e-mail: ahmad.albitar@cesbio.cnes.fr).

P. Richaume (e-mail: philippe.richaume@cesbio.cnes.fr).

J. P. Walker (e-mail: jeff.walker@monash.edu).

Y. H. Kerr (e-mail: yann.kerr@cesbio.cnes.fr).

Color versions of one or more of the figures in this paper are available online at http://ieeexplore.ieee.org.

Digital Object Identifier 10.1109/TGRS.2011.2175000

AACES-2 in September (Austral winter). The data collected in AACES include 1-km resolution airborne L-band brightness temperature mapped over a 500 km by 100 km area, 20 days of very intensive ground measurements and 20 5 km by 2 km ground sampling areas.

Even though the AACES ground measurements are very extensive, it is not feasible to cover the whole extent of a SMOS pixel by ground sampling alone. This is the reason why most validation strategies of spaceborne passive microwave data using *in situ* measurements have been based on the assumption that local observations are representative of a much larger spatial extent (i.e., the size of a microwave pixel). In the heterogeneous case where this assumption does not hold, upscaling approaches [12], [13] have been developed to relate the available ground observations to satellite scale soil moisture. Such approaches are very useful over sites which have been monitored for a long time and where extensive measurements have been made over a range of spatial scales. However, aggregation rules are difficult to build over sites which have been set up recently, or where no extensive field campaigns have been undertaken.

This study develops a methodology to facilitate the calibration and validation of SMOS data using localized ground measurements, such as those collected during AACES. The methodology combines upscaling (aggregation) and downscaling (disaggregation) approaches to make remote sensing and *in situ* observations match at an intermediate spatial resolution of 1 km. The key step in the procedure is a disaggregation algorithm of passive microwave soil moisture using kilometric optical data [14]–[16]. Disaggregating SMOS soil moisture can solve the disparity of spatial scales between satellite and *in situ* observations. However, the validation of spaceborne data by means of a disaggregation approach requires the uncertainties and potential error sources in downscaled data to be assessed. Generally speaking, disaggregation is a compromise between downscaling resolution and accuracy. The higher downscaling resolution, the more disaggregated values are spatially representative of ground observations, but typically have a lower accuracy and vice versa [17]. In this context, a disaggregation algorithm named Disaggregation based on Physical And Theoretical scale Change (DisPATCh) is applied to 40-km resolution SMOS soil moisture over the AACES area using 1-km resolution Moderate resolution Imaging Spectroradiometer (MODIS) data. The objective is to test DisPATCh under various surface and atmospheric conditions. Specifically, the impact of climatic (evaporative demand), meteorologic (presence of clouds), and vegetation (cover and water status) conditions on 1-km resolution disaggregated soil moisture is evaluated both qualitatively by visual assessment of disaggregation images and quantitatively by comparing DisPATCh output with AACES intensive ground measurements.

The AACES, SMOS, and MODIS data used in this study are first described. Next, the disaggregation methodology is presented followed by a step-by-step description of the DisPATCh algorithm. Results of the comparison between disaggregated SMOS soil moisture and *in situ* measurements are then reported. To test DisPATCh under various surface and atmospheric conditions, the algorithm is run during AACES-1 and AACES-2 in different modes, by including (or not) a correction for vegetation and atmospheric effects. Finally, some perspectives in the use of DisPATCh for validating SMOS data using ground-based sampling are given.

II. Data Collection and Preprocessing

The AACES experiments were planned to provide ground and airborne soil moisture data over an area of approximately 500 km by 100 km during the two main seasons in the Murrumbidgee river catchment, in southeastern Australia. The first AACES campaign (AACES-1) was undertaken in summer 2010 from January 18 to February 21, and the second campaign (AACES-2) was undertaken in the following Austral winter from September 11 to September 24 [11]. Fig. 1 presents the study area including the 20 5 km by 2 km ground sampling focus areas. The background image is the MODIS 250-m resolution 16-day normalized difference vegetation index (NDVI) product of February 2, 2010. The climate of the Murrumbidgee catchment area ranges from semi-arid in the west to alpine in the east, with a strong rainfall and potential evapotranspiration gradient in the west-east direction. Land use is extensive grazing in the west, cropping in the center, and mostly grazing/forest in the east (refer to [11] for a detailed account of AACES).

A. HDAS

During both AACES-1 and AACES-2, a spatially enabled platform (Hydraprobe Data Acquisition System, HDAS) was used to collect extensive measurements of near-surface soil moisture. HDAS is a handheld system combining a soil dielectric sensor (Hydraprobe) and a pocket PC with GPS receiver, allowing for direct storage of location and measurement within the GIS software. HDAS measurements were calibrated using the approach presented in [18] with a root mean square error of point estimate of about 0.03 m^3/m^3. The sampling coverage was two 5 km by 2 km farms per day during AACES-1 and one 5 km by 2 km farm per day during AACES-2. Within each farm, a total of six adjacent 5 km long transects separated by 330 m were walked to cover each area of 10 km^2, and three separate HDAS measurements were made along transects every 50 m.

In this study, HDAS soil moisture data are aggregated at 1-km resolution by averaging all measurements made within each pixel of the MODIS resolution grid. Out of concern for spatial representativeness of *in situ* observations, only the 1-km pixels whose ground sampling covers more than two third of its surface area are kept for comparison with disaggregation results. The 1-km average of HDAS measurements is denoted $\langle \mathrm{SM}_{\mathrm{HDAS}} \rangle$ and the standard deviation of *in situ* measurements (denoted σ_{HDAS}) computed to estimate the subpixel variability at 1-km resolution.

B. SMOS

The version-4 SMOS level-2 soil moisture product is used. This product (released on March 24, 2011) was produced from the reprocessed level 1C data, and the version-4 level-2 soil moisture algorithm. SMOS has a 6 am (ascending) and 6 pm

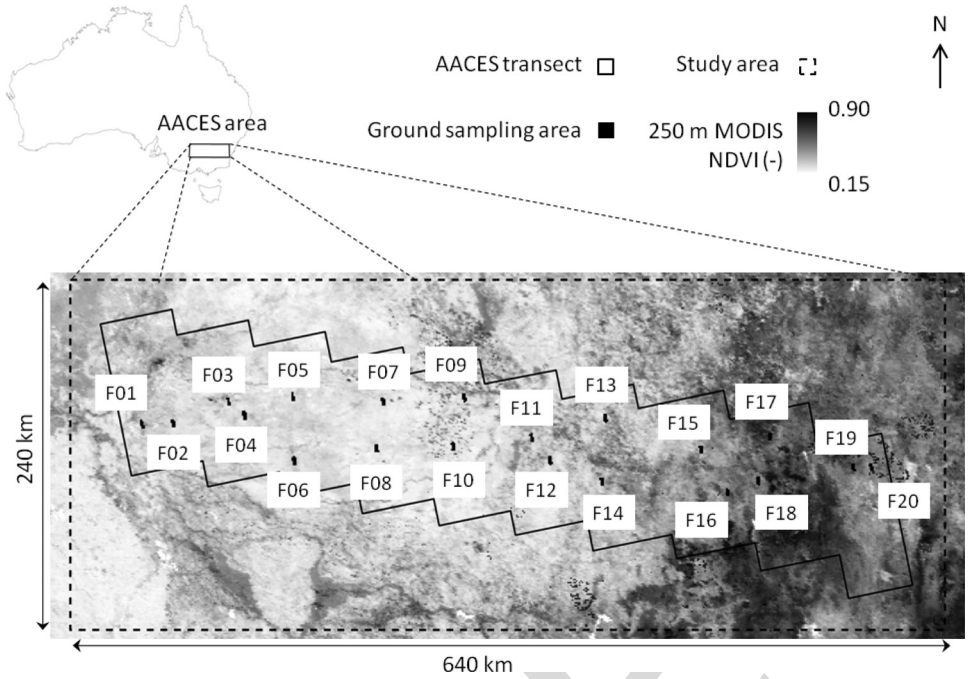

Fig. 1. Overview of the study area. During AACES, ten 100 km by 50 km patches were overflown by an airborne L-band radiometer. Within each patch, two 5 km by 2 km subareas were sampled to collect spatial soil moisture measurements. In this study, DisPATCh is run over a 640 by 240 km area including the whole AACES area, and disaggregation results are evaluated over the ground sampling areas.

(descending) equator crossing time. The sampling grid of the SMOS level-2 soil moisture product is called DGG or discrete global grid [19], [20] and has a node separation of about 15 km. The DGG provides a discretization that is higher than the SMOS natural pixel size, which is 40 km on average, ranging from 30 km at boresight to 90 km at high incidence angles. In this study, the disaggregation procedure takes advantage of the oversampling of SMOS data to potentially reduce (and provide an estimate of) random errors in disaggregated SMOS data. Instead of using a single snapshot SMOS image, DisPATCh uses four (overlapping) independent snapshots, which are generated by: 1) sliding a 40-km resolution grid; and 2) extracting the DGG nodes approximately centered on each 40 km pixel. The extraction of SMOS DGG nodes is presented in [21]. The DGG node(s) that fall(s) near the center of the 40-km resolution pixels with a $+/-10$-km tolerance are selected. If more than one DGG is selected, the associated soil moisture values are averaged to produce a single value for each 40-km resolution pixel. The 40-km resolution grid that fits the study area corresponds to what is termed here Resampling 1. Similarly, Resampling 2, 3, and 4 are performed by sliding the 40-km resolution grid to coordinates $(+20$ km, 0), $(0, -20$ km), and $(+20$ km, -20 km), respectively. The four 40-km resolution SMOS data sets are then used independently as input to DisPATCh.

C. MODIS

The MODIS data used in this paper are composed of:

- Version-5 MODIS/Terra land surface temperature and emissivity daily level-3 global 1-km grid product (MOD11A1) and version-5 MODIS/Aqua land surface temperature and emissivity daily level-3 global 1-km grid product (MYD11A1). The land surface temperature data set is the main component of DisPATCh. It is used to estimate 1-km resolution soil evaporative efficiency at 10 am (Terra data) and 1 pm (Aqua data) [22].
- Version-5 MODIS/Terra vegetation indices 16-day level-3 global 1-km grid product (MOD13A2). The NDVI data set is used in DisPATCh to estimate the fractional vegetation cover at 1-km resolution [23].
- Version-5 MODIS/Terra+Aqua albedo 16-day level-3 global 1-km grid product (MCD43B3). The surface albedo data set is used in DisPATCh to estimate the vegetation temperature at maximum water stress from the space land surface temperature albedo [24]. The MCD43B3 product provides 1-km data describing both directional hemispherical reflectance (black-sky albedo) at local solar noon and bihemispherical reflectance (white-sky albedo). In this study, surface albedo refers to the MODIS shortwave white sky albedo.
- MODIS/Terra level-1B calibrated radiances swath 1-km grid product (MOD021KM) and MODIS/Aqua level-1B calibrated radiances swath 1-km grid product (MYD021KM). The radiance data set is used to derive a land surface temperature data set that differs from the official MOD11A1 and MYD11A1 products with respect to atmospheric correction.

Products MOD11A1, MYD11A1, MOD13A2, and MCD43B3 were downloaded through the NASA Warehouse Inventory Search Tool (WIST http://wist.echo.nasa.gov/) and products MOD021KM and MYD021KM were downloaded through the NASA Level 1 and Atmosphere Archive and Distribution System (LAADS http://ladsweb.nascom.nasa.gov).

TABLE I
SCALE AND OFFSET VALUES USED TO CONVERT TERRA (AND AQUA) MODIS RADIANCE DATA TO PHYSICAL RADIANCE VALUES OVER THE AACES AREA

Thermal band	Scale (W m^{-2} sr^{-1})	Offset (-)
31	$8.4002{\cdot}10^{-4}$ ($6.5081{\cdot}10^{-4}$)	1577 (2036)
32	$7.2970{\cdot}10^{-4}$ ($5.7100{\cdot}10^{-4}$)	1658 (2119)

All products were projected in UTM 55 South with a sampling interval of 1000 m using the MODIS reprojection tool.

The level-1B calibrated radiance data (R_{31} and R_{32} for bands 31 and 32, respectively) were converted from digital number (DN) to radiance in W m^{-2} sr^{-1} using the radiance scales and offsets provided with each MODIS granule as listed in Table I

$$R_\lambda = \text{Scale}_\lambda \times (\text{DN}_\lambda - \text{Offset}_\lambda) \quad (1)$$

The radiance values were then converted to brightness temperature in K using the inverse of the Planck function [25]

$$Tb_\lambda = \frac{c_2}{\lambda \ln\left(1 + \frac{c_1}{R_\lambda \lambda^5}\right)} \quad (2)$$

with $c_1 = 1.19107 \times 10^8$ μm^5 W m^{-2} sr^{-1} and $c_2 = 1.43883 \times 10^4$ μm K, for center wavelength of the given band (11.0186 μm and 12.0325 μm for 31 and 32 band, respectively).

D. Overlapping HDAS, SMOS, and MODIS Data and Generating an Input Data Set

As indicated in Table II, HDAS soil moisture, SMOS soil moisture, and cloud-free MODIS land surface temperature data have overlapped on five days during AACES-1 (on January 28 and 30 and February 15, 18, and 20) and on five days during AACES-2 (on September 11, 13, 21, 22, and 24). On each sampling day, two farms were sampled during AACES-1 (except on February 18 when three farms were sampled), and one farm was sampled during AACES-2, so that disaggregation results can be evaluated for ten date-farm units during AACES-1 and five date-farm units during AACES-2.

DisPATCh is applied to an input ensemble composed of the different combinations of available SMOS (ascending orbit at 6 am and/or descending orbit at 6 pm) and MODIS (onboard Terra platform at 10 am and/or Aqua platform at 1 pm) data. To increase the quantity of input data sets, the MODIS data collected on the day before and the day after the SMOS overpass date are also included. For SMOS data on day of year (DoY) 51, the clear sky MODIS data collected on DoY 54 are used. Note that one implicitly assumes that no rainfall occurs between MODIS and SMOS overpasses, and that the spatial variability captured by MODIS is relatively similar to the actual variability of surface soil moisture at the time of SMOS overpass. Moreover, the SMOS data oversampling is used to generate four (overlapping) 40-km resolution SMOS grids on which DisPATCh is run independently, thus increasing the number of downscaled data that could be used in the validation. It is reminded that the spacing (about 15 km) between neighboring SMOS DGG nodes is smaller than the SMOS resolution (about 40 km). By combining the four SMOS grids, the two potential SMOS data sets (two orbits in one day) and the six potential MODIS data sets (three days including two overpasses each), the maximum number of input data sets is 48. The generation of input data sets is shown in Fig. 2 and the number of daily input data sets is indicated for each date-farm unit in Table II.

III. DISAGGGREGATION ALGORITHM

DisPATCh converts 1-km resolution MODIS-derived soil temperature fields into 1-km resolution surface soil moisture fields given a semi-empirical soil evaporative efficiency model [26] and a first-order Taylor series expansion around the 40-km resolution SMOS observation. DisPATCh is an improved version of the algorithms in [16] and [27], and mainly differs with regard to the representation of the vegetation water status. In previous versions [16], [27], the soil temperature was derived from MODIS land surface temperature by assuming that vegetation was unstressed so that vegetation temperature was uniformly set to the minimum surface temperature observed within the SMOS pixel. In this study, the approach in [28] is implemented to take into account vegetation water status in the estimation of soil temperature.

A. Disaggregation Methodology

The disaggregation procedure decouples the soil evaporation from the 0–5 cm soil layer and the vegetation transpiration from the root-zone soil layer by separating MODIS surface temperature into its soil and vegetation components as in the triangle or trapezoidal method [28], [29]. MODIS-derived soil temperature is then used to estimate soil evaporative efficiency, which is known to be relatively constant during the day on clear sky conditions. MODIS-derived soil evaporative efficiency is finally used as a proxy for surface (0–5 cm) soil moisture variability within the SMOS pixel. The link between surface soil moisture and soil evaporative efficiency at different scales is ensured by a downscaling relationship and a soil evaporative efficiency model, as described below in more detail. The originality of DisPATCh relies on a dynamical land cover classification (based on the hourglass approach in [28]) that takes into account the subpixel variability of the sensitivity of soil evaporative efficiency to surface soil moisture.

1) Downscaling Relationship: The downscaling relationship can be written as

$$\text{SM}_{1\text{ km}} = \mathbf{SM_{SMOS}} + \frac{\partial \mathbf{SM_{mod}}}{\partial \mathbf{SEE}} \times (\text{SEE}_{\text{MODIS,1 km}} - \langle \text{SEE}_{\text{MODIS,1 km}} \rangle_{\mathbf{40\ km}}) \quad (3)$$

with $\mathbf{SM_{SMOS}}$ being the SMOS soil moisture (for clarity, the variables defined at SMOS scale are written in bold), $\text{SEE}_{\text{MODIS}}$ the MODIS-derived soil evaporative efficiency (ratio of actual to potential evaporation), $\langle \text{SEE}_{\text{MODIS}} \rangle_{\mathbf{40\ km}}$ its average within a SMOS pixel and $\partial \mathbf{SM_{mod}}/\partial \mathbf{SEE}$ the partial derivative evaluated at SMOS scale of soil moisture with respect to soil evaporative efficiency. Note that the linearity of (3) implies that a possible bias in SMOS data would produce the

TABLE II
LIST OF OVERLAPPING HDAS, SMOS, AND MODIS (MOD11A1 AND MYD11A1) DATA DURING AACES-1 AND AACES-2. ONLY THE SMOS DATA COLLECTED ON THE SAME DAY AS GROUND SAMPLING HAVE BEEN CONSIDERED. THE MODIS DATA CONSIDERED AS INPUT TO DISPATCH HAVE BEEN COLLECTED WITHIN PLUS OR MINUS ONE DAY EITHER SIDE THE GROUND SAMPLING (AND SMOS OVERPASS) DATE. ON EACH SAMPLING DATE, THE RESULTANT NUMBER OF INPUT DATA SETS TO DISPATCH IS ALSO INDICATED

Experiment	Sampling date	DoY	Farm	SMOS overpass time	Cloud free MODIS data (DoY)	Number of input data sets to DisPATCh
AACES-1	28 January	28	F05	6 am	Terra (27,29) & Aqua (29)	3
	30 January	30	F07	6 am	Terra (29,30) & Aqua (29)	12
	’	’	F08	6 am	Terra (29,30) & Aqua (29)	9-12
	15 February	46	F15	6 am & 6 pm	Terra (46) & Aqua (47)	8-14
	’	’	F16	6 am & 6 pm	Terra (46) & Aqua (47)	8-10
	18 February	49	F17	6 am & 6 pm	Terra (48,50) & Aqua (48,49,50)	30-38
	’	’	F18	6 am & 6 pm	Terra (48,50) & Aqua (48,49,50)	24-30
	’	’	F20	6 am & 6 pm	Terra (48,50) & Aqua (48,49,50)	34-40
	20 February	51	F19	6 am & 6 pm	Terra (54) & Aqua (54)	6-8
	’	’	F20	6 am & 6 pm	Terra (54) & Aqua (54)	16
AACES-2	11 September	254	F09	6 am & 6 pm	Terra (253,254) & Aqua (254)	6-14
	13 September	256	F07	6 am & 6 pm	Terra (256)	8
	21 September	264	F13	6 am & 6 pm	Terra (263) & Aqua (264)	16
	22 September	265	F15	6 am & 6 pm	Terra (265) & Aqua (264,266)	16
	24 September	267	F09	6 am & 6 pm	Terra (267) & Aqua (266,267,268)	24-32

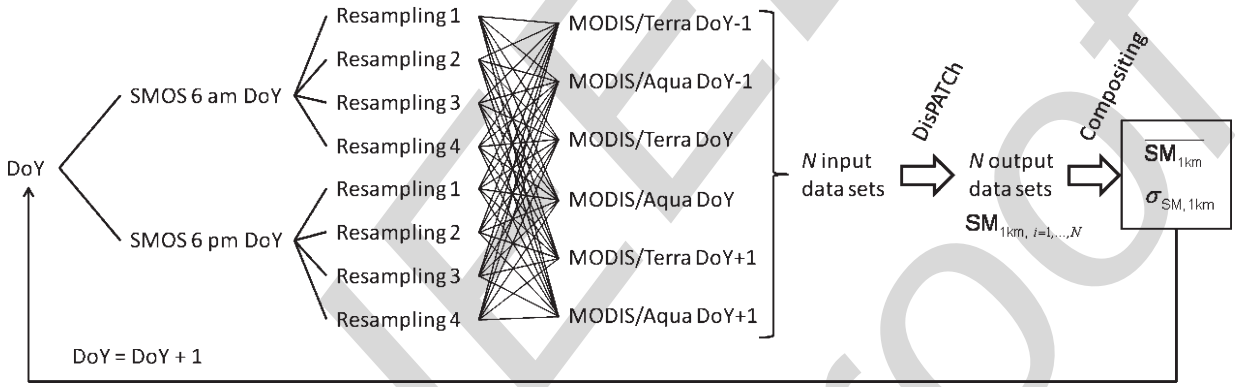

Fig. 2. Schematic diagram presenting the combination of SMOS and MODIS to generate an ensemble of input data to DisPATCh. The output data are composited at 1-km resolution by computing the average ($\overline{\mathrm{SM}_{1\ \mathrm{km}}}$) and standard deviation ($\sigma_{\mathrm{SM},1\ \mathrm{km}}$) of disaggregated SMOS soil moisture.

same bias in disaggregated data [30]. Consequently, although the possible presence of a bias in SMOS data limits the accuracy in the disaggregated soil moisture, it is not a limiting factor to the applicability of DisPATCh. MODIS derived soil evaporative efficiency is expressed as a linear function of soil temperature

$$\mathrm{SEE}_{\mathrm{MODIS},1\ \mathrm{km}} = \frac{\mathbf{T_{s,max}} - T_{\mathrm{s},1\ \mathrm{km}}}{\mathbf{T_{s,max}} - \mathbf{T_{s,min}}} \tag{4}$$

with T_{s} being the MODIS-derived soil skin temperature, $\mathbf{T_{s,max}}$ the soil skin temperature at $\mathrm{SEE} = 0$ and $\mathbf{T_{s,min}}$ the soil skin temperature at $\mathrm{SEE} = 1$. The linearity of the relationship between soil evaporative efficiency and surface soil temperature was verified using the physically based dual source energy budget model in [31] using a synthetic data set composed of a range of surface soil moisture values and different atmospheric conditions (results not shown). End-members $\mathbf{T_{s,min}}$ and $\mathbf{T_{s,max}}$ are estimated from the polygons obtained by plotting MODIS surface temperature against MODIS NDVI and MODIS albedo as in [24]. Derivation of soil temperature is based on a linear decomposition of the surface temperature into its soil and vegetation components as a good approximation of the relationship with fourth power for temperatures [32], [33] and consistent with the triangle method. MODIS-derived soil skin temperature is expressed as

$$T_{\mathrm{s},1\ \mathrm{km}} = \frac{T_{\mathrm{MODIS}} - f_{\mathrm{v},1\ \mathrm{km}} T_{\mathrm{v},1\ \mathrm{km}}}{1 - f_{\mathrm{v},1\ \mathrm{km}}} \tag{5}$$

with T_{MODIS} being the 1-km resolution MODIS land surface temperature, f_{v} the MODIS-derived fractional vegetation cover, and T_{v} the vegetation temperature. In this study, vegetation temperature is estimated using the approach proposed by [28]. In (5), fractional vegetation cover is written as

$$f_{\mathrm{v},1\ \mathrm{km}} = \frac{\mathrm{NDVI}_{\mathrm{MODIS}} - \mathbf{NDVI_s}}{\mathbf{NDVI_v} - \mathbf{NDVI_s}} \tag{6}$$

with $\mathrm{NDVI_{MODIS}}$ being the 1-km resolution MODIS NDVI, $\mathbf{NDVI_s}$ the NDVI corresponding to bare soil, and $\mathbf{NDVI_v}$ the NDVI corresponding to full-cover vegetation. Minimum and maximum NDVI values are set to 0.15 and 0.90, respectively.

In [16], the accuracy and robustness of the disaggregation methodology were tested using three different formulations of soil evaporative efficiency [26], [34], [35]. Results based on the NAFE'06 data set [36], which was collected over a 60 km by 40 km area in the AACES area, indicated that the model in [26] was better adapted for conditions where soil properties are unknown at high resolution. Consequently, the partial derivative in (3) is computed using the soil evaporative efficiency model in [26]

$$\mathrm{SEE_{mod}} = \frac{1}{2} - \frac{1}{2}\cos(\pi \cdot \mathrm{SM}/\mathbf{SM_p}) \tag{7}$$

with $\mathbf{SM_p}$ being a soil parameter (in soil moisture unit). In [26], $\mathbf{SM_p}$ was set to the soil moisture at field capacity. In DisPATCh, $\mathbf{SM_p}$ is retrieved at 40-km resolution from SMOS and aggregated MODIS data [16]. By inverting (7), one obtains

$$\mathrm{SM_{mod}} = \frac{\mathbf{SM_p}}{\pi}\cos^{-1}(1 - 2\,\mathrm{SEE}) \tag{8}$$

2) Vegetation Temperature: Vegetation temperature in (5) is estimated at 1-km resolution with the "hourglass" approach in [28]. By plotting the diagonals in the quadrilateral in Fig. 3, four areas are distinguished in the space defined by surface temperature and fractional vegetation cover. In zone A, land surface temperature is mainly controlled by soil evaporation leading to optimal sensitivity to surface soil moisture. In zone D, land surface temperature is mainly controlled by vegetation transpiration with no sensitivity to surface soil moisture. In zones B and C, land surface temperature is controlled by both soil evaporation and vegetation transpiration with intermediate (average) sensitivity to surface soil moisture. Based on this understanding, vegetation temperature is estimated in a different manner in each zone.

For a given data point located in Zone A, vegetation temperature is

$$T_{\mathrm{v,1\ km}} = (\mathbf{T_{v,min}} + \mathbf{T_{v,max}})/2 \tag{9}$$

with $\mathbf{T_{v,min}}$ and $\mathbf{T_{v,max}}$ being the vegetation temperature at minimum and maximum water stress, respectively. End-members $\mathbf{T_{v,min}}$ and $\mathbf{T_{v,max}}$ are estimated from the polygons obtained by plotting MODIS surface temperature against MODIS NDVI and MODIS albedo as in [24].

For a given data point located in Zone B, vegetation temperature is

$$T_{\mathrm{v,1\ km}} = (T_{\mathrm{v,min,1\ km}} + \mathbf{T_{v,max}})/2 \tag{10}$$

with $T_{\mathrm{v,min,1\ km}}$ being the vegetation temperature associated with $\mathrm{SEE} = 0$ ($T_{\mathrm{s}} = \mathbf{T_{s,max}}$).

For a given data point located in Zone C, vegetation temperature is

$$T_{\mathrm{v,1\ km}} = (\mathbf{T_{v,min}} + T_{\mathrm{v,max,1\ km}})/2 \tag{11}$$

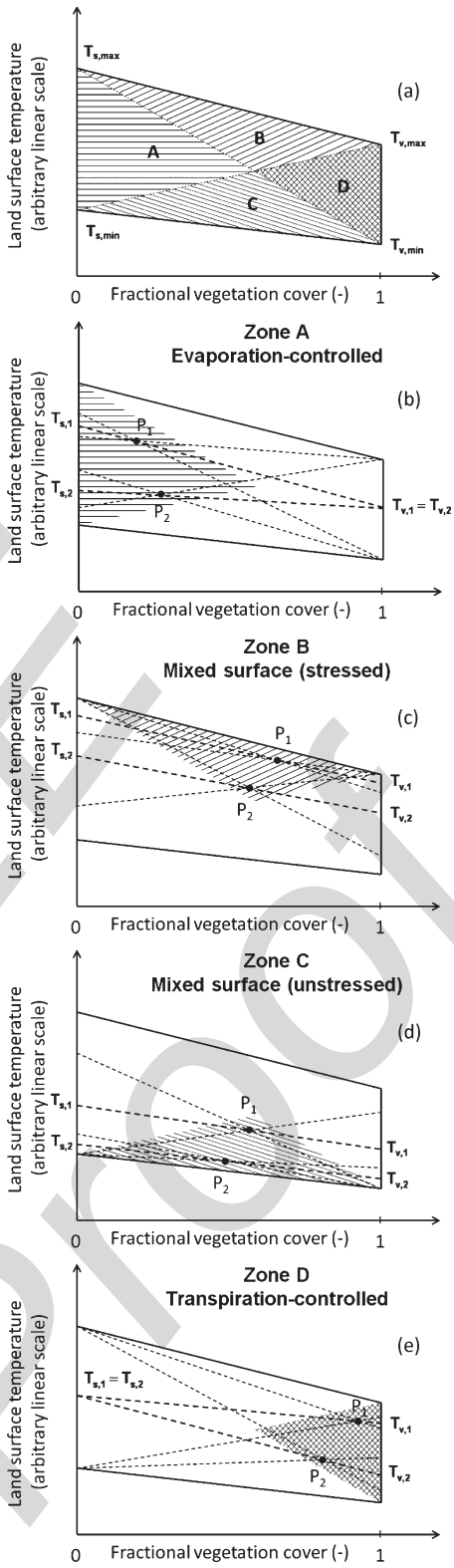

Fig. 3. Polygon defined in the land surface temperature-fractional vegetation cover space contains four distinct zones A, B, C, and D. In Zone A (soil-dominated area), the estimated vegetation temperature is constant leading to optimal sensitivity of estimated soil temperature to surface soil moisture. In Zone D, the estimated soil temperature is constant with no sensitivity to surface soil moisture. In Zone B and C (mixed surface), surface temperature is both controlled by soil evaporation and vegetation transpiration with intermediate (average) sensitivity of estimated soil temperature to surface soil moisture. DisPATCh can be run in the Zone A+B+C mode or in the Zone A only mode.

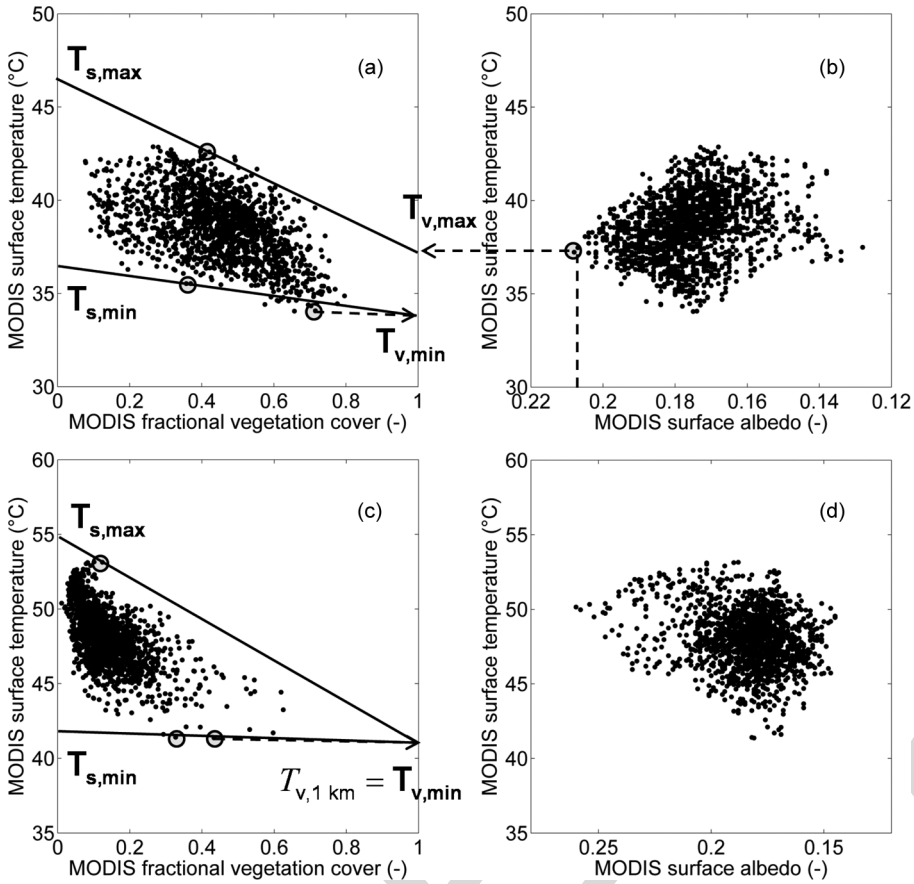

Fig. 4. Temperature end-members $\mathbf{T_{s,min}}$, $\mathbf{T_{s,max}}$, $\mathbf{T_{v,min}}$, and $\mathbf{T_{v,max}}$ are estimated from the surface temperature-fractional vegetation cover space and the surface temperature-surface albedo space within two given SMOS pixels. In (b), the pixel corresponding to the largest MODIS albedo has a fractional vegetation cover larger than 0.5, so that $\mathbf{T_{v,max}}$ is set to its surface temperature. In (d), the pixel corresponding to the largest MODIS albedo has a fractional vegetation cover lower than 0.5, so that $\mathbf{T_{v,max}}$ is set to $\mathbf{T_{v,min}}$.

with $T_{\mathrm{v,max,1\ km}}$ being the vegetation temperature associated with SEE $= 1$ ($T_{\mathrm{s}} = \mathbf{T_{s,min}}$).

For a given data point located in Zone D, vegetation temperature is

$$T_{\mathrm{v,1\ km}} = (T_{\mathrm{v,min,1\ km}} + T_{\mathrm{s,max,1\ km}})/2 \qquad (12)$$

3) End-Members: End-members $\mathbf{T_{s,min}}$, $\mathbf{T_{s,max}}$, $\mathbf{T_{v,min}}$ and $\mathbf{T_{v,max}}$ are estimated by combining the spatial information provided by the surface temperature-fractional vegetation cover space and the surface temperature-albedo space plotted using MODIS data collected in a 40-km resolution SMOS pixel. An illustration is provided in Fig. 4 for two given SMOS pixels.

- $\mathbf{T_{v,min}}$: the vegetation temperature at minimum vegetation water stress is set to the minimum MODIS surface temperature in the SMOS pixel [see Fig. 4(a) and (c)].
- $\mathbf{T_{v,max}}$: the vegetation temperature at maximum vegetation water stress is set to the MODIS surface temperature of the pixel with the maximum value of MODIS albedo in the SMOS pixel [see Fig. 4(b)]. If the fractional vegetation cover of that pixel is lower than 0.5 [see Fig. 4(d)], the vegetation temperature at maximum vegetation water stress is alternatively set to $\mathbf{T_{v,min}}$, meaning that vegetation is unstressed within the SMOS pixel. The condition based on fractional vegetation cover is lower than 0.5 aims to increase the robustness of the determination approach of $\mathbf{T_{v,max}}$, particularly in the SMOS pixels where all surface conditions are not met.
- $\mathbf{T_{s,min}}$: the soil temperature at SEE $= 1$ is extrapolated along the wet soil edge at $f_{\mathrm{v}} = 0$. The wet soil edge is defined as the line passing through $(1, \mathbf{T_{v,min}})$ and through the data point such that all the data points with $f_{\mathrm{v}} < 0.5$ are located above the wet soil edge [see Fig. 4(a) and (c)].
- $\mathbf{T_{s,max}}$: the soil temperature at SEE $= 0$ is extrapolated along the dry soil edge at $f_{\mathrm{v}} = 0$. The dry soil edge is defined as the line passing through $(1, \mathbf{T_{v,max}})$ and through the data point such that all the data points with $f_{\mathrm{v}} < 0.5$ are located below the dry soil edge [see Fig. 4(a) and (c)].

B. Atmospheric Correction

In MOD11A1 and MYD11A1 products, the land surface temperature is derived from MODIS thermal radiances using the split window algorithm [37]

$$T_{\mathrm{MODIS}} = C + \left(A_1 + A_2\frac{1-\epsilon}{\epsilon} + A_3\frac{\Delta\epsilon}{\epsilon^2}\right)\frac{Tb_{31}+Tb_{32}}{2} + \left(B_1 + B_2\frac{1-\epsilon}{\epsilon} + B_3\frac{\Delta\epsilon}{\epsilon^2}\right)\frac{Tb_{31}-Tb_{32}}{2} \qquad (13)$$

with Tb_{31} and Tb_{32} being the brightness temperatures measured in the MODIS bands 31 and 32, respectively, ϵ_{31} and ϵ_{32} the surface emissivities estimated in the respective bands, and A_1, A_2, A_3, B_1, B_2, B_3, and C regression coefficients. These coefficients are available during algorithm execution via a look up table stratified by subranges of near surface air temperature and total column water vapor. These input field are obtained at a 5-km resolution from the MODIS07_L2 product.

Given that regression coefficients in (13) are provided at 5-km resolution, the atmospheric corrections on the MODIS land surface temperature product are actually made at 5-km resolution. To test whether atmospheric corrections on MODIS temperature have an impact on disaggregation results, a different procedure is proposed to obtain another temperature data set whose atmospheric corrections are operated at the scale of a SMOS pixel, i.e., at 40-km resolution (instead of 5-km resolution for the official MODIS temperature product). The approach is to normalize the mean MODIS radiance-derived brightness temperature at the SMOS resolution. Normalization is done by adjusting the minimum and maximum mean MODIS brightness temperature to the minimum and maximum value of the official MODIS land surface temperature product within the SMOS pixel, respectively. The new temperature noted $T_{\mathrm{MODIS}}^{\mathrm{unif.\ corr.}}$ (uniform atmospheric corrections) is written

$$T_{\mathrm{MODIS}}^{\mathrm{unif.\ corr.}} = T_{\mathbf{MODIS,min}} + (T_{\mathbf{MODIS,max}} - T_{\mathbf{MODIS,min}}) \times \frac{Tb_{31} + Tb_{32} - \mathbf{Min}(Tb_{31} + Tb_{32})}{\mathbf{Max}(Tb_{31} + Tb_{32}) - \mathbf{Min}(Tb_{31} + Tb_{32})} \quad (14)$$

with $T_{\mathbf{MODIS,min}}$ and $T_{\mathbf{MODIS,max}}$ being the minimum and maximum MODIS land surface temperature within the SMOS pixel, and $\mathbf{Min}()$ and $\mathbf{Max}()$ the function that returns the minimum and maximum value within the SMOS pixel, respectively. Note that the underlying assumptions of (14) are:

- near surface air temperature and column water vapor vary at scales larger than 40 km (size of a SMOS pixel).
- surface emissivity is close to 1.

C. Algorithm

The steps used in applying DisPATCh include: 1) selecting the SMOS pixels with at least 90% (clear sky) MODIS-retrieved land surface temperature coverage; 2) computing soil evaporative efficiency over nominal MODIS pixels with (4); 3) estimating soil evaporative efficiency over non-nominal MODIS pixels; 4) retrieving parameter $\mathbf{SM_p}$; 5) applying the downscaling relationship of (3); 6) correcting disaggregated soil moisture by the SMOS pixel weighting function; and 7) compositing on a daily basis the disaggregation output ensemble [21]. The input and output data and their link within DisPATCh are summarized in Fig. 5.

1) Selecting Clear Sky SMOS Pixels: A threshold of 90% cloud-free MODIS coverage is used to select the SMOS pixels to be disaggregated. In the official MODIS land surface temperature product (MOD11A1 for Terra and MYD11A1 for Aqua), the data affected by the presence of clouds are already masked. Hence, selection of the 90% clear sky SMOS pixels is directly based on the MODIS land surface temperature product masking.

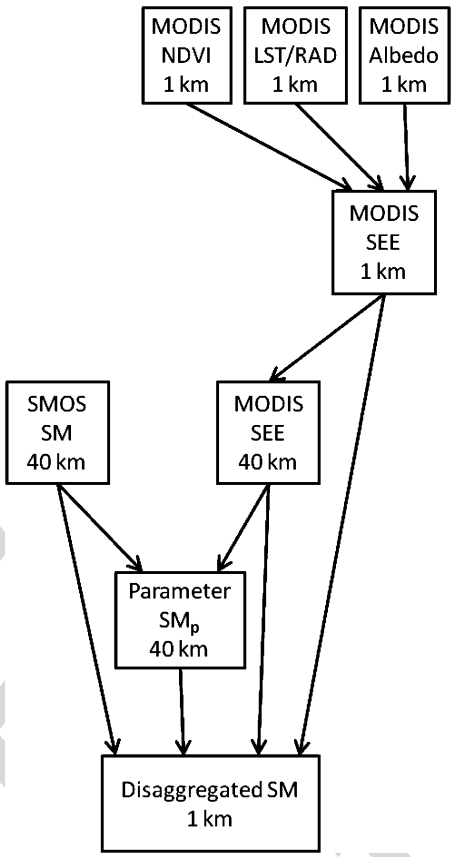

Fig. 5. Schematic diagram presenting the input and output data of DisPATCh.

2) Non-Nominal Pixels: Nominal MODIS pixels are defined as the 1-km resolution pixels that do not include open water and where land surface temperature is actually retrieved. Open water pixels are flagged in the algorithm when MODIS NDVI retrievals yield negative values. The soil evaporative efficiency of open water pixels is set to 1. The emerged pixels where land surface temperature is not retrieved (due to the presence of some clouds within the SMOS pixel) are processed as pixels with mean surface conditions. In practice, the soil evaporative efficiency of cloudy pixels (which represent less than 10% of the surface area within the SMOS pixel) is set to the mean soil evaporative efficiency calculated over the clear sky MODIS pixels. Allocating a soil evaporative efficiency value to non-nominal pixels allows DisPATCh to be run over a wider range of SMOS pixels, including those partially covered by clouds. However, non-nominal 1-km resolution pixels are flagged and discarded from the disaggregation output ensemble.

3) Forested Areas: In this study, DisPATCh is applied to all the SMOS pixels where the soil moisture retrieval is successful, even those including forest class, as long as the 1 km MODIS pixels are in Zone A, B or C (see Fig. 3). This choice is relevant here because the AACES extensive data were almost exclusively collected in agricultural areas (cropping/grazing), so forests for this study are not an issue. In the case of a mixed SMOS pixel including a significant fraction of forest, DisPATCh should be applied to the surface area of the dominant

class, thus excluding the surface area of the minority land cover classes.

4) Calibration: The soil moisture parameter $\mathbf{SM_p}$ used to compute $\partial\mathbf{SM_{mod}}/\partial\mathbf{SEE}$ in (3) is estimated by inverting the SEE model in (7) at SMOS resolution

$$\mathbf{SM_p} = \frac{\pi \cdot \mathbf{SM_{SMOS}}}{\cos^{-1}\left(1 - 2\langle \mathrm{SEE}_{\mathrm{MODIS,1\ km}}\rangle_{\mathbf{40}\ \mathrm{km}}\right)} \tag{15}$$

A value of $\mathbf{SM_p}$ is obtained for each SMOS pixel and each input data set. Note that the main assumption limiting validity of the calibration approach is the soil evaporative efficiency model [26] itself. The soil evaporative efficiency model in [26] was chosen for its simplicity (one parameter) and its ability to represent the general behavior of soil evaporative efficiency over the full range of soil moisture: particularly the null derivative at zero and at maximum soil moisture, and an inflexion point in between [38]. However, it has some inconsistencies. In particular, [38] have indicated that 1) potential evaporation is physically reached at soil saturation and not at field capacity; therefore the model in [26] should be (strictly speaking) parameterized by the soil moisture at saturation and not by the soil moisture at field capacity, and 2) soil evaporative efficiency varies with potential evaporation, meaning that the soil moisture parameter (set to the soil moisture at field capacity in [26]) should theoretically vary in time with atmospheric evaporative demand. Consequently, the $\mathbf{SM_p}$ retrieved from SMOS and MODIS data using the model in [26] is definitely not the soil moisture at field capacity as in [26], although it could be in part related to it. In this study, $\mathbf{SM_p}$ is therefore considered to be a fitting parameter self-estimated by DisPATCh.

5) Weighting Function: A SMOS pixel WEighting Function (WEF) is used to take into account the impact of soil moisture distribution on the SMOS scale soil moisture as seen by SMOS radiometer. A centrosymmetric analytical approximation MEAN_WEF is provided in [19], [20]

$$\mathrm{MEAN\_WEF}(\rho) = C_{\mathrm{MWEF2}} + \mathrm{WEF_A}\left(\frac{\rho}{C_{\mathrm{MWEF1}}} \cdot \frac{\pi}{C_{\mathrm{WEF1}}}\right) \tag{16}$$

with ρ being the distance from the SMOS pixel center, and $C_{\mathrm{MWEF1}} = 40$ km, $C_{\mathrm{MWEF2}} = 0.027$, $C_{\mathrm{WEF1}} = 73.30$ and

$$\mathrm{WEF_A}(\rho') = \frac{[\mathrm{sinc}(C_{\mathrm{WEF1}} \cdot \rho')]^{C_{\mathrm{WEF2}}}}{1 + C_{\mathrm{WEF3}} \cdot \rho'^{C_{\mathrm{WEF4}}}} \tag{17}$$

with ρ' being the distance in the director cosines coordinates, $\mathrm{sinc}(x) = \sin(x)/x$, and $C_{\mathrm{WEF2}} = 1.4936$, $C_{\mathrm{WEF3}} = 524.5$ and $C_{\mathrm{WEF4}} = 2.103$.

A correction is applied to disaggregated soil moisture in (3)

$$\mathrm{SM}_{1\ \mathrm{km}}^{\mathrm{wef\ corr.}} = \mathrm{SM}_{1\ \mathrm{km}} + \frac{\sum \mathrm{MEAN\_WEF}(\rho) \cdot \mathrm{SM}_{1\ \mathrm{km}}(\rho)}{\sum \mathrm{MEAN\_WEF}(\rho)} - \mathbf{SM_{SMOS}} \tag{18}$$

with $\mathrm{SM}_{1\ \mathrm{km}}^{\mathrm{wef\ corr.}}$ being the WEF-corrected disaggregated soil moisture. Mathematically speaking, one should replace $\mathbf{SM_{SMOS}}$ with $\sum \mathrm{MEAN\_WEF} \cdot \mathrm{SM}_{1\ \mathrm{km}} / \sum \mathrm{MEAN\_WEF}$ in (3) and (15) and run an iteration loop until convergence of $\mathrm{SM}_{1\ \mathrm{km}}^{\mathrm{wef\ corr.}}$ values. However, the impact of the WEF on disaggregated soil moisture is expected to be low so that the simple correction in (18) is considered to be sufficient for the purpose of the study.

6) Disaggregation Output: The downscaling relationship in (3) is applied to each input data set, and the disaggregated soil moisture data ensemble is averaged on each 1-km resolution pixel within the study area. Averaging is a way to reduce random uncertainties in the disaggregation output. In [17], [27], disaggregated soil moisture was averaged in space (aggregated) at the expense of downscaling resolution. Herein, temporal averaging [30] is preferred to keep an optimal downscaling resolution. Note that a condition to average disaggregated soil moisture in time is the availability of thermal infrared data at high temporal frequency. Another significant advantage of applying DisPATCh to an input ensemble is to provide an estimate of the uncertainty in 1-km resolution disaggregated soil moisture, e.g., by computing the standard deviation within the output ensemble.

IV. Application

To test DisPATCh under various surface and atmospheric conditions, the algorithm is run during AACES-1 and AACES-2 in different modes, by including (or not) a correction for vegetation and atmospheric effects. In each case, disaggregated SMOS soil moisture and HDAS measurements are compared at 1-km resolution for all date-farm units with overlapping HDAS/SMOS/MODIS data.

A. Null Hypothesis

In this study, the null hypothesis is defined as the application of DisPATCh with parameter $\mathbf{SM_p}$ set to zero in (8). Hence, the downscaling relationship in (3) becomes

$$\mathrm{SM}_{1\ \mathrm{km}} = \mathbf{SM_{SMOS}} \tag{19}$$

meaning that no 1-km information is used. Defining a null hypothesis is useful to test whether DisPATCh is able to reproduce the subpixel variability within the ~ 10 km^2 sampling farms with better skill than simply assuming a uniform moisture condition. Statistical results in terms of root mean square difference, mean difference, correlation coefficient, and slope of the linear regression between the SMOS soil moisture disaggregated with (19) and *in situ* measurements are listed in Table III. One observes that the root mean square difference is generally explained by a (negative) bias in SMOS data and that none of the correlations evaluated at 1-km resolution for each farm separately is statistically significant (all calculated p-values are larger than 0.10). Thus, the rationale for developing DisPATCh is to improve the correlation at fine scale between SMOS and ground soil moisture and to reduce the bias in disaggregated SMOS data in the specific case where the bias in SMOS data at the farm scale is due to the heterogeneity of soil moisture within the SMOS pixel.

TABLE III
DISPATCH IS RUN WITH NO 1-km INFORMATION ($\mathbf{SM_p}$ SET TO ZERO) AND STATISTICAL RESULTS ARE LISTED IN TERMS OF ROOT MEAN SQUARE DIFFERENCE (RMSD), MEAN DIFFERENCE (BIAS), CORRELATION COEFFICIENT (R), AND SLOPE OF THE LINEAR REGRESSION BETWEEN 1-km RESOLUTION DISAGGREGATED SMOS SOIL MOISTURE AND 1-km AGGREGATED *IN SITU* MEASUREMENTS. THE MEAN AND STANDARD DEVIATION OF GROUND MEASUREMENTS ($\langle SM_{HDAS}\rangle$ AND σ_{HDAS}), THE NUMBER OF CONSIDERED 1-km PIXELS, AND STATISTICAL SIGNIFICANCE (P-VALUE) ARE ALSO LISTED FOR EACH DATE-FARM UNIT

DoY/Farm	$\langle SM_{HDAS}\rangle$ (m^3/m^3)	σ_{HDAS} (m^3/m^3)	Number of 1 km pixels	RMSD (m^3/m^3)	Bias (m^3/m^3)	R† (-)	Slope† (-)	p-value (-)
28/F05	0.04	0.02	7	0.04	−0.04	-	-	1.0
30/F07	0.02	0.03	8	0.02	−0.02	-	-	1.0
30/F08	0.03	0.02	7	0.02	−0.02	-	-	0.69
46/F15	0.29	0.05	8	0.04	0.03	-	-	0.91
46/F16	0.34	0.06	8	0.09	−0.08	-	-	1.0
49/F17	0.21	0.06	8	0.04	−0.04	-	-	0.66
49/F18	0.25	0.07	6	0.08	−0.08	-	-	0.42
49/F20	0.20	0.09	4	0.02	−0.007	-	-	0.87
51/F19	0.24	0.08	6	0.13	−0.13	-	-	0.77
51/F20	0.20	0.10	6	0.09	−0.08	-	-	0.79
AACES-1 mean‡	-	-	-	-	-	-	-	>0.10
254/F09	0.33	0.07	9	0.13	−0.13	-	-	0.13
256/F07	0.36	0.10	8	0.19	−0.18	-	-	0.15
264/F13	0.30	0.07	8	0.18	−0.17	-	-	1.0
265/F15	0.25	0.06	7	0.05	−0.05	-	-	1.0
267/F09	0.21	0.07	9	0.14	−0.14	-	-	0.43
AACES-2 mean‡	-	-	-	-	-	-	-	>0.10

† R and slope values are reported if p-value<0.10.

‡ the mean values computed for AACES-1 and AACES-2 include only statistically significant (p-value<0.10) results.

B. Visual Assessment of Disaggregation Images

As an example, DisPATCh is applied on DoY 49 over a 120 km by 80 km subarea including the farms F16, F17, F18, F19, and F20. The images of 1-km resolution disaggregated SMOS soil moisture are presented in Fig. 6. DisPATCh is run with $\mathbf{SM_p}$ set to zero (null hypothesis) and in four distinct modes corresponding to the combinations of the "LST" (the official MODIS land surface temperature product is used) and "RAD" [the land surface temperature is derived from MODIS radiances using (14)] modes and the "Zone A+B+C" (the vegetation-transpiration dominated 1-km pixels are discarded) and "Zone A only" (only the soil evaporation-dominated 1-km pixels are selected) modes.

In Fig. 6, the SMOS DGG nodes where level-2 soil moisture is successfully retrieved are overlaid on the image corresponding to the null hypothesis (resampled SMOS data with no 1-km information) for 6 am and 6 pm overpass times separately. The gaps in SMOS data in the lower middle part of the images are due to topography flagging over the Australian Alps. In the version-4 SMOS level-2 processor, soil moisture is not retrieved at the DGG nodes where the topography effects on simulated brightness temperatures exceed a certain threshold, so as to prevent large errors in soil moisture values. The apparent resolution of the null hypothesis image is 20 km because it is generated from the composition of four 40-km resolution resampled SMOS snapshot images, whose resampling grids are separated by 20 km (the SMOS level-2 data resampling strategy was described in Section II-B.).

Note that the disaggregation products in the Zone A+B+C mode cover an area larger than the area sampled by SMOS data, because the SMOS resolution (about 40 km) is larger than the SMOS product sampling length (about 15 km), but does not provide disaggregated values at a distance larger than 20 km from the successful retrieval nodes. Concerning the Zone A only mode, disaggregation products do not cover an area larger than the SMOS sampling area because the Australian Alps are surrounded by forests where the fraction of bare soil is less than elsewhere in the area, and which correspond to Zone B or C in the hourglass in Fig. 3.

When looking at the images obtained in the Zone A+B+C mode in Fig. 6, one observes that the spatial structures of 1-km disaggregated SMOS soil moisture encompass, but does not seem to be correlated with, the SMOS data sampling length. However, a "boxy artifact" is still apparent at 20-km resolution, which is the separation length of the SMOS data resampling grids as explained in Section II-B. The notion of "boxy artifact" was introduced by [39] to analyze the quality of a disaggregation approach. The less apparent the low-resolution boxes, the better the disaggregation skill of the algorithm to spatially connect high-resolution disaggregated values between neighboring low-resolution pixels, and thus to derive a realistic high-resolution soil moisture field. When comparing the images obtained in the Zone A+B+C mode with those obtained in the

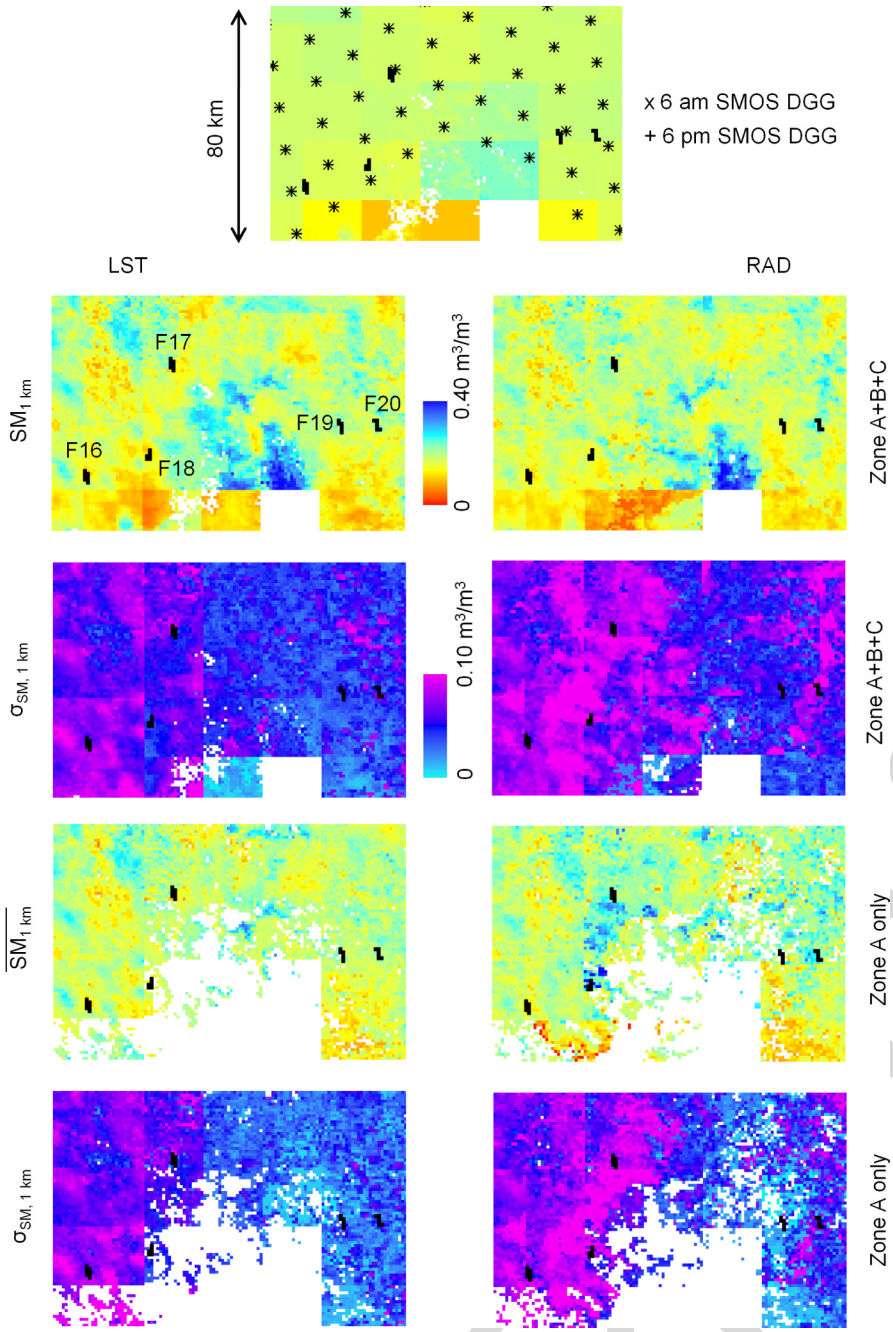

Fig. 6. Images of disaggregation results over a 120 km by 80 km subarea on DoY 49. The disaggregated soil moisture ($\overline{\mathrm{SM}_{1\ \mathrm{km}}}$) and its estimated uncertainty ($\sigma_{\mathrm{SM},1\ \mathrm{km}}$) are compared in the LST and RAD modes and in the Zone A+B+C and Zone A only modes. Sampling farms are overlaid on all images. SMOS DGG nodes are overlaid on the image corresponding to the null hypothesis (no 1-km resolution information) presented at top.

Zone A only mode, one observes that the 20-km resolution boxy artifact is less apparent in the Zone A only mode, consistent with the better sensitivity of MODIS-derived SEE with soil-dominated pixels (Zone A) than with mixed-surface (Zone B and C) pixels. In Fig. 6, the images obtained in the LST and RAD mode highlight different spatial structures. In general, there are less data gaps in the RAD than in the LST mode. However, ground validation data are required to assess their relative quality/accuracy.

As an assessment of the uncertainty in composited soil moisture disaggregation, the standard deviation within the disaggregation output ensemble is also reported for each disaggregation product in Fig. 6. The same observations can be made as with the soil moisture images: spatial structures are more visible, and the boxy artifact is less apparent in the RAD than in the LST mode. In general, the estimated uncertainty in disaggregated products is larger in the RAD than in the LST mode, regardless of the Zone (A+B+C or A only) mode.

C. SMOS Weighting Function

To evaluate the impact of the SMOS instrument weighting function on disaggregation results, DisPATCh is run with (and without) the WEF correction in (18). The expected effect of the

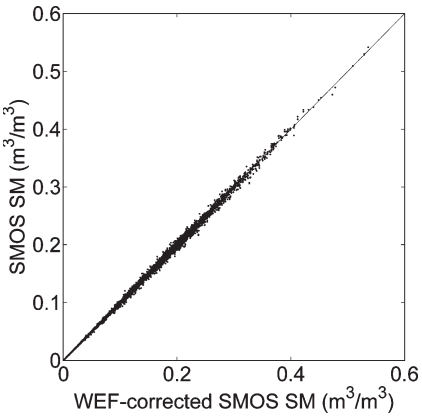

Fig. 7. Uncorrected versus WEF-corrected SMOS soil moisture for the entire data set.

WEF is a bias at 40 km resolution on disaggregated soil moisture. Fig. 7 plots the uncorrected against WEF-corrected SMOS soil moisture for the entire data set including both AACES-1 and AACES-2 experiments. The WEF correction has very little impact on disaggregated soil moisture with a maximum difference between uncorrected and WEF-corrected SMOS soil moisture of 0.02 m^3/m^3, a mean difference of approximately zero, and a standard deviation of 0.003 m^3/m^3. Although the difference is small with this data set, WEF-corrected products are expected to be more realistic. Therefore, the correction in (18) is used in all the DisPATCh runs that follow.

D. Quantitative Comparison With In Situ Measurements

Fig. 8 presents the scatterplots of 1-km resolution disaggregated SMOS soil moisture versus 1-km resolution aggregated *in situ* measurements for the ten date-farm units during AACES-1. On each graph are plotted the soil moisture disaggregated in the Zone A+B+C mode (empty squares) and the soil moisture disaggregated in the Zone A only mode (black squares). At the beginning of AACES-1, conditions are very dry so that SMOS retrievals are close to zero and the variability of *in situ* measurements is low (about 0.02 m^3/m^3). In such conditions, no useful information is expected from the application of DisPATCh, and the statistical results in terms of spatial correlation are not meaningful for DoY 28/F05, DoY 30/F07 and DoY 30/F08. While wetter conditions occur after DoY 30, cloud cover prevents DisPATCh to be run (MODIS data are unavailable) until DoY 46. On DoY 46, the average and standard deviation of *in situ* soil moisture measurements is 0.32 m^3/m^3 and 0.06 m^3/m^3, respectively. The spatial variability of 1-km soil moisture is nicely captured by DisPATCh notably in the RAD mode. On DoY 49, the disaggregated SMOS soil moisture is still correlated with the *in situ* measurements made in three farms (F17, F18, and F20). On the last ground sampling day, disaggregation results are significantly correlated with *in situ* measurements in F19, but not in F20. The poor results obtained with DoY 51/F20 is probably due to the time gap (3 days) between ground sampling date (DoY 51) and MODIS overpass day (DoY 54).

Statistical results in terms of root mean square difference, mean difference, correlation coefficient, and slope of the linear regression between the SMOS soil moisture disaggregated in the Zone A+B+C mode and aggregated *in situ* measurements are listed in Table IV. Statistical significance (p-value) is also reported for each date-farm unit to select statistically significant (p-value < 0.10) results. Although the disaggregation of SMOS data on extensively dry DoY 30 does not provide any additional information (soil is uniformly dry), the observed correlation between disaggregated (LST mode) and *in situ* soil moisture is statistically significant, and the correlation coefficient value is negative (-0.70 and -0.95 at F07 and F08, respectively). One plausible explanation is the opposite effect of soil temperature on HDAS soil moisture measurements and on MODIS-derived soil evaporative efficiency: a slight undercorrection of the temperature-corrected hydraprobe measurements at high temperature [18] results in a slight increase of soil moisture estimate with soil temperature, while an increase of soil temperature makes soil evaporative efficiency decrease. Nevertheless, the possible impact of soil temperature on HDAS measurements is very low with a slope of the linear regression between disaggregated SMOS and *in situ* soil moisture calculated as -0.08 and -0.03 for F07 and F08, respectively. When selecting statistically significant results (p-value < 0.10) and discarding data for DoY 30, the mean correlation coefficient and slope in RAD mode are 0.75 and 0.58, respectively.

Fig. 9 presents the scatterplots of 1-km resolution disaggregated SMOS soil moisture versus 1-km resolution aggregated *in situ* measurements for the five date-farm units during AACES-2. On each graph are plotted the soil moisture disaggregated in the Zone A+B+C mode (empty squares) and the soil moisture disaggregated in the Zone A only mode (black squares). The surface conditions of AACES-2 were relatively wet with a mean soil moisture value estimated as 0.29 m^3/m^3. The disaggregated SMOS soil moisture does not correlate well with *in situ* measurements with a p-value larger than 0.10 for all sampling days, except for DoY 256/F07 in LST mode (see Table IV). The negative correlation coefficient (-0.73) obtained on DoY 256 is discussed when comparing the Zone A+B+C and Zone A only modes in Section IV-F. In general, statistical results in Table IV indicate that DisPATCh does not succeed in representing the variability of soil moisture at 1-km resolution during AACES-2. In fact, DisPATCh is based on the tight coupling that occurs between soil moisture and evaporation under high evaporative demand conditions [40]. This coupling seems to be weak in September over the study area so that the disaggregation results at 1-km resolution are not reliable.

For DoY 264/F13, however, an interesting feature is observed on the graph corresponding to the RAD and Zone A only modes. When removing the (three) black squares with the largest errorbars, the correlation coefficient and the slope of the linear regression between disaggregated and *in situ* observations becomes 0.9 and 0.7, respectively. This suggests that: 1) the standard deviation within the disaggregation output ensemble can be a good estimate of the uncertainty in the composited disaggregation product; and 2) the applicability of DisPATCh is greatly dependent on the quality of MODIS land surface temperature. Note that in this study, a choice was made to maximize the number of data points used in the comparison with *in situ* measurements. Consequently, all the cloud-free

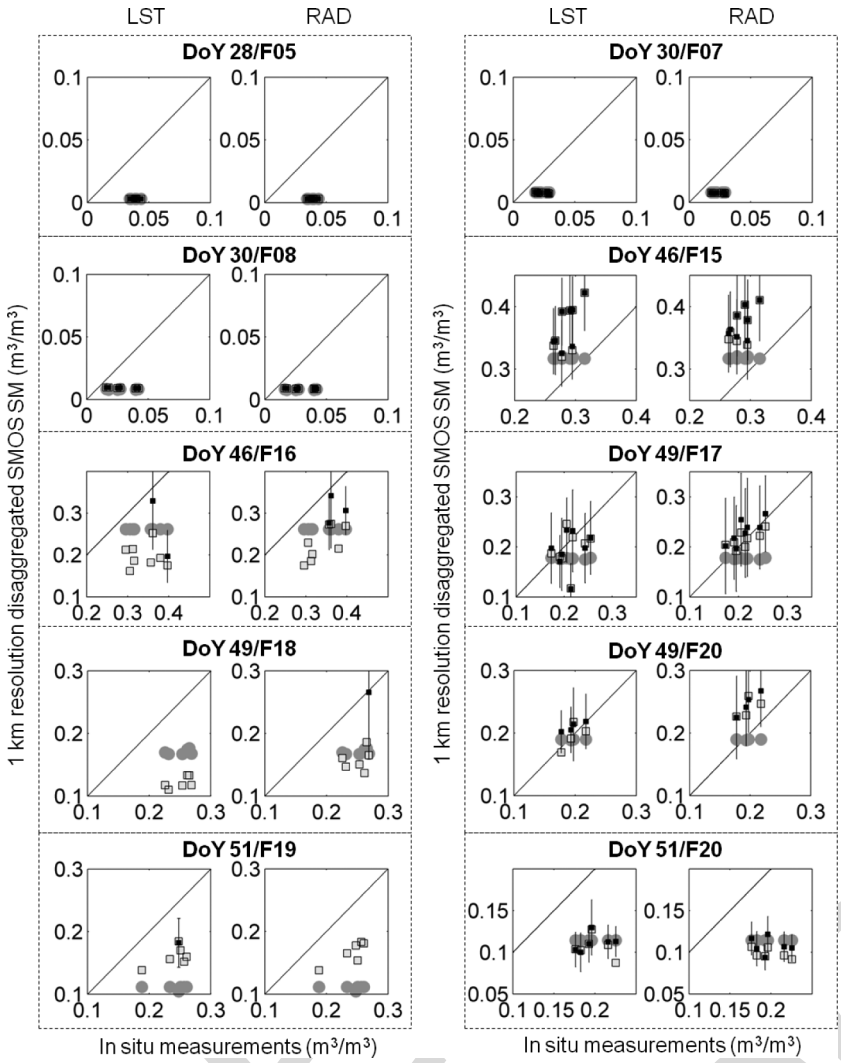

Fig. 8. Scatterplots of 1-km resolution disaggregated SMOS soil moisture versus 1-km resolution aggregated *in situ* measurements for each of the ten date-farm data sets during AACES-1. The filled circles correspond to disaggregation with no 1-km information, empty squares to Zone A+B+C mode and black squares to Zone A only mode. For the Zone A only mode, the uncertainty in disaggregated soil moisture is represented by vertical errorbars.

MODIS land surface temperature data were used regardless of the MODIS land surface temperature quality index. Further research should be conducted to assess whether selecting the MODIS pixel with the best MODIS land surface temperature quality index would improve the disaggregation results. This would be possible using the AACES airborne data, which cover a much larger area than *in situ* measurements.

E. Atmospheric Corrections

The impact of atmospheric corrections on DisPATCh output is analyzed by comparing the disaggregation results obtained in the LST and RAD mode. Quantitative comparison between LST and RAD modes is provided in Table IV in terms of root mean square difference, mean difference, correlation coefficient, and slope of the linear regression between disaggregated SMOS soil moisture and aggregated *in situ* measurements. Correlation coefficient and slope values are reported only if the p-value (statistical significance) is lower than 0.10. It is apparent that statistical results are better in the RAD than in the LST mode. When including all dates, the mean bias is decreased from -0.05 m^3/m^3 in LST mode to -0.03 m^3/m^3 in RAD mode during AACES-1. When selecting statistically significant results (p-value < 0.10) and discarding data for DoY 30, the mean correlation coefficient and slope is 0.75 and 0.58 in RAD mode, and 0.65 and 1.5 in LST mode, respectively. Note that the improvement is very significant for DoY 46/F16 with a correlation coefficient and slope increasing from about zero to 0.7 and 0.8, respectively.

The fact that the results obtained in RAD mode are superior to those obtained in LST mode indicates that the atmospheric corrections of the official MODIS land surface temperature add significant uncertainties in the disaggregation products. One rationale may be that the information used in atmospheric corrections (notably air temperature and water vapor profile data) are subjected to large uncertainties at 5-km resolution. As DisPATCh is based on the spatial variations of MODIS temperature relative to the 40 km scale mean, the atmospheric corrections on the land surface temperature data are not necessary at 5 km (as it is done in the MODIS temperature

TABLE IV
DISPATCH IS RUN IN THE ZONE A+B+C MODE AND STATISTICAL RESULTS ARE LISTED IN TERMS OF ROOT MEAN SQUARE DIFFERENCE (RMSD), MEAN DIFFERENCE (BIAS), CORRELATION COEFFICIENT (R), AND SLOPE OF THE LINEAR REGRESSION BETWEEN 1-km RESOLUTION DISAGGREGATED SMOS SOIL MOISTURE AND 1-km AGGREGATED *IN SITU* MEASUREMENTS. THE RESULTS OBTAINED USING THE RADIANCE-DERIVED LAND SURFACE TEMPERATURE DATA (RAD MODE) AND USING THE OFFICIAL MODIS LAND SURFACE TEMPERATURE DATA (LST MODE IN PARENTHESIS) ARE COMPARED. THE MEAN AND STANDARD DEVIATION OF GROUND MEASUREMENTS ($\langle SM_{HDAS} \rangle$ AND σ_{HDAS}), THE NUMBER OF CONSIDERED 1-km PIXELS AND STATISTICAL SIGNIFICANCE (P-VALUE) ARE ALSO LISTED FOR EACH DATE-FARM UNIT

DoY/Farm	$\langle SM_{HDAS} \rangle$ (m^3/m^3)	σ_{HDAS} (m^3/m^3)	Number of 1 km pixels	RMSD (m^3/m^3)	Bias (m^3/m^3)	R† (-)	Slope† (-)	p-value (-)
28/F05	0.04	0.02	7 (7)	0.04 (0.04)	−0.04 (−0.04)	- (-)	- (-)	0.72 (0.80)
30/F07	0.02	0.03	8 (8)	0.02 (0.02)	−0.02 (−0.02)	- (−0.70)	- (−0.08)	0.20 (0.05)
30/F08	0.03	0.02	7 (7)	0.02 (0.02)	−0.02 (−0.02)	- (−0.95)	- (−0.03)	0.11 (0.001)
46/F15	0.29	0.05	8 (8)	0.09 (0.09)	0.09 (0.08)	- (0.65)	- (1.5)	0.12 (0.08)
46/F16	0.34	0.06	8 (8)	0.12 (0.15)	−0.11 (−0.14)	0.72 (-)	0.76 (-)	0.04 (0.95)
49/F17	0.21	0.06	8 (8)	0.02 (0.04)	0.00 (−0.02)	0.70 (-)	0.42 (-)	0.05 (0.54)
49/F18	0.25	0.07	6 (6)	0.10 (0.13)	−0.09 (−0.13)	- (-)	- (-)	0.60 (0.20)
49/F20	0.20	0.09	4 (4)	0.05 (0.01)	0.04 (0.00)	- (-)	- (-)	0.41 (0.32)
51/F19	0.24	0.08	6 (6)	0.07 (0.08)	−0.07 (−0.08)	0.84 (-)	0.56 (-)	0.04 (0.19)
51/F20	0.20	0.10	6 (6)	0.10 (0.09)	−0.10 (−0.09)	- (-)	- (-)	0.17 (0.51)
AACES-1 mean‡	0.26 (0.29)	0.07 (0.05)	7 (8)	0.07 (0.09)	−0.06 (−0.08)	0.75 (0.65)	0.58 (1.5)	0.04 (0.08)
254/F09	0.33	0.07	9 (9)	0.18 (0.14)	−0.16 (−0.11)	- (-)	- (-)	0.17 (0.74)
256/F07	0.36	0.10	8 (9)	0.12 (0.19)	−0.10 (−0.18)	- (−0.73)	- (−0.47)	0.12 (0.04)
264/F13	0.30	0.07	8 (8)	0.16 (0.19)	−0.14 (−0.16)	- (-)	- (-)	0.59 (0.47)
265/F15	0.25	0.06	7 (7)	0.16 (0.18)	0.01 (0.03)	- (-)	- (-)	0.32 (0.34)
267/F09	0.21	0.07	9 (9)	0.16 (0.15)	−0.15 (−0.15)	- (-)	- (-)	0.90 (0.86)
AACES-2 mean‡	0.36	0.10	- (9)	- (0.19)	- (−0.18)	- (−0.73)	- (−0.47)	>0.10 (0.04)

† R and slope values are reported if p-value<0.10.

‡ the mean values computed for AACES-1 and AACES-2 include only statistically significant (p-value<0.10) results and discard extensive dry days DoY 28-30.

algorithm). An atmospheric correction at 40-km resolution is sufficient and provides even better disaggregation results that applying an atmospheric correction at 5-km resolution.

F. Vegetation Cover

The impact of vegetation cover on DisPATCh output during AACES-1 is analyzed by comparing the disaggregation results obtained in the Zone A+B+C and Zone A only mode. Quantitative comparison between Zone A+B+C and Zone A only modes is provided in Tables IV and V in terms of root mean square difference, mean difference, correlation coefficient, and slope of the linear regression between disaggregated SMOS soil moisture and aggregated *in situ* measurements. It is apparent that statistical results are generally better in the Zone A only than in the Zone A+B+C mode for both LST and RAD modes. In the RAD mode for instance, the mean correlation coefficient is increased from 0.75 in the Zone A+B+C mode (Table IV) to 0.89 in the Zone A only mode (Table V). Also the mean slope is closer to 1 as it switches from 0.58 in the Zone A+B+C mode (Table IV) to 0.91 in the Zone A only mode (Table V). Consequently, results are consistent with the hourglass approach in Fig. 3 that predicts a lower sensitivity of MODIS-derived soil temperature to soil moisture in Zone B and C, Zone A having the highest potential for estimating soil moisture variability from MODIS temperature.

On DoY 256, the negative correlation appearing in Zone A+B+C mode (Table IV) is not significant in Zone A only mode (Table V), suggesting that the contradictory result obtained on DoY 256 is probably an artifact due to the small sample size.

Note that one drawback of the Zone A only mode is the larger amount of data gaps in the soil moisture images. Therefore, the use of both modes is a compromise between application coverage and accuracy in the disaggregation output.

G. Distinguishing Between SMOS and DisPATCh Errors

By solving the extent mismatch between 40-km resolution remote sensing observation and localized *in situ* measurements, DisPATCh could be used as a tool to help improve the validation strategies of SMOS data in low-vegetated semi-arid regions. It also would reduce the coverage requirements identified by [41] for airborne validation campaigns. However, such a validation approach requires separating the different error sources that may be attributed to SMOS soil moisture and to DisPATCh. One solution is to estimate the errors attributed to DisPATCh and then deduce the errors attributed to SMOS soil moisture. To estimate the errors that are associated with the disaggregation

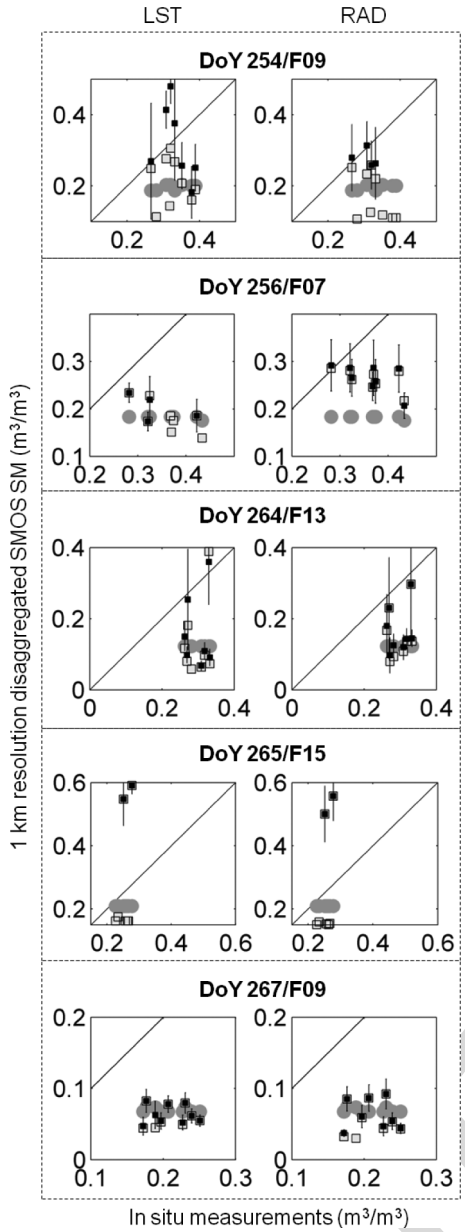

Fig. 9. Scatterplots of 1-km resolution disaggregated SMOS soil moisture versus 1-km resolution aggregated *in situ* measurements for each of the five date-farm data sets during AACES-2. The filled circles correspond to disaggregation with no 1-km information, empty squares to Zone A+B+C mode and black squares to Zone A only mode. For the Zone A only mode, the uncertainty in disaggregated soil moisture is represented by vertical errorbars.

methodology, it is suggested to analyze the spatial correlation between 1-km disaggregated SMOS soil moisture and *in situ* measurements. If the correlation is significant, then the disaggregation product is likely to be sufficiently accurate for validating SMOS data.

Note that the errors in DisPATCh are in part coupled with the errors in SMOS soil moisture, particularly because SMOS is an input to DisPATCh. However, any uncertainties in SMOS soil moisture should not impact the disaggregation results at a distance shorter than the SMOS data sampling length (15 km). This is the reason why such a validation strategy should be conducted with ground measurements made within a distance radius of 15 km.

In this study case, five date-farm units including DoY 46/F15, DoY 46/F16, DoY 49/F17, DoY 49/F18, and DoY 49/F20 indicate a significant correlation between disaggregated SMOS soil moisture and *in situ* measurements. For these units, the root mean square error in disaggregated SMOS soil moisture is mainly explained by a bias in disaggregated soil moisture (see Table IV). However, no conclusion can be drawn from these data because: 1) the bias is sometimes positive (DoY 46/F15, DoY 49/F20), and sometimes negative (DoY 46/F16, DoY 49/F17, DoY 49/F18); and 2) the comparison is made only once for each farm, which does not allow analyzing the temporal behavior. Such a validation approach could be undertaken in the near future using the OzNet (http://www.oznet.org.au/, [42]) soil moisture monitoring network, providing continuous measurements at 68 sites within the Murrumbidgee catchment area.

H. Subpixel Variability and Assimilation Perspectives

DisPATCh is successively run in LST or RAD mode and in Zone A+B+C or Zone A only mode during AACES-1. Fig. 10 plots for each case the estimated uncertainty in disaggregated soil moisture (computed as the standard deviation of the disaggregation output ensemble) against the subpixel variability of 1-km resolution *in situ* measurements (computed as the standard deviation of the *in situ* measurements made within 1-km pixels). The data corresponding to DoY 51 are plotted separately because of the time gap between HDAS/SMOS (DoY 51) and MODIS (DoY 54) collection time. It is interesting to observe that the estimated uncertainty in disaggregated soil moisture is closely related to the observed subpixel variability of *in situ* measurements. Hence, $\sigma_{\mathrm{SM,1\ km}}$ could be used as a proxy for representing the soil moisture variability at scales finer than 1-km resolution. Concerning the data on DoY 51, the linear regression is clearly off the 1:1 line. This is consistent with a decrease of the spatial variability in soil moisture during a dry down period [43]. In particular, the spatial variability in soil moisture is expected to be lower on DoY 54 than on DoY 51.

The correlation between the estimated uncertainty in disaggregated soil moisture and the subpixel soil moisture variability makes an additional link between DisPATCh output and assimilation schemes into hydrological models. A number of optimal assimilation methodologies have been developed to combine model predictions with remote sensing observations. However, any so-called optimal assimilation technique stops being optimal if the uncertainty in remotely sensed data is unknown or estimated with a large uncertainty. In the perspective of assimilating disaggregated SMOS data into land surface models, one should keep in mind that the error information on observable variables is as crucial as the observations themselves, e.g., [44].

V. Summary and Conclusion

DisPATCh is an algorithm dedicated to the disaggregation of soil moisture observations using high-resolution soil temperature data. It converts soil temperature fields into soil moisture fields given a semi-empirical soil evaporative efficiency model

TABLE V
DISPATCH IS RUN IN THE ZONE A ONLY MODE, AND STATISTICAL RESULTS ARE LISTED IN TERMS OF ROOT MEAN SQUARE DIFFERENCE (RMSD), MEAN DIFFERENCE (BIAS), CORRELATION COEFFICIENT (R), AND SLOPE OF THE LINEAR REGRESSION BETWEEN 1-km RESOLUTION DISAGGREGATED SMOS SOIL MOISTURE AND 1-km AGGREGATED *IN SITU* MEASUREMENTS. THE RESULTS OBTAINED USING THE RADIANCE-DERIVED LAND SURFACE TEMPERATURE DATA (RAD MODE) AND USING THE OFFICIAL MODIS LAND SURFACE TEMPERATURE DATA (LST MODE IN PARENTHESIS) ARE COMPARED. THE MEAN AND STANDARD DEVIATION OF GROUND MEASUREMENTS ($\langle SM_{HDAS} \rangle$ AND σ_{HDAS}), THE NUMBER OF CONSIDERED 1-km PIXELS AND STATISTICAL SIGNIFICANCE (P-VALUE) ARE ALSO LISTED FOR EACH DATE-FARM UNIT

DoY/Farm	$\langle SM_{HDAS} \rangle$ (m^3/m^3)	σ_{HDAS} (m^3/m^3)	Number of 1 km pixels	RMSD* (m^3/m^3)	Bias* (m^3/m^3)	R† (-)	Slope† (-)	p-value (-)
28/F05	0.04	0.02	7 (7)	0.04 (0.04)	−0.04 (−0.04)	- (-)	- (-)	0.72 (0.80)
30/F07	0.02	0.03	8 (8)	0.02 (0.02)	−0.02 (−0.02)	- (−0.70)	- (−0.08)	0.20 (0.05)
30/F08	0.03	0.02	7 (7)	0.02 (0.02)	−0.02 (−0.02)	- (−0.95)	- (−0.03)	0.11 (0.001)
46/F15	0.29	0.05	8 (8)	0.09 (0.09)	0.09 (0.08)	- (0.66)	- (1.4)	0.13 (0.07)
46/F16	0.34	0.06	3 (2)	0.07 (0.14)	−0.06 (−0.12)	- (-)	- (-)	0.96 (-)
49/F17	0.21	0.06	8 (8)	0.02 (0.04)	0.02 (−0.02)	0.79 (-)	0.71 (-)	0.02 (0.64)
49/F18	0.25	0.07	1 (0)	- (-)	- (-)	- (-)	- (-)	0.20 (0.20)
49/F20	0.20	0.09	4 (4)	0.05 (0.02)	0.05 (0.01)	0.98 (0.92)	1.1 (0.42)	0.02 (0.08)
51/F19	0.24	0.08	0 (1)	- (-)	- (-)	- (-)	- (-)	0.19 (0.19)
51/F20	0.20	0.10	6 (6)	0.09 (0.09)	−0.09 (−0.09)	- (-)	- (-)	0.70 (0.45)
AACES-1 mean‡	0.21 (0.25)	0.08 (0.07)	6 (6)	0.04 (0.06)	0.04 (0.05)	0.89 (0.79)	0.91 (0.91)	0.02 (0.08)
254/F09	0.33	0.07	4 (7)	0.05 (0.12)	−0.03 (−0.02)	- (-)	- (-)	0.70 (0.30)
256/F07	0.36	0.10	8 (4)	0.12 (0.15)	−0.10 (−0.13)	- (-)	- (-)	0.13 (0.43)
264/F13	0.30	0.07	8 (7)	0.14 (0.17)	−0.13 (−0.14)	- (-)	- (-)	0.64 (0.86)
265/F15	0.25	0.06	2 (2)	0.26 (0.30)	0.26 (0.30)	- (-)	- (-)	- (-)
267/F09	0.21	0.07	8 (9)	0.15 (0.15)	−0.15 (−0.15)	- (-)	- (-)	0.77 (0.85)
AACES-2 mean‡	-	-	- (-)	- (-)	- (-)	- (-)	- (-)	>0.10 (>0.10)

* RMSD and bias values are computed if the number of 1 km pixels>1.

† R and slope values are reported if p-value<0.10.

‡ the mean values computed for AACES-1 and AACES-2 include only statistically significant (p-value<0.10) results and discard extensive dry days DoY 28-30.

and a first-order Taylor series expansion around the field-mean soil moisture. In this study, the disaggregation approach is applied to 40-km resolution version-4 SMOS level-2 soil moisture using 1-km resolution MODIS data. The objective is to test DisPATCh under different surface and atmospheric conditions using the very intensive ground measurements collected in southeastern Australia during the 2010 summer and winter AACES campaigns. Those measurements are aggregated at the downscaling resolution (1 km) and subsequently compared to the disaggregated SMOS soil moisture. Over the study area, climatic (evaporative demand), meteorologic (presence of clouds), and vegetation (cover and water status) conditions are strong constraints on disaggregation results. The quality of disaggregation products varies greatly according to season: while the correlation coefficient between disaggregated and *in situ* soil moisture is 0.7 during the summer AACES, it is about zero during the winter AACES, consistent with a weaker coupling between evaporation and surface moisture in temperate than in semi-arid climate. Moreover, vegetation cover prevents the soil temperature to be retrieved from thermal infrared data and the vegetation water stress may increase the remotely sensed land surface temperature independent of near-surface soil moisture. By separating the 1-km pixels where MODIS temperature is mainly controlled by soil evaporation, from those where MODIS temperature is controlled by both soil evaporation and vegetation transpiration, the correlation coefficient between disaggregated and *in situ* soil moisture is increased from 0.70 to 0.85 during the summer AACES campaign. Also, cloud cover totally obscures the surface during rain events, and on clear sky days, the water vapor in the atmosphere significantly affects the quality of land surface temperature data. It is found that the 5-km resolution atmospheric correction of the official MODIS temperature data has significant impact on DisPATCh output. An alternative atmospheric correction at 40-km resolution increases the correlation coefficient between disaggregated and *in situ* soil moisture from 0.72 to 0.82 during the summer AACES.

The above limitations must be kept in mind when using DisPATCh as a tool for validating SMOS soil moisture. Over semi-arid areas, disaggregation can solve the extent mismatch between the 40-km resolution SMOS data and localized *in situ* measurements. However, the validation of SMOS using DisPATCh requires separation of the errors associated with SMOS data and the errors associated with DisPATCh. As SMOS data are an input to DisPATCh, the errors in DisPATCh are also linked to the uncertainty in SMOS soil moisture. Nevertheless, one way to identify the error sources specifically attributed to DisPATCh is to analyze the spatial correlation between

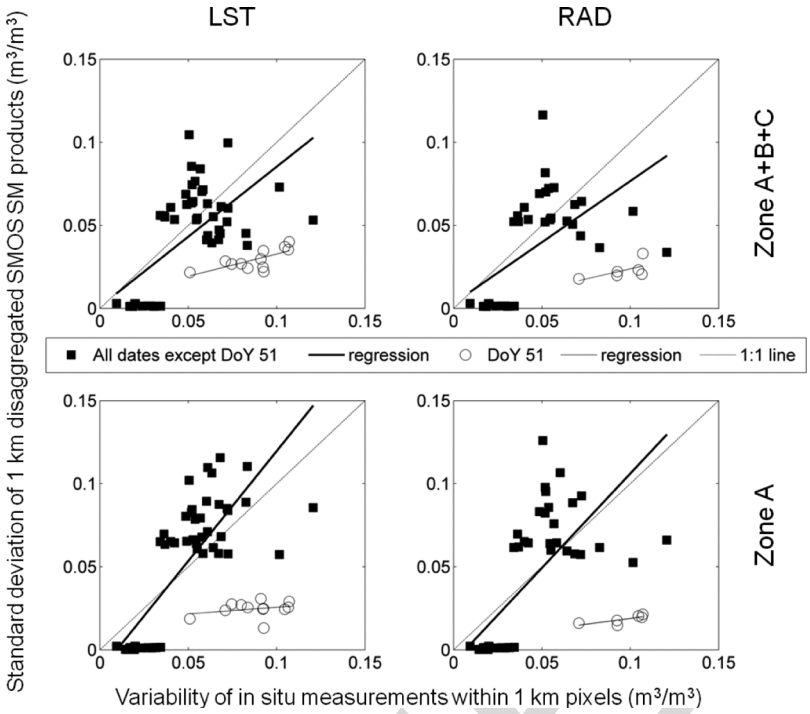

Fig. 10. Estimated uncertainty in disaggregated soil moisture ($\sigma_{\mathrm{SM}}, 1\ \mathrm{km}$) versus subpixel variability of 1 km resolution *in situ* measurements for DisPATCh run in LST or RAD mode and Zone A+B+C or Zone A only mode.

disaggregated SMOS data and the *in situ* measurements made at a distance larger than the downscaling resolution (1 km with MODIS data) and smaller than the SMOS data sampling length (15 km).

Based on the results obtained using the AACES *in situ* measurements, several improvements of DisPATCh can be suggested:

- Use of the MODIS land surface temperature quality index to select the SMOS pixels with the highest MODIS data quality.
- Correcting the MODIS land surface temperature for topography and illumination effects [45]. Within a 40-km SMOS resolution pixel, the elevation range may be very significant and thus induce a variability in land surface temperature that is not attributed to surface soil moisture.
- Use of ancillary air temperature data to constrain the estimation of end-members. The unstressed vegetation temperature $\mathbf{T_{v,min}}$ could be set to the air temperature instead of the minimum MODIS land surface temperature. This would make the estimation of $\mathbf{T_{v,min}}$ less dependent on the representativeness of the surface conditions met within the SMOS pixel [24].
- Accounting for the dependency of soil evaporative efficiency to potential evaporation, by replacing the model in [26] with the model in [38].
- Estimating an optimal downscaling resolution for each season: as the sensitivity of soil evaporative efficiency to soil moisture is lower in the winter months than in the summer months, aggregating DisPATCh output may improve the quality of disaggregation products at the expense of spatial resolution [17].

A robust disaggregation methodology of SMOS soil moisture at 1-km resolution, which would provide both disaggregated soil moisture and its uncertainty at 1-km resolution is a crucial step toward the application of SMOS data to hydrological studies.

REFERENCES

[1] E. G. Njoku and L. Li, "Retrieval of land surface parameters using passive microwave measurements at 6–18 GHz," *IEEE Trans. Geosci. Remote Sens.*, vol. 37, no. 1, pp. 79–93, Jan. 1999.

[2] C. S. Draper, J. P. Walker, P. J. Steinle, R. A. M. D. Jeu, and T. R. H. Holmes, "An evaluation of AMSR-E derived soil moisture over Australia," *Remote Sens. Environ.*, vol. 113, no. 4, pp. 703–710, Apr. 2009. doi:10.1016/j.rse.2008.11.011.

[3] C. Kummerow, W. S. Olson, and L. Giglio, "A simplified scheme for obtaining precipitation and vertical hydrometeor profiles from passive microwave sensors," *IEEE Trans. Geosci. Remote Sens.*, vol. 34, no. 5, pp. 1213–1232, Sep. 1996.

[4] M. Grecu and E. N. Anagnostou, "Overland precipitation estimation from TRMM passive microwave observations," *J. Appl. Meteor.*, vol. 40, no. 8, pp. 1367–1380, Aug. 2001.

[5] T. J. Jackson, M. H. Cosh, R. Bindlish, P. J. Starks, D. D. Bosch, M. Seyfried, D. C. Goodrich, M. S. Moran, and J. Du, "Validation of advanced microwave scanning radiometer soil moisture products," *IEEE Trans. Geosci. Remote Sens.*, vol. 48, no. 12, pp. 4256–4272, Dec. 2010. doi:10.1109/TGRS.2010.2051035.

[6] Y. H. Kerr, P. Waldteufel, J.-P. Wigneron, S. Delwart, F. Cabot, J. Boutin, M. J. Escorihuela, J. Font, N. Reul, C. Gruhier, S. E. Juglea, M. R. Drinkwater, A. Hahne, M. Martin-Neira, and S. Mecklenburg, "The SMOS mission: New tool for monitoring key elements of the global water cycle," *Proc. IEEE*, vol. 98, no. 5, pp. 666–687, May 2010. doi:10.1109/JPROC.2010.2043032.

[7] P. Matos, A. Gutiérrez, and F. Moreira, *SMOS L1 Processor Discrete Global Grids Document*, vol. SMOS-DMS-TN-5200. Lisboa, Portugal: DEIMOS Engenharia, 2004, V1.4.

[8] S. Bircher, J. E. Balling, N. Skou, and Y. Kerr, "SMOS validation by means of an airborne campaign in the Skjern river catchment, Western Denmark," *IEEE Trans. Geosci. Remote Sens.*, 2011, to be published. AQ1

[9] C. Gruhier, P. de Rosnay, S. Hasenauer, T. Holmes, R. de Jeu, Y. Kerr, E. Mougin, E. Njoku, F. Timouk, W. Wagner, and M. Zribi

(2010, Jan.). Soil moisture active and passive microwave products: Intercomparison and evaluation over a Sahelian site. *Hydrol. Earth Syst. Sci.* [Online]. *14(1)*, pp. 141–156. Available: www.hydrol-earth-syst-sci.net/14/141/2010/

[10] J.-C. Calvet, N. Fritz, F. Froissard, D. Suquia, A. Petitpa, and B. Piguet, "In situ soil moisture observations for the CAL/VAL of SMOS: The SMOSMANIA network," in *Proc. IGARSS*, Barcelona, Spain, 2007, pp. 1196–1199.

[11] S. Peischl, J. P. Walker, M. Allahmoradi, D. Barrett, R. Gurney, Y. Kerr, E. Kim, J. Le Marshall, C. Rüdiger, D. Ryu, and N. Ye, "Towards validation of SMOS using airborne and ground data over the Murrumbidgee catchment," in *Proc. MODSIM*, Cairns, Australia, 2009, pp. 3733–3739.

[12] M. H. Cosh, T. J. Jackson, S. M. Moran, and R. Bindlish, "Temporal persistence and stability of surface soil moisture in a semi-arid watershed," *Remote Sens. Environ.*, vol. 112, no. 2, pp. 304–313, Feb. 2008. doi:10.1016/j.rse.2007.07.001.

[13] P. de Rosnay, C. Gruhier, F. Timouk, F. Baup, E. Mougin, P. Hiernaux, L. Kergoat, and V. Le Dantec, "Multi-scale soil moisture measurements at the Gourma meso-scale site in Mali," *J. Hydrol.*, vol. 375, no. 1/2, pp. 241–252, Aug. 2009. doi:10.1016/j.jhydrol.2009.01.015.

[14] N. S. Chauhan, S. Miller, and P. Ardanuy, "Spaceborne soil moisture estimation at high resolution: A microwave-optical/IR synergistic approach," *Int. J. Remote Sens.*, vol. 24, no. 22, pp. 4599–4622, Nov. 2003.

[15] M. Piles, A. Camps, M. Vall-llossera, I. Corbella, R. Panciera, C. Rüdiger, Y. H. Kerr, and J. P. Walker, "Downscaling SMOS-derived soil moisture using MODIS visible/infrared data," *IEEE Trans. Geosci. Remote Sens.*, vol. 49, no. 9, pp. 3156–3166, Sep. 2011.

[16] O. Merlin, A. Al Bitar, J. P. Walker, and Y. Kerr, "An improved algorithm for disaggregating microwave-derived soil moisture based on red, near-infrared and thermal-infrared data," *Remote Sens. Environ.*, vol. 114, no. 10, pp. 2305–2316, Oct. 2010. doi:10.1016/j.rse.2010.05.007.

[17] O. Merlin, A. Al Bitar, J. P. Walker, and Y. Kerr, "A sequential model for disaggregating near-surface soil moisture observations using multi-resolution thermal sensors," *Remote Sens. Environ.*, vol. 113, no. 10, pp. 2275–2284, Oct. 2009. doi:10.1016/j.rse.2009.06.012.

[18] O. Merlin, J. Walker, R. Panciera, R. Young, J. Kalma, and E. Kim, "Soil moisture measurement in heterogeneous terrain," in *Proc. MODSIM—International Congress Modelling Simulation Modelling Simulation Society Australia New Zealand*, Dec. 2007, pp. 2604–2610.

[19] Y. H. Kerr, P. Waldteufel, P. Richaume, P. Ferrazzoli, and J.-P. Wigneron, *SMOS Level 2 Processor Soil Moisture Algorithm Theoretical Basis Document (ATBD)*, vol. SO-TN-ESL-SM-GS-0001. Toulouse, France: CESBIO, May 2011, V3.f.

[20] Y. H. Kerr, P. Waldteufel, P. Richaume, J. P. Wigneron, P. Ferrazzoli, A. Mahmoodi, A. Al Bitar, F. Cabot, C. Gruhier, D. Leroux, A. Mialon, and S. Delwart, "The SMOS soil moisture retrieval algorithm," *IEEE Trans. Geosci. Remote Sens.*, 2011.

[21] O. Merlin, C. Rüdiger, P. Richaume, A. Al Bitar, A. Mialon, J. P. Walker, and Y. Kerr, "Disaggregation as a top-down approach for evaluating 40 km resolution SMOS data using point-scale measurements: Application to AACES-1," in *Proc. SPIE, Remote Sens. Agriculture, Ecosystems, Hydrol. XII*, Toulouse, France, 2010, pp. 782 40I-1–782 40I-8.

[22] K. Nishida, R. R. Nemani, J. M. Glassy, and S. W. Running, "Development of an evapotranspiration index from Aqua/MODIS for monitoring surface moisture status," *IEEE Trans. Geosci. Remote Sens.*, vol. 41, no. 2, pp. 493–501, Feb. 2003.

[23] G. Gutman and A. Ignatov, "The derivation of the green vegetation fraction from NOAA/AVHRR data for use in numerical weather prediction models," *Int. J. Remote Sens.*, vol. 19, pp. 1533–1543, 1998.

[24] O. Merlin, B. Duchemin, O. Hagolle, F. Jacob, B. Coudert, G. Chehbouni, G. Dedieu, J. Garatuza, and Y. Kerr, "Disaggregation of MODIS surface temperature over an agricultural area using a time series of Formosat-2 images," *Remote Sens. Environ.*, vol. 114, no. 11, pp. 2500–2512, Nov. 2010. doi:10.1016/j.rse.2010.05.025.

[25] A. C. T. Pinheiro, J. Descloitres, J. L. Privette, J. Susskind, L. Iredell, and J. Schmaltz, "Near-real time retrievals of land surface temperature within the MODIS rapid response system," *Remote Sens. Environ.*, vol. 106, no. 3, pp. 326–336, Feb. 2007. doi:10.1016/j.rse.2006.09.006.

[26] J. Noilhan and S. Planton, "A simple parameterization of land surface processes for meteorological models," *Monthly Weather Rev.*, vol. 117, no. 3, pp. 536–549, 1989.

[27] O. Merlin, J. P. Walker, A. Chehbouni, and Y. Kerr, "Towards deterministic downscaling of SMOS soil moisture using MODIS derived soil evaporative efficiency," *Remote Sens. Environ.*, vol. 112, no. 10, pp. 3935–3946, Oct. 2008. doi:10.1016/j.rse.2008.06.012.

[28] M. S. Moran, T. R. Clarke, Y. Inoue, and A. Vidal, "Estimating crop water deficit using the relation between surface-air temperature and spectral vegetation index," *Remote Sens. Environ.*, vol. 49, no. 3, pp. 246–263, 1994.

[29] T. N. Carlson, R. R. Gillies, and E. M. Perry, "A method to make use of thermal infrared temperature and NDVI measurements to infer soil water content and fractional vegetation cover," *Remote Sens. Rev.*, vol. 52, pp. 45–49, 1994.

[30] O. Merlin, G. Chehbouni, J. P. Walker, R. Panciera, and Y. Kerr, "A simple method to disaggregate passive microwave based soil moisture," *IEEE Trans. Geosci. Remote Sens.—SMOS Special Issue*, vol. 46, no. 3, pp. 786–796, Mar. 2008. doi:10.1109/TGRS.2007.914807.

[31] W. P. Kustas and J. M. Norman, "Evaluation of soil and vegetation heat flux predictions using a simple two-source model with radiometric temperatures for partial canopy cover," *Agricultural Forest Meteorol.*, vol. 94, no. 1, pp. 13–29, 1999.

[32] M. C. Anderson, J. M. Norman, G. R. Diak, W. P. Kustas, and J. R. Mecikalski, "A two-source time-integrated model for estimating surface fluxes using thermal infrared remote sensing," *Remote Sens. Environ.*, vol. 60, no. 2, pp. 195–216, May 1997.

[33] O. Merlin and G. Chehbouni, "Different approaches in estimating heat flux using dual angle observations of radiative surface temperature," *Int. J. Remote Sens.*, vol. 25, no. 1, pp. 275–289, 2004.

[34] T. J. Lee and R. A. Pielke, "Estimating the soil surface specific humidity," *J. Appl. Meteorol.*, vol. 31, no. 5, pp. 480–484, 1992.

[35] T. S. Komatsu, "Towards a robust phenomenological expression of evaporation efficiency for unsaturated soil surfaces," *J. Appl. Meteorol.*, vol. 42, no. 9, pp. 1330–1334, Sep. 2003.

[36] O. Merlin, J. P. Walker, J. D. Kalma, E. J. Kim, J. Hacker, R. Panciera, R. Young, G. Summerell, J. Hornbuckle, M. Hafeez, and T. J. Jackson, "The NAFE'06 data set: Towards soil moisture retrieval at intermediate resolution," *Adv. Water Resour.*, vol. 31, pp. 1444–1455, 2008. doi:10.1016/j.advwatres.2008.01.018.

[37] Z. Wan and J. Dozier, "A generalized split-window algorithm for retrieving land-surface temperature from space," *IEEE Trans. Geosci. Remote Sens.*, vol. 34, no. 4, pp. 892–905, Jul. 1996.

[38] O. Merlin, A. Al Bitar, V. Rivalland, P. Béziat, E. Ceschia, and G. Dedieu, "An analytical model of evaporation efficiency for unsaturated soil surfaces with an arbitrary thickness," *J. Appl. Meteorol. Climatol.*, vol. 50, no. 2, pp. 457–471, Feb. 2011. doi:10.1175/2010JAMC2418.1.

[39] N. Agam, W. P. Kustas, M. C. Anderson, F. Li, and C. M. U. Neale, "A vegetation index based technique for spatial sharpening of thermal imagery," *Remote Sens. Environ.*, vol. 107, no. 4, pp. 545–558, 2007.

[40] E. E. Small and S. A. Kurc, "Tight coupling between soil moisture and the surface radiation budget in semiarid environments: Implications for land-atmosphere interactions," *Water Resour. Res.*, vol. 39, no. 10, p. 1278, Oct. 2003. doi:10.1029/2002WR001297.

[41] C. Rüdiger, J. P. Walker, and Y. H. Kerr, "On the airborne spatial coverage requirement for microwave satellite validation," *IEEE Geosci. Remote Sens. Lett.*, vol. 8, no. 4, pp. 824–828, Jul. 2011.

[42] R. Young, J. Walker, N. Yeoh, A. Smith, K. Ellett, O. Merlin, and A. Western, *Soil Moisture and Meteorological Observations from the Murrumbidgee Catchment*. Melbourne, Australia: Dept. Civil Environ. Eng., Univ. Melbourne, 2008.

[43] A. J. Teuling, R. Uijlenhoet, R. Hurkmans, O. Merlin, R. Panciera, J. Walker, and P. A. Troch, "Dry-end surface soil moisture variability during NAFE'06," *Geophys. Res. Lett.*, vol. 34, no. L17 402, Sep. 2007.

[44] W. T. Crow and E. F. Wood, "The assimilation of remotely sensed soil brightness temperature imagery into a land surface model using Ensemble Kalman filtering: A case study based on ESTAR measurements during SGP97," *Adv. Water Resour.*, vol. 26, pp. 137–149, 2003.

[45] Q. K. Hassan, C. P.-A. Bourque, F.-R. Meng, and R. M. Cox, "A wetness index using terrain-corrected surface temperature and normalized difference vegetation index derived from standard MODIS products: An evaluation of its use in a humid forest-dominated region of eastern Canada," *Sensors*, vol. 7, no. 10, pp. 2028–2048, 2007.

Olivier Merlin, photograph and biography not available at the time of publication.

Christoph Rüdiger, photograph and biography not available at the time of publication.

Ahmad Al Bitar, photograph and biography not available at the time of publication.

Philippe Richaume, photograph and biography not available at the time of publication.

Jeffrey P. Walker, photograph and biography not available at the time of publication.

Yann H. Kerr, photograph and biography not available at the time of publication.

AUTHOR QUERIES

AUTHOR PLEASE ANSWER ALL QUERIES

Please be aware that the authors are required to pay overlength page charges ($200 per page) if the paper is longer than 6 pages. If you cannot pay any or all of these charges please let us know.

AQ1 = Please provide publication update in Ref. [8].
AQ2 = Please provide volume. issue number, page range and month of publication in [20].

END OF ALL QUERIES

Disaggregation of SMOS Soil Moisture in Southeastern Australia

Olivier Merlin, Christoph Rüdiger, Ahmad Al Bitar, Philippe Richaume, Jeffrey P. Walker, and Yann H. Kerr

***Abstract*—Disaggregation based on Physical And Theoretical scale Change (DisPATCh) is an algorithm dedicated to the disaggregation of soil moisture observations using high-resolution soil temperature data. DisPATCh converts soil temperature fields into soil moisture fields given a semi-empirical soil evaporative efficiency model and a first-order Taylor series expansion around the field-mean soil moisture. In this study, the disaggregation approach is applied to soil moisture and ocean salinity (SMOS) data over the 500 km by 100 km AACES (Australian Airborne Calibration/validation Experiments for SMOS) area. The 40-km resolution SMOS surface soil moisture pixels are disaggregated at 1-km resolution using the soil skin temperature derived from moderate resolution imaging spectroradiometer (MODIS) data, and subsequently compared with the AACES intensive ground measurements aggregated at 1-km resolution. The objective is to test DisPATCh under various surface and atmospheric conditions. It is found that the accuracy of disaggregation products varies greatly according to season: while the correlation coefficient between disaggregated and *in situ* soil moisture is about 0.7 during the summer AACES, it is approximately zero during the winter AACES, consistent with a weaker coupling between evaporation and surface soil moisture in temperate than in semi-arid climate. Moreover, during the summer AACES, the correlation coefficient between disaggregated and *in situ* soil moisture is increased from 0.70 to 0.85, by separating the 1-km pixels where MODIS temperature is mainly controlled by soil evaporation, from those where MODIS temperature is controlled by both soil evaporation and vegetation transpiration. It is also found that the 5-km resolution atmospheric correction of the official MODIS temperature data has a significant impact on DisPATCh output. An alternative atmospheric correction at 40-km resolution increases the correlation coefficient between disaggregated and *in situ* soil moisture from 0.72 to 0.82 during the summer AACES. Results indicate that DisPATCh has a strong potential in low-vegetated semi-arid areas where it can be used as a tool to evaluate SMOS data (by reducing the mismatch in spatial extent between SMOS observations and localized *in situ* measurements), and as a further step, to derive a 1-km resolution soil moisture product adapted for large-scale hydrological studies.**

***Index Terms*—AACES, calibration/validation, disaggregation, Disaggregation based on Physical And Theoretical scale Change (DisPATCh), field campaign, moderate resolution imaging spectroradiometer (MODIS), soil moisture and ocean salinity (SMOS).**

I. Introduction

PASSIVE MICROWAVE remote sensing has the capability to provide key elements of the terrestrial hydrological cycle such as surface soil moisture [1], [2] and overland precipitation [3], [4]. Nevertheless, due to the large discrepancy between the observation scale (several tens of km) and the scale of physical interactions with the land surface (one wavelength or several cm), the radiative transfer models applied to passive microwave remote sensing data are only semiphysically based. Consequently, the retrieval process of land surface parameters from microwave brightness temperatures requires ancillary data for calibration and validation purposes [5]. It also requires a strategy to use such ancillary data since ground-based sampling is often made over a small area/point, which constrasts with the large integrated extent of spaceborne passive microwave observations.

The soil moisture and ocean salinity (SMOS), [6]) satellite was launched on November 2, 2009. Over land, the SMOS mission aims at providing $\sim$5 cm surface soil moisture data at a spatial resolution better than 50 km and a repeat cycle of less than 3 days. The payload is a 2-D interferometer equipped with 69 individual L-band antennas regularly spaced along Y-shaped arms. This new concept allows observing all pixels in the 1000 km wide field of view at a range of incidence angles. It also allows reconstructing brightness temperatures on a fixed sampling grid [7].

Since the SMOS launch, various field experiments (the HOBE site in Denmark [8], the Mali site in Western Africa [9], the SMOSMANIA site in Southwestern France [10] just to name a few) have been undertaken to validate SMOS reconstructed brightness temperatures and soil moisture retrievals. The AACES (Australian Airborne Calibration/validation Experiment for SMOS, [11]) is one of the most comprehensive campaigns worldwide dedicated to SMOS calibration/validation. A series of two experiments were undertaken in 2010, AACES-1 in January-February (Austral summer) and

Manuscript received March 31, 2011; revised September 1, 2011; accepted October 30, 2011. The AACES participants are gratefully acknowledged for their participation in collecting this extensive data set. The Australian Airborne Calibration/validation Experiments for SMOS have been made possible through infrastructure (LE0453434) and research (DP0879212) funding from the Australian Research Council, and the collaboration of a large number of scientists from throughout Australia, United States and Europe. Initial setup and maintenance of the study catchments was funded by two research Grants (DP0343778, DP0557543) from the Australian Research Council and by the CRC for Catchment Hydrology. This work was funded by the CNES TOSCA (Terre solide, Océan, Surfaces Continentales et Atmosphère) program and the Centre National de la Recherche Scientifique.

O. Merlin is with the Centre d'Etudes Spatiales de la Biosphère (CESBIO), 31401 Toulouse, France (e-mail: olivier.merlin@cesbio.cnes.fr).

C. Rüdiger (e-mail: chris.rudiger@monash.edu).

A. Al Bitar (e-mail: ahmad.albitar@cesbio.cnes.fr).

P. Richaume (e-mail: philippe.richaume@cesbio.cnes.fr).

J. P. Walker (e-mail: jeff.walker@monash.edu).

Y. H. Kerr (e-mail: yann.kerr@cesbio.cnes.fr).

Color versions of one or more of the figures in this paper are available online at http://ieeexplore.ieee.org.

Digital Object Identifier 10.1109/TGRS.2011.2175000

AACES-2 in September (Austral winter). The data collected in AACES include 1-km resolution airborne L-band brightness temperature mapped over a 500 km by 100 km area, 20 days of very intensive ground measurements and 20 5 km by 2 km ground sampling areas.

Even though the AACES ground measurements are very extensive, it is not feasible to cover the whole extent of a SMOS pixel by ground sampling alone. This is the reason why most validation strategies of spaceborne passive microwave data using *in situ* measurements have been based on the assumption that local observations are representative of a much larger spatial extent (i.e., the size of a microwave pixel). In the heterogeneous case where this assumption does not hold, upscaling approaches [12], [13] have been developed to relate the available ground observations to satellite scale soil moisture. Such approaches are very useful over sites which have been monitored for a long time and where extensive measurements have been made over a range of spatial scales. However, aggregation rules are difficult to build over sites which have been set up recently, or where no extensive field campaigns have been undertaken.

This study develops a methodology to facilitate the calibration and validation of SMOS data using localized ground measurements, such as those collected during AACES. The methodology combines upscaling (aggregation) and downscaling (disaggregation) approaches to make remote sensing and *in situ* observations match at an intermediate spatial resolution of 1 km. The key step in the procedure is a disaggregation algorithm of passive microwave soil moisture using kilometric optical data [14]–[16]. Disaggregating SMOS soil moisture can solve the disparity of spatial scales between satellite and *in situ* observations. However, the validation of spaceborne data by means of a disaggregation approach requires the uncertainties and potential error sources in downscaled data to be assessed. Generally speaking, disaggregation is a compromise between downscaling resolution and accuracy. The higher downscaling resolution, the more disaggregated values are spatially representative of ground observations, but typically have a lower accuracy and vice versa [17]. In this context, a disaggregation algorithm named Disaggregation based on Physical And Theoretical scale Change (DisPATCh) is applied to 40-km resolution SMOS soil moisture over the AACES area using 1-km resolution Moderate resolution Imaging Spectroradiometer (MODIS) data. The objective is to test DisPATCh under various surface and atmospheric conditions. Specifically, the impact of climatic (evaporative demand), meteorologic (presence of clouds), and vegetation (cover and water status) conditions on 1-km resolution disaggregated soil moisture is evaluated both qualitatively by visual assessment of disaggregation images and quantitatively by comparing DisPATCh output with AACES intensive ground measurements.

The AACES, SMOS, and MODIS data used in this study are first described. Next, the disaggregation methodology is presented followed by a step-by-step description of the DisPATCh algorithm. Results of the comparison between disaggregated SMOS soil moisture and *in situ* measurements are then reported. To test DisPATCh under various surface and atmospheric conditions, the algorithm is run during AACES-1 and AACES-2 in different modes, by including (or not) a correction for vegetation and atmospheric effects. Finally, some perspectives in the use of DisPATCh for validating SMOS data using ground-based sampling are given.

II. Data Collection and Preprocessing

The AACES experiments were planned to provide ground and airborne soil moisture data over an area of approximately 500 km by 100 km during the two main seasons in the Murrumbidgee river catchment, in southeastern Australia. The first AACES campaign (AACES-1) was undertaken in summer 2010 from January 18 to February 21, and the second campaign (AACES-2) was undertaken in the following Austral winter from September 11 to September 24 [11]. Fig. 1 presents the study area including the 20 5 km by 2 km ground sampling focus areas. The background image is the MODIS 250-m resolution 16-day normalized difference vegetation index (NDVI) product of February 2, 2010. The climate of the Murrumbidgee catchment area ranges from semi-arid in the west to alpine in the east, with a strong rainfall and potential evapotranspiration gradient in the west-east direction. Land use is extensive grazing in the west, cropping in the center, and mostly grazing/forest in the east (refer to [11] for a detailed account of AACES).

A. HDAS

During both AACES-1 and AACES-2, a spatially enabled platform (Hydraprobe Data Acquisition System, HDAS) was used to collect extensive measurements of near-surface soil moisture. HDAS is a handheld system combining a soil dielectric sensor (Hydraprobe) and a pocket PC with GPS receiver, allowing for direct storage of location and measurement within the GIS software. HDAS measurements were calibrated using the approach presented in [18] with a root mean square error of point estimate of about 0.03 m^3/m^3. The sampling coverage was two 5 km by 2 km farms per day during AACES-1 and one 5 km by 2 km farm per day during AACES-2. Within each farm, a total of six adjacent 5 km long transects separated by 330 m were walked to cover each area of 10 km^2, and three separate HDAS measurements were made along transects every 50 m.

In this study, HDAS soil moisture data are aggregated at 1-km resolution by averaging all measurements made within each pixel of the MODIS resolution grid. Out of concern for spatial representativeness of *in situ* observations, only the 1-km pixels whose ground sampling covers more than two third of its surface area are kept for comparison with disaggregation results. The 1-km average of HDAS measurements is denoted $\langle \mathrm{SM}_{\mathrm{HDAS}} \rangle$ and the standard deviation of *in situ* measurements (denoted σ_{HDAS}) computed to estimate the subpixel variability at 1-km resolution.

B. SMOS

The version-4 SMOS level-2 soil moisture product is used. This product (released on March 24, 2011) was produced from the reprocessed level 1C data, and the version-4 level-2 soil moisture algorithm. SMOS has a 6 am (ascending) and 6 pm

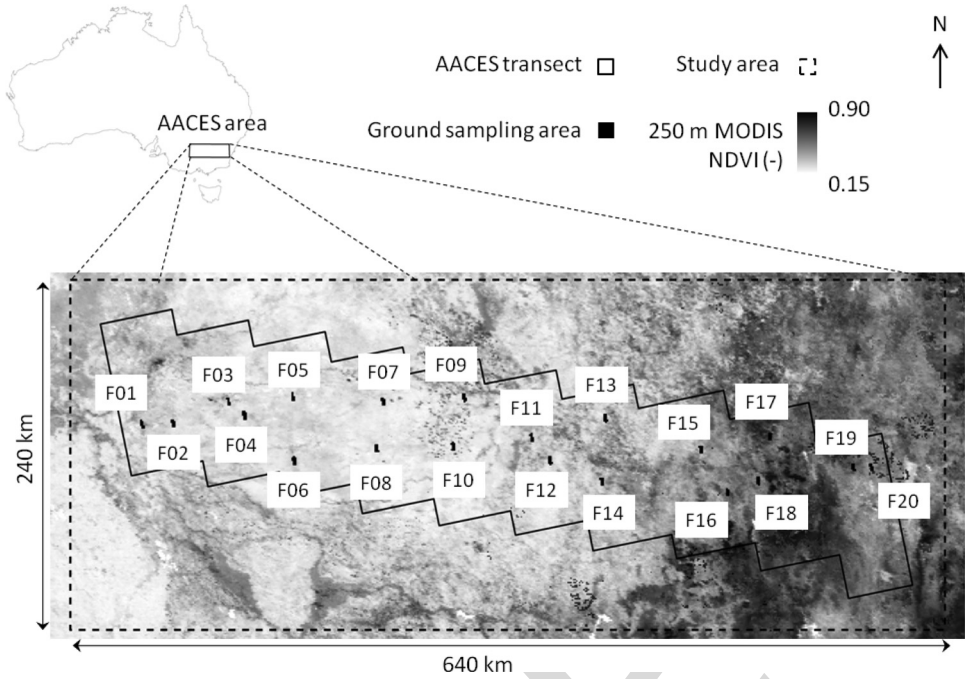

Fig. 1. Overview of the study area. During AACES, ten 100 km by 50 km patches were overflown by an airborne L-band radiometer. Within each patch, two 5 km by 2 km subareas were sampled to collect spatial soil moisture measurements. In this study, DisPATCh is run over a 640 by 240 km area including the whole AACES area, and disaggregation results are evaluated over the ground sampling areas.

(descending) equator crossing time. The sampling grid of the SMOS level-2 soil moisture product is called DGG or discrete global grid [19], [20] and has a node separation of about 15 km. The DGG provides a discretization that is higher than the SMOS natural pixel size, which is 40 km on average, ranging from 30 km at boresight to 90 km at high incidence angles. In this study, the disaggregation procedure takes advantage of the oversampling of SMOS data to potentially reduce (and provide an estimate of) random errors in disaggregated SMOS data. Instead of using a single snapshot SMOS image, DisPATCh uses four (overlapping) independent snapshots, which are generated by: 1) sliding a 40-km resolution grid; and 2) extracting the DGG nodes approximately centered on each 40 km pixel. The extraction of SMOS DGG nodes is presented in [21]. The DGG node(s) that fall(s) near the center of the 40-km resolution pixels with a $+/-10$-km tolerance are selected. If more than one DGG is selected, the associated soil moisture values are averaged to produce a single value for each 40-km resolution pixel. The 40-km resolution grid that fits the study area corresponds to what is termed here Resampling 1. Similarly, Resampling 2, 3, and 4 are performed by sliding the 40-km resolution grid to coordinates $(+20$ km, 0), $(0, -20$ km), and $(+20$ km, -20 km), respectively. The four 40-km resolution SMOS data sets are then used independently as input to DisPATCh.

C. MODIS

The MODIS data used in this paper are composed of:

- Version-5 MODIS/Terra land surface temperature and emissivity daily level-3 global 1-km grid product (MOD11A1) and version-5 MODIS/Aqua land surface temperature and emissivity daily level-3 global 1-km grid product (MYD11A1). The land surface temperature data set is the main component of DisPATCh. It is used to estimate 1-km resolution soil evaporative efficiency at 10 am (Terra data) and 1 pm (Aqua data) [22].
- Version-5 MODIS/Terra vegetation indices 16-day level-3 global 1-km grid product (MOD13A2). The NDVI data set is used in DisPATCh to estimate the fractional vegetation cover at 1-km resolution [23].
- Version-5 MODIS/Terra+Aqua albedo 16-day level-3 global 1-km grid product (MCD43B3). The surface albedo data set is used in DisPATCh to estimate the vegetation temperature at maximum water stress from the space land surface temperature albedo [24]. The MCD43B3 product provides 1-km data describing both directional hemispherical reflectance (black-sky albedo) at local solar noon and bihemispherical reflectance (white-sky albedo). In this study, surface albedo refers to the MODIS shortwave white sky albedo.
- MODIS/Terra level-1B calibrated radiances swath 1-km grid product (MOD021KM) and MODIS/Aqua level-1B calibrated radiances swath 1-km grid product (MYD021KM). The radiance data set is used to derive a land surface temperature data set that differs from the official MOD11A1 and MYD11A1 products with respect to atmospheric correction.

Products MOD11A1, MYD11A1, MOD13A2, and MCD43B3 were downloaded through the NASA Warehouse Inventory Search Tool (WIST http://wist.echo.nasa.gov/) and products MOD021KM and MYD021KM were downloaded through the NASA Level 1 and Atmosphere Archive and Distribution System (LAADS http://ladsweb.nascom.nasa.gov).

TABLE I
SCALE AND OFFSET VALUES USED TO CONVERT TERRA (AND AQUA) MODIS RADIANCE DATA TO PHYSICAL RADIANCE VALUES OVER THE AACES AREA

Thermal band	Scale (W m^{-2} sr^{-1})	Offset (-)
31	$8.4002{\cdot}10^{-4}$ ($6.5081{\cdot}10^{-4}$)	1577 (2036)
32	$7.2970{\cdot}10^{-4}$ ($5.7100{\cdot}10^{-4}$)	1658 (2119)

All products were projected in UTM 55 South with a sampling interval of 1000 m using the MODIS reprojection tool.

The level-1B calibrated radiance data (R_{31} and R_{32} for bands 31 and 32, respectively) were converted from digital number (DN) to radiance in W m^{-2} sr^{-1} using the radiance scales and offsets provided with each MODIS granule as listed in Table I

$$R_\lambda = \text{Scale}_\lambda \times (\text{DN}_\lambda - \text{Offset}_\lambda) \quad (1)$$

The radiance values were then converted to brightness temperature in K using the inverse of the Planck function [25]

$$Tb_\lambda = \frac{c_2}{\lambda \ln\left(1 + \frac{c_1}{R_\lambda \lambda^5}\right)} \quad (2)$$

with $c_1 = 1.19107 \times 10^8$ μm^5 W m^{-2} sr^{-1} and $c_2 = 1.43883 \times 10^4$ μm K, for center wavelength of the given band (11.0186 μm and 12.0325 μm for 31 and 32 band, respectively).

D. Overlapping HDAS, SMOS, and MODIS Data and Generating an Input Data Set

As indicated in Table II, HDAS soil moisture, SMOS soil moisture, and cloud-free MODIS land surface temperature data have overlapped on five days during AACES-1 (on January 28 and 30 and February 15, 18, and 20) and on five days during AACES-2 (on September 11, 13, 21, 22, and 24). On each sampling day, two farms were sampled during AACES-1 (except on February 18 when three farms were sampled), and one farm was sampled during AACES-2, so that disaggregation results can be evaluated for ten date-farm units during AACES-1 and five date-farm units during AACES-2.

DisPATCh is applied to an input ensemble composed of the different combinations of available SMOS (ascending orbit at 6 am and/or descending orbit at 6 pm) and MODIS (onboard Terra platform at 10 am and/or Aqua platform at 1 pm) data. To increase the quantity of input data sets, the MODIS data collected on the day before and the day after the SMOS overpass date are also included. For SMOS data on day of year (DoY) 51, the clear sky MODIS data collected on DoY 54 are used. Note that one implicitly assumes that no rainfall occurs between MODIS and SMOS overpasses, and that the spatial variability captured by MODIS is relatively similar to the actual variability of surface soil moisture at the time of SMOS overpass. Moreover, the SMOS data oversampling is used to generate four (overlapping) 40-km resolution SMOS grids on which DisPATCh is run independently, thus increasing the number of downscaled data that could be used in the validation. It is reminded that the spacing (about 15 km) between neighboring SMOS DGG nodes is smaller than the SMOS resolution (about 40 km). By combining the four SMOS grids, the two potential SMOS data sets (two orbits in one day) and the six potential MODIS data sets (three days including two overpasses each), the maximum number of input data sets is 48. The generation of input data sets is shown in Fig. 2 and the number of daily input data sets is indicated for each date-farm unit in Table II.

III. DISAGGGREGATION ALGORITHM

DisPATCh converts 1-km resolution MODIS-derived soil temperature fields into 1-km resolution surface soil moisture fields given a semi-empirical soil evaporative efficiency model [26] and a first-order Taylor series expansion around the 40-km resolution SMOS observation. DisPATCh is an improved version of the algorithms in [16] and [27], and mainly differs with regard to the representation of the vegetation water status. In previous versions [16], [27], the soil temperature was derived from MODIS land surface temperature by assuming that vegetation was unstressed so that vegetation temperature was uniformly set to the minimum surface temperature observed within the SMOS pixel. In this study, the approach in [28] is implemented to take into account vegetation water status in the estimation of soil temperature.

A. Disaggregation Methodology

The disaggregation procedure decouples the soil evaporation from the 0–5 cm soil layer and the vegetation transpiration from the root-zone soil layer by separating MODIS surface temperature into its soil and vegetation components as in the triangle or trapezoidal method [28], [29]. MODIS-derived soil temperature is then used to estimate soil evaporative efficiency, which is known to be relatively constant during the day on clear sky conditions. MODIS-derived soil evaporative efficiency is finally used as a proxy for surface (0–5 cm) soil moisture variability within the SMOS pixel. The link between surface soil moisture and soil evaporative efficiency at different scales is ensured by a downscaling relationship and a soil evaporative efficiency model, as described below in more detail. The originality of DisPATCh relies on a dynamical land cover classification (based on the hourglass approach in [28]) that takes into account the subpixel variability of the sensitivity of soil evaporative efficiency to surface soil moisture.

1) Downscaling Relationship: The downscaling relationship can be written as

$$\text{SM}_{1\text{ km}} = \mathbf{SM_{SMOS}} + \frac{\partial \mathbf{SM_{mod}}}{\partial \mathbf{SEE}} \times (\text{SEE}_{\text{MODIS,1 km}} - \langle \text{SEE}_{\text{MODIS,1 km}} \rangle_{\mathbf{40\ km}}) \quad (3)$$

with $\mathbf{SM_{SMOS}}$ being the SMOS soil moisture (for clarity, the variables defined at SMOS scale are written in bold), $\text{SEE}_{\text{MODIS}}$ the MODIS-derived soil evaporative efficiency (ratio of actual to potential evaporation), $\langle \text{SEE}_{\text{MODIS}} \rangle_{\mathbf{40\ km}}$ its average within a SMOS pixel and $\partial \mathbf{SM_{mod}}/\partial \mathbf{SEE}$ the partial derivative evaluated at SMOS scale of soil moisture with respect to soil evaporative efficiency. Note that the linearity of (3) implies that a possible bias in SMOS data would produce the

TABLE II
LIST OF OVERLAPPING HDAS, SMOS, AND MODIS (MOD11A1 AND MYD11A1) DATA DURING AACES-1 AND AACES-2. ONLY THE SMOS DATA COLLECTED ON THE SAME DAY AS GROUND SAMPLING HAVE BEEN CONSIDERED. THE MODIS DATA CONSIDERED AS INPUT TO DISPATCH HAVE BEEN COLLECTED WITHIN PLUS OR MINUS ONE DAY EITHER SIDE THE GROUND SAMPLING (AND SMOS OVERPASS) DATE. ON EACH SAMPLING DATE, THE RESULTANT NUMBER OF INPUT DATA SETS TO DISPATCH IS ALSO INDICATED

Experiment	Sampling date	DoY	Farm	SMOS overpass time	Cloud free MODIS data (DoY)	Number of input data sets to DisPATCh
AACES-1	28 January	28	F05	6 am	Terra (27,29) & Aqua (29)	3
	30 January	30	F07	6 am	Terra (29,30) & Aqua (29)	12
	’	’	F08	6 am	Terra (29,30) & Aqua (29)	9-12
	15 February	46	F15	6 am & 6 pm	Terra (46) & Aqua (47)	8-14
	’	’	F16	6 am & 6 pm	Terra (46) & Aqua (47)	8-10
	18 February	49	F17	6 am & 6 pm	Terra (48,50) & Aqua (48,49,50)	30-38
	’	’	F18	6 am & 6 pm	Terra (48,50) & Aqua (48,49,50)	24-30
	’	’	F20	6 am & 6 pm	Terra (48,50) & Aqua (48,49,50)	34-40
	20 February	51	F19	6 am & 6 pm	Terra (54) & Aqua (54)	6-8
	’	’	F20	6 am & 6 pm	Terra (54) & Aqua (54)	16
AACES-2	11 September	254	F09	6 am & 6 pm	Terra (253,254) & Aqua (254)	6-14
	13 September	256	F07	6 am & 6 pm	Terra (256)	8
	21 September	264	F13	6 am & 6 pm	Terra (263) & Aqua (264)	16
	22 September	265	F15	6 am & 6 pm	Terra (265) & Aqua (264,266)	16
	24 September	267	F09	6 am & 6 pm	Terra (267) & Aqua (266,267,268)	24-32

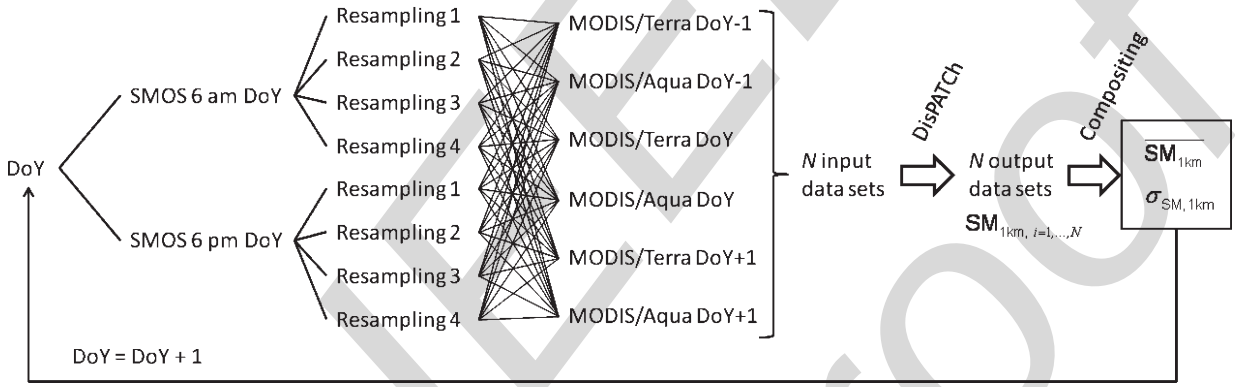

Fig. 2. Schematic diagram presenting the combination of SMOS and MODIS to generate an ensemble of input data to DisPATCh. The output data are composited at 1-km resolution by computing the average ($\overline{\mathrm{SM}_{1\ \mathrm{km}}}$) and standard deviation ($\sigma_{\mathrm{SM},1\ \mathrm{km}}$) of disaggregated SMOS soil moisture.

same bias in disaggregated data [30]. Consequently, although the possible presence of a bias in SMOS data limits the accuracy in the disaggregated soil moisture, it is not a limiting factor to the applicability of DisPATCh. MODIS derived soil evaporative efficiency is expressed as a linear function of soil temperature

$$\mathrm{SEE}_{\mathrm{MODIS},1\ \mathrm{km}} = \frac{\mathbf{T_{s,max}} - T_{\mathrm{s},1\ \mathrm{km}}}{\mathbf{T_{s,max}} - \mathbf{T_{s,min}}} \tag{4}$$

with T_{s} being the MODIS-derived soil skin temperature, $\mathbf{T_{s,max}}$ the soil skin temperature at $\mathrm{SEE} = 0$ and $\mathbf{T_{s,min}}$ the soil skin temperature at $\mathrm{SEE} = 1$. The linearity of the relationship between soil evaporative efficiency and surface soil temperature was verified using the physically based dual source energy budget model in [31] using a synthetic data set composed of a range of surface soil moisture values and different atmospheric conditions (results not shown). End-members $\mathbf{T_{s,min}}$ and $\mathbf{T_{s,max}}$ are estimated from the polygons obtained by plotting MODIS surface temperature against MODIS NDVI and MODIS albedo as in [24]. Derivation of soil temperature is based on a linear decomposition of the surface temperature into its soil and vegetation components as a good approximation of the relationship with fourth power for temperatures [32], [33] and consistent with the triangle method. MODIS-derived soil skin temperature is expressed as

$$T_{\mathrm{s},1\ \mathrm{km}} = \frac{T_{\mathrm{MODIS}} - f_{\mathrm{v},1\ \mathrm{km}} T_{\mathrm{v},1\ \mathrm{km}}}{1 - f_{\mathrm{v},1\ \mathrm{km}}} \tag{5}$$

with T_{MODIS} being the 1-km resolution MODIS land surface temperature, f_{v} the MODIS-derived fractional vegetation cover, and T_{v} the vegetation temperature. In this study, vegetation temperature is estimated using the approach proposed by [28]. In (5), fractional vegetation cover is written as

$$f_{\mathrm{v},1\ \mathrm{km}} = \frac{\mathrm{NDVI}_{\mathrm{MODIS}} - \mathbf{NDVI_s}}{\mathbf{NDVI_v} - \mathbf{NDVI_s}} \tag{6}$$

with $\mathrm{NDVI_{MODIS}}$ being the 1-km resolution MODIS NDVI, $\mathbf{NDVI_s}$ the NDVI corresponding to bare soil, and $\mathbf{NDVI_v}$ the NDVI corresponding to full-cover vegetation. Minimum and maximum NDVI values are set to 0.15 and 0.90, respectively.

In [16], the accuracy and robustness of the disaggregation methodology were tested using three different formulations of soil evaporative efficiency [26], [34], [35]. Results based on the NAFE'06 data set [36], which was collected over a 60 km by 40 km area in the AACES area, indicated that the model in [26] was better adapted for conditions where soil properties are unknown at high resolution. Consequently, the partial derivative in (3) is computed using the soil evaporative efficiency model in [26]

$$\mathrm{SEE_{mod}} = \frac{1}{2} - \frac{1}{2}\cos(\pi \cdot \mathrm{SM}/\mathbf{SM_p}) \tag{7}$$

with $\mathbf{SM_p}$ being a soil parameter (in soil moisture unit). In [26], $\mathbf{SM_p}$ was set to the soil moisture at field capacity. In DisPATCh, $\mathbf{SM_p}$ is retrieved at 40-km resolution from SMOS and aggregated MODIS data [16]. By inverting (7), one obtains

$$\mathrm{SM_{mod}} = \frac{\mathbf{SM_p}}{\pi}\cos^{-1}(1 - 2\,\mathrm{SEE}) \tag{8}$$

2) Vegetation Temperature: Vegetation temperature in (5) is estimated at 1-km resolution with the "hourglass" approach in [28]. By plotting the diagonals in the quadrilateral in Fig. 3, four areas are distinguished in the space defined by surface temperature and fractional vegetation cover. In zone A, land surface temperature is mainly controlled by soil evaporation leading to optimal sensitivity to surface soil moisture. In zone D, land surface temperature is mainly controlled by vegetation transpiration with no sensitivity to surface soil moisture. In zones B and C, land surface temperature is controlled by both soil evaporation and vegetation transpiration with intermediate (average) sensitivity to surface soil moisture. Based on this understanding, vegetation temperature is estimated in a different manner in each zone.

For a given data point located in Zone A, vegetation temperature is

$$T_{\mathrm{v,1\ km}} = (\mathbf{T_{v,min}} + \mathbf{T_{v,max}})/2 \tag{9}$$

with $\mathbf{T_{v,min}}$ and $\mathbf{T_{v,max}}$ being the vegetation temperature at minimum and maximum water stress, respectively. End-members $\mathbf{T_{v,min}}$ and $\mathbf{T_{v,max}}$ are estimated from the polygons obtained by plotting MODIS surface temperature against MODIS NDVI and MODIS albedo as in [24].

For a given data point located in Zone B, vegetation temperature is

$$T_{\mathrm{v,1\ km}} = (T_{\mathrm{v,min,1\ km}} + \mathbf{T_{v,max}})/2 \tag{10}$$

with $T_{\mathrm{v,min,1\ km}}$ being the vegetation temperature associated with $\mathrm{SEE} = 0$ ($T_{\mathrm{s}} = \mathbf{T_{s,max}}$).

For a given data point located in Zone C, vegetation temperature is

$$T_{\mathrm{v,1\ km}} = (\mathbf{T_{v,min}} + T_{\mathrm{v,max,1\ km}})/2 \tag{11}$$

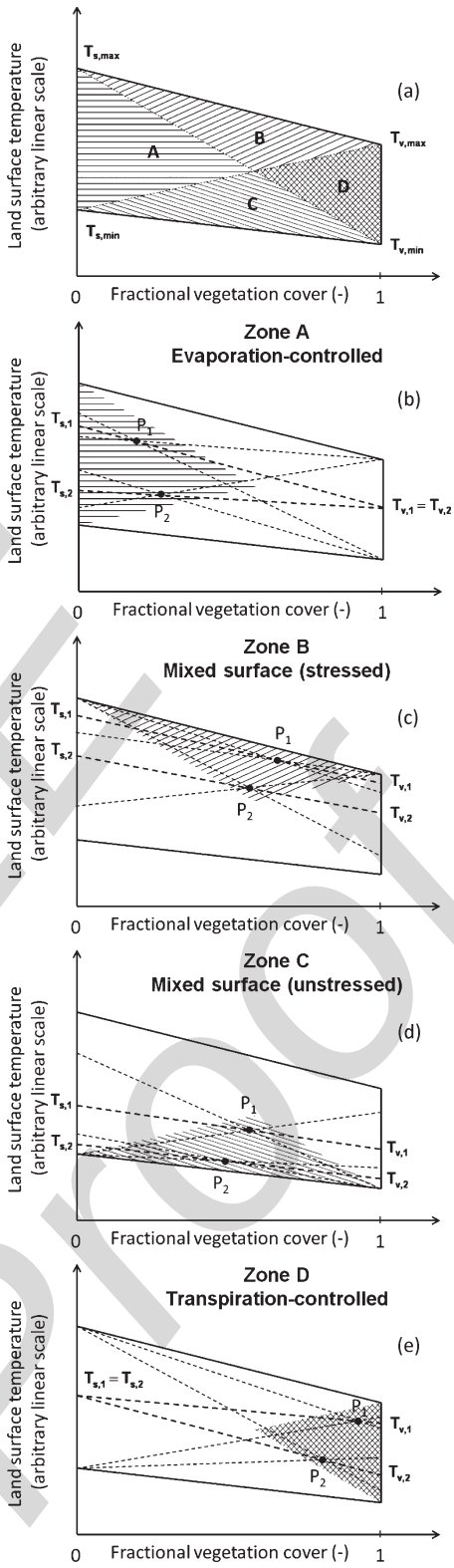

Fig. 3. Polygon defined in the land surface temperature-fractional vegetation cover space contains four distinct zones A, B, C, and D. In Zone A (soil-dominated area), the estimated vegetation temperature is constant leading to optimal sensitivity of estimated soil temperature to surface soil moisture. In Zone D, the estimated soil temperature is constant with no sensitivity to surface soil moisture. In Zone B and C (mixed surface), surface temperature is both controlled by soil evaporation and vegetation transpiration with intermediate (average) sensitivity of estimated soil temperature to surface soil moisture. DisPATCh can be run in the Zone A+B+C mode or in the Zone A only mode.

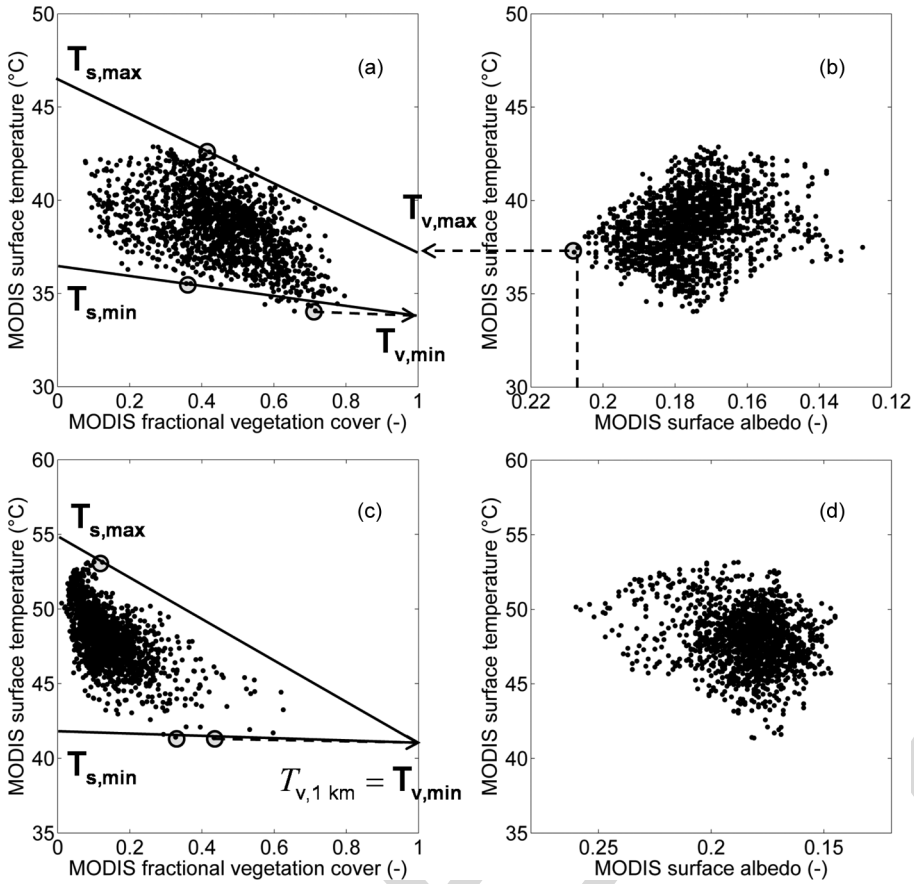

Fig. 4. Temperature end-members $\mathbf{T_{s,min}}$, $\mathbf{T_{s,max}}$, $\mathbf{T_{v,min}}$, and $\mathbf{T_{v,max}}$ are estimated from the surface temperature-fractional vegetation cover space and the surface temperature-surface albedo space within two given SMOS pixels. In (b), the pixel corresponding to the largest MODIS albedo has a fractional vegetation cover larger than 0.5, so that $\mathbf{T_{v,max}}$ is set to its surface temperature. In (d), the pixel corresponding to the largest MODIS albedo has a fractional vegetation cover lower than 0.5, so that $\mathbf{T_{v,max}}$ is set to $\mathbf{T_{v,min}}$.

with $T_{\mathrm{v,max,1\ km}}$ being the vegetation temperature associated with SEE $= 1$ ($T_{\mathrm{s}} = \mathbf{T_{s,min}}$).

For a given data point located in Zone D, vegetation temperature is

$$T_{\mathrm{v,1\ km}} = (T_{\mathrm{v,min,1\ km}} + T_{\mathrm{s,max,1\ km}})/2 \qquad (12)$$

3) End-Members: End-members $\mathbf{T_{s,min}}$, $\mathbf{T_{s,max}}$, $\mathbf{T_{v,min}}$ and $\mathbf{T_{v,max}}$ are estimated by combining the spatial information provided by the surface temperature-fractional vegetation cover space and the surface temperature-albedo space plotted using MODIS data collected in a 40-km resolution SMOS pixel. An illustration is provided in Fig. 4 for two given SMOS pixels.

- $\mathbf{T_{v,min}}$: the vegetation temperature at minimum vegetation water stress is set to the minimum MODIS surface temperature in the SMOS pixel [see Fig. 4(a) and (c)].
- $\mathbf{T_{v,max}}$: the vegetation temperature at maximum vegetation water stress is set to the MODIS surface temperature of the pixel with the maximum value of MODIS albedo in the SMOS pixel [see Fig. 4(b)]. If the fractional vegetation cover of that pixel is lower than 0.5 [see Fig. 4(d)], the vegetation temperature at maximum vegetation water stress is alternatively set to $\mathbf{T_{v,min}}$, meaning that vegetation is unstressed within the SMOS pixel. The condition based on fractional vegetation cover is lower than 0.5 aims to increase the robustness of the determination approach of $\mathbf{T_{v,max}}$, particularly in the SMOS pixels where all surface conditions are not met.
- $\mathbf{T_{s,min}}$: the soil temperature at SEE $= 1$ is extrapolated along the wet soil edge at $f_{\mathrm{v}} = 0$. The wet soil edge is defined as the line passing through $(1, \mathbf{T_{v,min}})$ and through the data point such that all the data points with $f_{\mathrm{v}} < 0.5$ are located above the wet soil edge [see Fig. 4(a) and (c)].
- $\mathbf{T_{s,max}}$: the soil temperature at SEE $= 0$ is extrapolated along the dry soil edge at $f_{\mathrm{v}} = 0$. The dry soil edge is defined as the line passing through $(1, \mathbf{T_{v,max}})$ and through the data point such that all the data points with $f_{\mathrm{v}} < 0.5$ are located below the dry soil edge [see Fig. 4(a) and (c)].

B. Atmospheric Correction

In MOD11A1 and MYD11A1 products, the land surface temperature is derived from MODIS thermal radiances using the split window algorithm [37]

$$T_{\mathrm{MODIS}} = C + \left(A_1 + A_2\frac{1-\epsilon}{\epsilon} + A_3\frac{\Delta\epsilon}{\epsilon^2}\right)\frac{Tb_{31}+Tb_{32}}{2} + \left(B_1 + B_2\frac{1-\epsilon}{\epsilon} + B_3\frac{\Delta\epsilon}{\epsilon^2}\right)\frac{Tb_{31}-Tb_{32}}{2} \qquad (13)$$

with Tb_{31} and Tb_{32} being the brightness temperatures measured in the MODIS bands 31 and 32, respectively, ϵ_{31} and ϵ_{32} the surface emissivities estimated in the respective bands, and A_1, A_2, A_3, B_1, B_2, B_3, and C regression coefficients. These coefficients are available during algorithm execution via a look up table stratified by subranges of near surface air temperature and total column water vapor. These input field are obtained at a 5-km resolution from the MODIS07_L2 product.

Given that regression coefficients in (13) are provided at 5-km resolution, the atmospheric corrections on the MODIS land surface temperature product are actually made at 5-km resolution. To test whether atmospheric corrections on MODIS temperature have an impact on disaggregation results, a different procedure is proposed to obtain another temperature data set whose atmospheric corrections are operated at the scale of a SMOS pixel, i.e., at 40-km resolution (instead of 5-km resolution for the official MODIS temperature product). The approach is to normalize the mean MODIS radiance-derived brightness temperature at the SMOS resolution. Normalization is done by adjusting the minimum and maximum mean MODIS brightness temperature to the minimum and maximum value of the official MODIS land surface temperature product within the SMOS pixel, respectively. The new temperature noted $T_{\mathrm{MODIS}}^{\mathrm{unif.\ corr.}}$ (uniform atmospheric corrections) is written

$$T_{\mathrm{MODIS}}^{\mathrm{unif.\ corr.}} = T_{\mathbf{MODIS,min}} + (T_{\mathbf{MODIS,max}} - T_{\mathbf{MODIS,min}}) \times \frac{Tb_{31} + Tb_{32} - \mathbf{Min}(Tb_{31} + Tb_{32})}{\mathbf{Max}(Tb_{31} + Tb_{32}) - \mathbf{Min}(Tb_{31} + Tb_{32})} \quad (14)$$

with $T_{\mathbf{MODIS,min}}$ and $T_{\mathbf{MODIS,max}}$ being the minimum and maximum MODIS land surface temperature within the SMOS pixel, and $\mathbf{Min}()$ and $\mathbf{Max}()$ the function that returns the minimum and maximum value within the SMOS pixel, respectively. Note that the underlying assumptions of (14) are:

- near surface air temperature and column water vapor vary at scales larger than 40 km (size of a SMOS pixel).
- surface emissivity is close to 1.

C. Algorithm

The steps used in applying DisPATCh include: 1) selecting the SMOS pixels with at least 90% (clear sky) MODIS-retrieved land surface temperature coverage; 2) computing soil evaporative efficiency over nominal MODIS pixels with (4); 3) estimating soil evaporative efficiency over non-nominal MODIS pixels; 4) retrieving parameter $\mathbf{SM_p}$; 5) applying the downscaling relationship of (3); 6) correcting disaggregated soil moisture by the SMOS pixel weighting function; and 7) compositing on a daily basis the disaggregation output ensemble [21]. The input and output data and their link within DisPATCh are summarized in Fig. 5.

1) Selecting Clear Sky SMOS Pixels: A threshold of 90% cloud-free MODIS coverage is used to select the SMOS pixels to be disaggregated. In the official MODIS land surface temperature product (MOD11A1 for Terra and MYD11A1 for Aqua), the data affected by the presence of clouds are already masked. Hence, selection of the 90% clear sky SMOS pixels is directly based on the MODIS land surface temperature product masking.

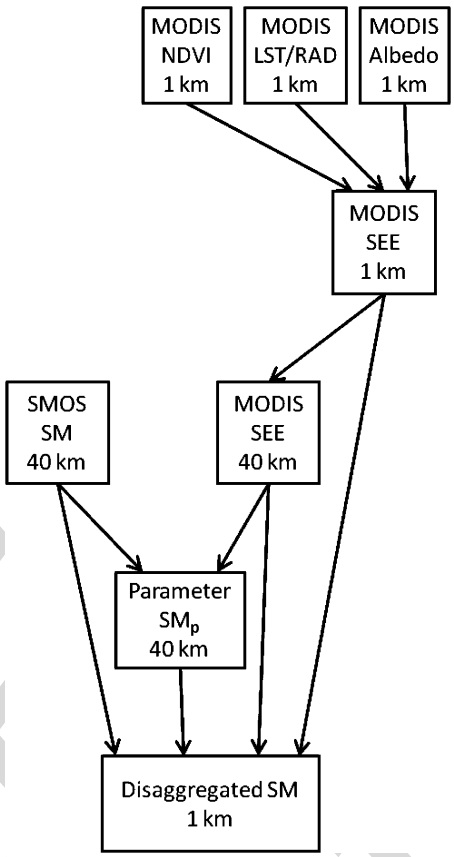

Fig. 5. Schematic diagram presenting the input and output data of DisPATCh.

2) Non-Nominal Pixels: Nominal MODIS pixels are defined as the 1-km resolution pixels that do not include open water and where land surface temperature is actually retrieved. Open water pixels are flagged in the algorithm when MODIS NDVI retrievals yield negative values. The soil evaporative efficiency of open water pixels is set to 1. The emerged pixels where land surface temperature is not retrieved (due to the presence of some clouds within the SMOS pixel) are processed as pixels with mean surface conditions. In practice, the soil evaporative efficiency of cloudy pixels (which represent less than 10% of the surface area within the SMOS pixel) is set to the mean soil evaporative efficiency calculated over the clear sky MODIS pixels. Allocating a soil evaporative efficiency value to non-nominal pixels allows DisPATCh to be run over a wider range of SMOS pixels, including those partially covered by clouds. However, non-nominal 1-km resolution pixels are flagged and discarded from the disaggregation output ensemble.

3) Forested Areas: In this study, DisPATCh is applied to all the SMOS pixels where the soil moisture retrieval is successful, even those including forest class, as long as the 1 km MODIS pixels are in Zone A, B or C (see Fig. 3). This choice is relevant here because the AACES extensive data were almost exclusively collected in agricultural areas (cropping/grazing), so forests for this study are not an issue. In the case of a mixed SMOS pixel including a significant fraction of forest, DisPATCh should be applied to the surface area of the dominant

class, thus excluding the surface area of the minority land cover classes.

4) Calibration: The soil moisture parameter $\mathbf{SM_p}$ used to compute $\partial\mathbf{SM_{mod}}/\partial\mathbf{SEE}$ in (3) is estimated by inverting the SEE model in (7) at SMOS resolution

$$\mathbf{SM_p} = \frac{\pi \cdot \mathbf{SM_{SMOS}}}{\cos^{-1}\left(1 - 2\langle \mathrm{SEE}_{\mathrm{MODIS,1\ km}}\rangle_{\mathbf{40}\ \mathrm{km}}\right)} \tag{15}$$

A value of $\mathbf{SM_p}$ is obtained for each SMOS pixel and each input data set. Note that the main assumption limiting validity of the calibration approach is the soil evaporative efficiency model [26] itself. The soil evaporative efficiency model in [26] was chosen for its simplicity (one parameter) and its ability to represent the general behavior of soil evaporative efficiency over the full range of soil moisture: particularly the null derivative at zero and at maximum soil moisture, and an inflexion point in between [38]. However, it has some inconsistencies. In particular, [38] have indicated that 1) potential evaporation is physically reached at soil saturation and not at field capacity; therefore the model in [26] should be (strictly speaking) parameterized by the soil moisture at saturation and not by the soil moisture at field capacity, and 2) soil evaporative efficiency varies with potential evaporation, meaning that the soil moisture parameter (set to the soil moisture at field capacity in [26]) should theoretically vary in time with atmospheric evaporative demand. Consequently, the $\mathbf{SM_p}$ retrieved from SMOS and MODIS data using the model in [26] is definitely not the soil moisture at field capacity as in [26], although it could be in part related to it. In this study, $\mathbf{SM_p}$ is therefore considered to be a fitting parameter self-estimated by DisPATCh.

5) Weighting Function: A SMOS pixel WEighting Function (WEF) is used to take into account the impact of soil moisture distribution on the SMOS scale soil moisture as seen by SMOS radiometer. A centrosymmetric analytical approximation MEAN_WEF is provided in [19], [20]

$$\mathrm{MEAN\_WEF}(\rho) = C_{\mathrm{MWEF2}} + \mathrm{WEF_A}\left(\frac{\rho}{C_{\mathrm{MWEF1}}} \cdot \frac{\pi}{C_{\mathrm{WEF1}}}\right) \tag{16}$$

with ρ being the distance from the SMOS pixel center, and $C_{\mathrm{MWEF1}} = 40$ km, $C_{\mathrm{MWEF2}} = 0.027$, $C_{\mathrm{WEF1}} = 73.30$ and

$$\mathrm{WEF_A}(\rho') = \frac{[\mathrm{sinc}(C_{\mathrm{WEF1}} \cdot \rho')]^{C_{\mathrm{WEF2}}}}{1 + C_{\mathrm{WEF3}} \cdot \rho'^{C_{\mathrm{WEF4}}}} \tag{17}$$

with ρ' being the distance in the director cosines coordinates, $\mathrm{sinc}(x) = \sin(x)/x$, and $C_{\mathrm{WEF2}} = 1.4936$, $C_{\mathrm{WEF3}} = 524.5$ and $C_{\mathrm{WEF4}} = 2.103$.

A correction is applied to disaggregated soil moisture in (3)

$$\mathrm{SM}_{1\ \mathrm{km}}^{\mathrm{wef\ corr.}} = \mathrm{SM}_{1\ \mathrm{km}} + \frac{\sum \mathrm{MEAN\_WEF}(\rho) \cdot \mathrm{SM}_{1\ \mathrm{km}}(\rho)}{\sum \mathrm{MEAN\_WEF}(\rho)} - \mathbf{SM_{SMOS}} \tag{18}$$

with $\mathrm{SM}_{1\ \mathrm{km}}^{\mathrm{wef\ corr.}}$ being the WEF-corrected disaggregated soil moisture. Mathematically speaking, one should replace $\mathbf{SM_{SMOS}}$ with $\sum \mathrm{MEAN\_WEF} \cdot \mathrm{SM}_{1\ \mathrm{km}} / \sum \mathrm{MEAN\_WEF}$ in (3) and (15) and run an iteration loop until convergence of $\mathrm{SM}_{1\ \mathrm{km}}^{\mathrm{wef\ corr.}}$ values. However, the impact of the WEF on disaggregated soil moisture is expected to be low so that the simple correction in (18) is considered to be sufficient for the purpose of the study.

6) Disaggregation Output: The downscaling relationship in (3) is applied to each input data set, and the disaggregated soil moisture data ensemble is averaged on each 1-km resolution pixel within the study area. Averaging is a way to reduce random uncertainties in the disaggregation output. In [17], [27], disaggregated soil moisture was averaged in space (aggregated) at the expense of downscaling resolution. Herein, temporal averaging [30] is preferred to keep an optimal downscaling resolution. Note that a condition to average disaggregated soil moisture in time is the availability of thermal infrared data at high temporal frequency. Another significant advantage of applying DisPATCh to an input ensemble is to provide an estimate of the uncertainty in 1-km resolution disaggregated soil moisture, e.g., by computing the standard deviation within the output ensemble.

IV. Application

To test DisPATCh under various surface and atmospheric conditions, the algorithm is run during AACES-1 and AACES-2 in different modes, by including (or not) a correction for vegetation and atmospheric effects. In each case, disaggregated SMOS soil moisture and HDAS measurements are compared at 1-km resolution for all date-farm units with overlapping HDAS/SMOS/MODIS data.

A. Null Hypothesis

In this study, the null hypothesis is defined as the application of DisPATCh with parameter $\mathbf{SM_p}$ set to zero in (8). Hence, the downscaling relationship in (3) becomes

$$\mathrm{SM}_{1\ \mathrm{km}} = \mathbf{SM_{SMOS}} \tag{19}$$

meaning that no 1-km information is used. Defining a null hypothesis is useful to test whether DisPATCh is able to reproduce the subpixel variability within the ~ 10 km^2 sampling farms with better skill than simply assuming a uniform moisture condition. Statistical results in terms of root mean square difference, mean difference, correlation coefficient, and slope of the linear regression between the SMOS soil moisture disaggregated with (19) and *in situ* measurements are listed in Table III. One observes that the root mean square difference is generally explained by a (negative) bias in SMOS data and that none of the correlations evaluated at 1-km resolution for each farm separately is statistically significant (all calculated p-values are larger than 0.10). Thus, the rationale for developing DisPATCh is to improve the correlation at fine scale between SMOS and ground soil moisture and to reduce the bias in disaggregated SMOS data in the specific case where the bias in SMOS data at the farm scale is due to the heterogeneity of soil moisture within the SMOS pixel.

TABLE III
DISPATCH IS RUN WITH NO 1-km INFORMATION ($\mathbf{SM_p}$ SET TO ZERO) AND STATISTICAL RESULTS ARE LISTED IN TERMS OF ROOT MEAN SQUARE DIFFERENCE (RMSD), MEAN DIFFERENCE (BIAS), CORRELATION COEFFICIENT (R), AND SLOPE OF THE LINEAR REGRESSION BETWEEN 1-km RESOLUTION DISAGGREGATED SMOS SOIL MOISTURE AND 1-km AGGREGATED *IN SITU* MEASUREMENTS. THE MEAN AND STANDARD DEVIATION OF GROUND MEASUREMENTS ($\langle SM_{HDAS}\rangle$ AND σ_{HDAS}), THE NUMBER OF CONSIDERED 1-km PIXELS, AND STATISTICAL SIGNIFICANCE (P-VALUE) ARE ALSO LISTED FOR EACH DATE-FARM UNIT

DoY/Farm	$\langle SM_{HDAS}\rangle$ (m^3/m^3)	σ_{HDAS} (m^3/m^3)	Number of 1 km pixels	RMSD (m^3/m^3)	Bias (m^3/m^3)	R† (-)	Slope† (-)	p-value (-)
28/F05	0.04	0.02	7	0.04	−0.04	-	-	1.0
30/F07	0.02	0.03	8	0.02	−0.02	-	-	1.0
30/F08	0.03	0.02	7	0.02	−0.02	-	-	0.69
46/F15	0.29	0.05	8	0.04	0.03	-	-	0.91
46/F16	0.34	0.06	8	0.09	−0.08	-	-	1.0
49/F17	0.21	0.06	8	0.04	−0.04	-	-	0.66
49/F18	0.25	0.07	6	0.08	−0.08	-	-	0.42
49/F20	0.20	0.09	4	0.02	−0.007	-	-	0.87
51/F19	0.24	0.08	6	0.13	−0.13	-	-	0.77
51/F20	0.20	0.10	6	0.09	−0.08	-	-	0.79
AACES-1 mean‡	-	-	-	-	-	-	-	>0.10
254/F09	0.33	0.07	9	0.13	−0.13	-	-	0.13
256/F07	0.36	0.10	8	0.19	−0.18	-	-	0.15
264/F13	0.30	0.07	8	0.18	−0.17	-	-	1.0
265/F15	0.25	0.06	7	0.05	−0.05	-	-	1.0
267/F09	0.21	0.07	9	0.14	−0.14	-	-	0.43
AACES-2 mean‡	-	-	-	-	-	-	-	>0.10

† R and slope values are reported if p-value<0.10.

‡ the mean values computed for AACES-1 and AACES-2 include only statistically significant (p-value<0.10) results.

B. Visual Assessment of Disaggregation Images

As an example, DisPATCh is applied on DoY 49 over a 120 km by 80 km subarea including the farms F16, F17, F18, F19, and F20. The images of 1-km resolution disaggregated SMOS soil moisture are presented in Fig. 6. DisPATCh is run with $\mathbf{SM_p}$ set to zero (null hypothesis) and in four distinct modes corresponding to the combinations of the "LST" (the official MODIS land surface temperature product is used) and "RAD" [the land surface temperature is derived from MODIS radiances using (14)] modes and the "Zone A+B+C" (the vegetation-transpiration dominated 1-km pixels are discarded) and "Zone A only" (only the soil evaporation-dominated 1-km pixels are selected) modes.

In Fig. 6, the SMOS DGG nodes where level-2 soil moisture is successfully retrieved are overlaid on the image corresponding to the null hypothesis (resampled SMOS data with no 1-km information) for 6 am and 6 pm overpass times separately. The gaps in SMOS data in the lower middle part of the images are due to topography flagging over the Australian Alps. In the version-4 SMOS level-2 processor, soil moisture is not retrieved at the DGG nodes where the topography effects on simulated brightness temperatures exceed a certain threshold, so as to prevent large errors in soil moisture values. The apparent resolution of the null hypothesis image is 20 km because it is generated from the composition of four 40-km resolution resampled SMOS snapshot images, whose resampling grids are separated by 20 km (the SMOS level-2 data resampling strategy was described in Section II-B.).

Note that the disaggregation products in the Zone A+B+C mode cover an area larger than the area sampled by SMOS data, because the SMOS resolution (about 40 km) is larger than the SMOS product sampling length (about 15 km), but does not provide disaggregated values at a distance larger than 20 km from the successful retrieval nodes. Concerning the Zone A only mode, disaggregation products do not cover an area larger than the SMOS sampling area because the Australian Alps are surrounded by forests where the fraction of bare soil is less than elsewhere in the area, and which correspond to Zone B or C in the hourglass in Fig. 3.

When looking at the images obtained in the Zone A+B+C mode in Fig. 6, one observes that the spatial structures of 1-km disaggregated SMOS soil moisture encompass, but does not seem to be correlated with, the SMOS data sampling length. However, a "boxy artifact" is still apparent at 20-km resolution, which is the separation length of the SMOS data resampling grids as explained in Section II-B. The notion of "boxy artifact" was introduced by [39] to analyze the quality of a disaggregation approach. The less apparent the low-resolution boxes, the better the disaggregation skill of the algorithm to spatially connect high-resolution disaggregated values between neighboring low-resolution pixels, and thus to derive a realistic high-resolution soil moisture field. When comparing the images obtained in the Zone A+B+C mode with those obtained in the

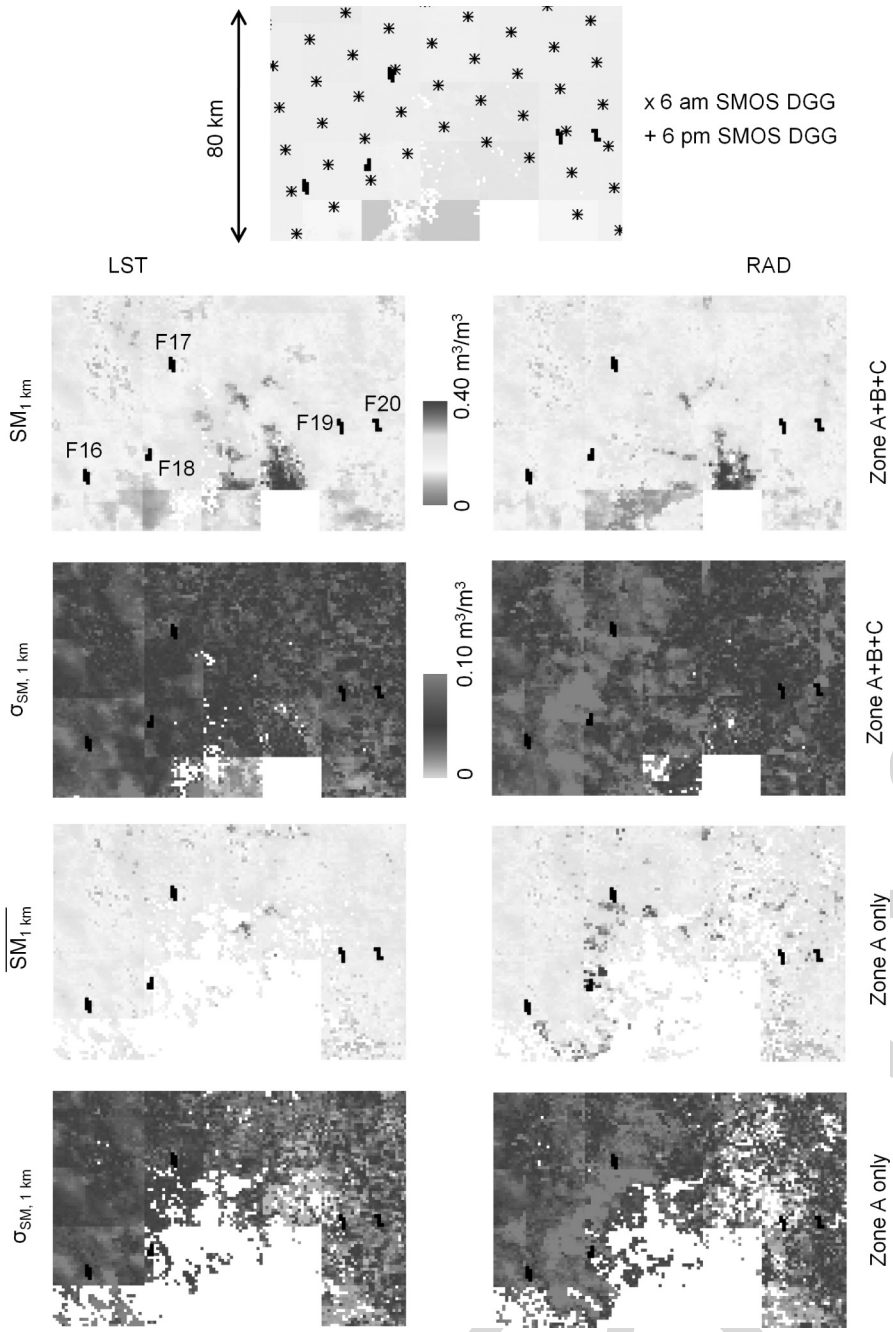

Fig. 6. Images of disaggregation results over a 120 km by 80 km subarea on DoY 49. The disaggregated soil moisture ($\overline{\mathrm{SM}_{1\ \mathrm{km}}}$) and its estimated uncertainty ($\sigma_{\mathrm{SM},1\ \mathrm{km}}$) are compared in the LST and RAD modes and in the Zone A+B+C and Zone A only modes. Sampling farms are overlaid on all images. SMOS DGG nodes are overlaid on the image corresponding to the null hypothesis (no 1-km resolution information) presented at top.

Zone A only mode, one observes that the 20-km resolution boxy artifact is less apparent in the Zone A only mode, consistent with the better sensitivity of MODIS-derived SEE with soil-dominated pixels (Zone A) than with mixed-surface (Zone B and C) pixels. In Fig. 6, the images obtained in the LST and RAD mode highlight different spatial structures. In general, there are less data gaps in the RAD than in the LST mode. However, ground validation data are required to assess their relative quality/accuracy.

As an assessment of the uncertainty in composited soil moisture disaggregation, the standard deviation within the disaggregation output ensemble is also reported for each disaggregation product in Fig. 6. The same observations can be made as with the soil moisture images: spatial structures are more visible, and the boxy artifact is less apparent in the RAD than in the LST mode. In general, the estimated uncertainty in disaggregated products is larger in the RAD than in the LST mode, regardless of the Zone (A+B+C or A only) mode.

C. SMOS Weighting Function

To evaluate the impact of the SMOS instrument weighting function on disaggregation results, DisPATCh is run with (and without) the WEF correction in (18). The expected effect of the

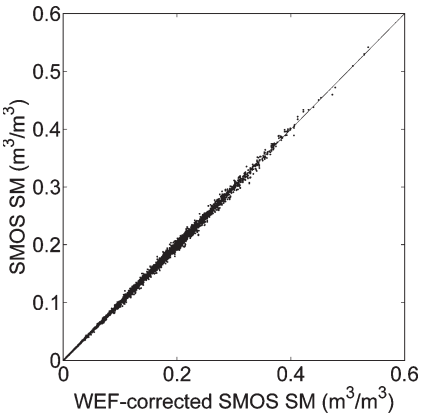

Fig. 7. Uncorrected versus WEF-corrected SMOS soil moisture for the entire data set.

WEF is a bias at 40 km resolution on disaggregated soil moisture. Fig. 7 plots the uncorrected against WEF-corrected SMOS soil moisture for the entire data set including both AACES-1 and AACES-2 experiments. The WEF correction has very little impact on disaggregated soil moisture with a maximum difference between uncorrected and WEF-corrected SMOS soil moisture of 0.02 m^3/m^3, a mean difference of approximately zero, and a standard deviation of 0.003 m^3/m^3. Although the difference is small with this data set, WEF-corrected products are expected to be more realistic. Therefore, the correction in (18) is used in all the DisPATCh runs that follow.

D. Quantitative Comparison With In Situ Measurements

Fig. 8 presents the scatterplots of 1-km resolution disaggregated SMOS soil moisture versus 1-km resolution aggregated *in situ* measurements for the ten date-farm units during AACES-1. On each graph are plotted the soil moisture disaggregated in the Zone A+B+C mode (empty squares) and the soil moisture disaggregated in the Zone A only mode (black squares). At the beginning of AACES-1, conditions are very dry so that SMOS retrievals are close to zero and the variability of *in situ* measurements is low (about 0.02 m^3/m^3). In such conditions, no useful information is expected from the application of DisPATCh, and the statistical results in terms of spatial correlation are not meaningful for DoY 28/F05, DoY 30/F07 and DoY 30/F08. While wetter conditions occur after DoY 30, cloud cover prevents DisPATCh to be run (MODIS data are unavailable) until DoY 46. On DoY 46, the average and standard deviation of *in situ* soil moisture measurements is 0.32 m^3/m^3 and 0.06 m^3/m^3, respectively. The spatial variability of 1-km soil moisture is nicely captured by DisPATCh notably in the RAD mode. On DoY 49, the disaggregated SMOS soil moisture is still correlated with the *in situ* measurements made in three farms (F17, F18, and F20). On the last ground sampling day, disaggregation results are significantly correlated with *in situ* measurements in F19, but not in F20. The poor results obtained with DoY 51/F20 is probably due to the time gap (3 days) between ground sampling date (DoY 51) and MODIS overpass day (DoY 54).

Statistical results in terms of root mean square difference, mean difference, correlation coefficient, and slope of the linear regression between the SMOS soil moisture disaggregated in the Zone A+B+C mode and aggregated *in situ* measurements are listed in Table IV. Statistical significance (p-value) is also reported for each date-farm unit to select statistically significant (p-value < 0.10) results. Although the disaggregation of SMOS data on extensively dry DoY 30 does not provide any additional information (soil is uniformly dry), the observed correlation between disaggregated (LST mode) and *in situ* soil moisture is statistically significant, and the correlation coefficient value is negative (-0.70 and -0.95 at F07 and F08, respectively). One plausible explanation is the opposite effect of soil temperature on HDAS soil moisture measurements and on MODIS-derived soil evaporative efficiency: a slight undercorrection of the temperature-corrected hydraprobe measurements at high temperature [18] results in a slight increase of soil moisture estimate with soil temperature, while an increase of soil temperature makes soil evaporative efficiency decrease. Nevertheless, the possible impact of soil temperature on HDAS measurements is very low with a slope of the linear regression between disaggregated SMOS and *in situ* soil moisture calculated as -0.08 and -0.03 for F07 and F08, respectively. When selecting statistically significant results (p-value < 0.10) and discarding data for DoY 30, the mean correlation coefficient and slope in RAD mode are 0.75 and 0.58, respectively.

Fig. 9 presents the scatterplots of 1-km resolution disaggregated SMOS soil moisture versus 1-km resolution aggregated *in situ* measurements for the five date-farm units during AACES-2. On each graph are plotted the soil moisture disaggregated in the Zone A+B+C mode (empty squares) and the soil moisture disaggregated in the Zone A only mode (black squares). The surface conditions of AACES-2 were relatively wet with a mean soil moisture value estimated as 0.29 m^3/m^3. The disaggregated SMOS soil moisture does not correlate well with *in situ* measurements with a p-value larger than 0.10 for all sampling days, except for DoY 256/F07 in LST mode (see Table IV). The negative correlation coefficient (-0.73) obtained on DoY 256 is discussed when comparing the Zone A+B+C and Zone A only modes in Section IV-F. In general, statistical results in Table IV indicate that DisPATCh does not succeed in representing the variability of soil moisture at 1-km resolution during AACES-2. In fact, DisPATCh is based on the tight coupling that occurs between soil moisture and evaporation under high evaporative demand conditions [40]. This coupling seems to be weak in September over the study area so that the disaggregation results at 1-km resolution are not reliable.

For DoY 264/F13, however, an interesting feature is observed on the graph corresponding to the RAD and Zone A only modes. When removing the (three) black squares with the largest errorbars, the correlation coefficient and the slope of the linear regression between disaggregated and *in situ* observations becomes 0.9 and 0.7, respectively. This suggests that: 1) the standard deviation within the disaggregation output ensemble can be a good estimate of the uncertainty in the composited disaggregation product; and 2) the applicability of DisPATCh is greatly dependent on the quality of MODIS land surface temperature. Note that in this study, a choice was made to maximize the number of data points used in the comparison with *in situ* measurements. Consequently, all the cloud-free

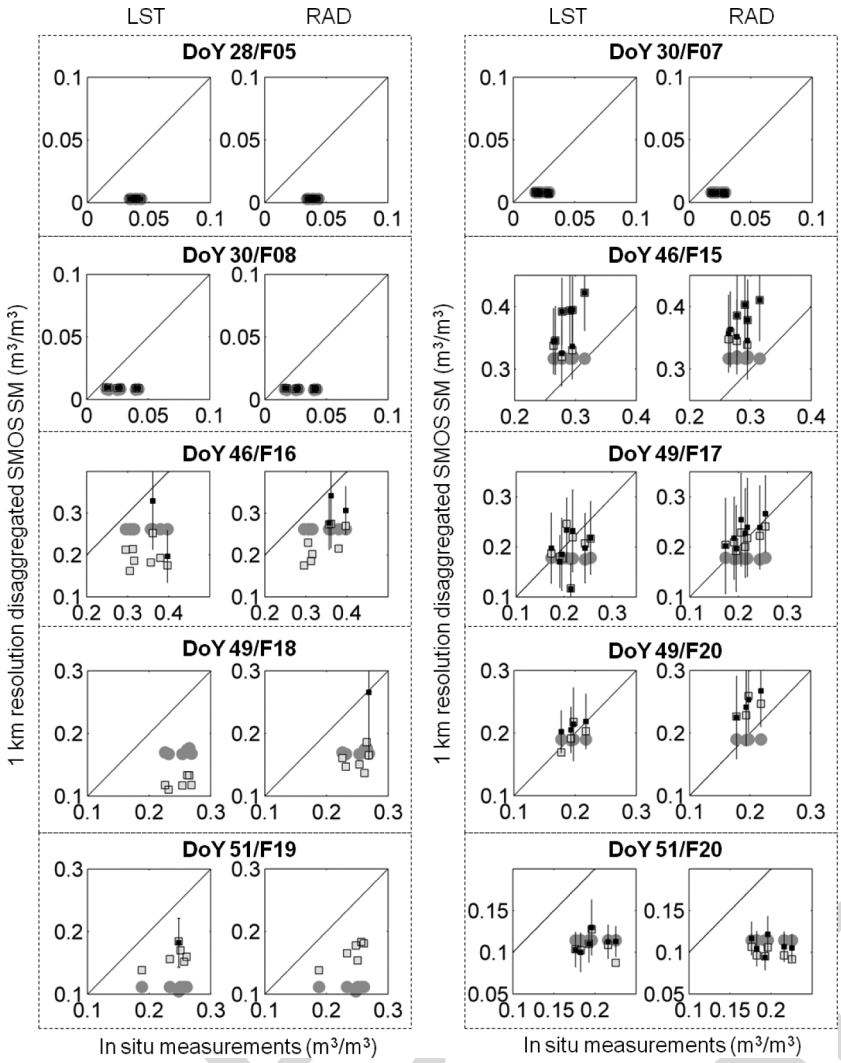

Fig. 8. Scatterplots of 1-km resolution disaggregated SMOS soil moisture versus 1-km resolution aggregated *in situ* measurements for each of the ten date-farm data sets during AACES-1. The filled circles correspond to disaggregation with no 1-km information, empty squares to Zone A+B+C mode and black squares to Zone A only mode. For the Zone A only mode, the uncertainty in disaggregated soil moisture is represented by vertical errorbars.

MODIS land surface temperature data were used regardless of the MODIS land surface temperature quality index. Further research should be conducted to assess whether selecting the MODIS pixel with the best MODIS land surface temperature quality index would improve the disaggregation results. This would be possible using the AACES airborne data, which cover a much larger area than *in situ* measurements.

E. Atmospheric Corrections

The impact of atmospheric corrections on DisPATCh output is analyzed by comparing the disaggregation results obtained in the LST and RAD mode. Quantitative comparison between LST and RAD modes is provided in Table IV in terms of root mean square difference, mean difference, correlation coefficient, and slope of the linear regression between disaggregated SMOS soil moisture and aggregated *in situ* measurements. Correlation coefficient and slope values are reported only if the p-value (statistical significance) is lower than 0.10. It is apparent that statistical results are better in the RAD than in the LST mode. When including all dates, the mean bias is decreased from -0.05 m^3/m^3 in LST mode to -0.03 m^3/m^3 in RAD mode during AACES-1. When selecting statistically significant results (p-value < 0.10) and discarding data for DoY 30, the mean correlation coefficient and slope is 0.75 and 0.58 in RAD mode, and 0.65 and 1.5 in LST mode, respectively. Note that the improvement is very significant for DoY 46/F16 with a correlation coefficient and slope increasing from about zero to 0.7 and 0.8, respectively.

The fact that the results obtained in RAD mode are superior to those obtained in LST mode indicates that the atmospheric corrections of the official MODIS land surface temperature add significant uncertainties in the disaggregation products. One rationale may be that the information used in atmospheric corrections (notably air temperature and water vapor profile data) are subjected to large uncertainties at 5-km resolution. As DisPATCh is based on the spatial variations of MODIS temperature relative to the 40 km scale mean, the atmospheric corrections on the land surface temperature data are not necessary at 5 km (as it is done in the MODIS temperature

TABLE IV
DISPATCH IS RUN IN THE ZONE A+B+C MODE AND STATISTICAL RESULTS ARE LISTED IN TERMS OF ROOT MEAN SQUARE DIFFERENCE (RMSD), MEAN DIFFERENCE (BIAS), CORRELATION COEFFICIENT (R), AND SLOPE OF THE LINEAR REGRESSION BETWEEN 1-km RESOLUTION DISAGGREGATED SMOS SOIL MOISTURE AND 1-km AGGREGATED *IN SITU* MEASUREMENTS. THE RESULTS OBTAINED USING THE RADIANCE-DERIVED LAND SURFACE TEMPERATURE DATA (RAD MODE) AND USING THE OFFICIAL MODIS LAND SURFACE TEMPERATURE DATA (LST MODE IN PARENTHESIS) ARE COMPARED. THE MEAN AND STANDARD DEVIATION OF GROUND MEASUREMENTS ($\langle SM_{HDAS} \rangle$ AND σ_{HDAS}), THE NUMBER OF CONSIDERED 1-km PIXELS AND STATISTICAL SIGNIFICANCE (P-VALUE) ARE ALSO LISTED FOR EACH DATE-FARM UNIT

DoY/Farm	$\langle SM_{HDAS} \rangle$ (m^3/m^3)	σ_{HDAS} (m^3/m^3)	Number of 1 km pixels	RMSD (m^3/m^3)	Bias (m^3/m^3)	R† (-)	Slope† (-)	p-value (-)
28/F05	0.04	0.02	7 (7)	0.04 (0.04)	−0.04 (−0.04)	- (-)	- (-)	0.72 (0.80)
30/F07	0.02	0.03	8 (8)	0.02 (0.02)	−0.02 (−0.02)	- (−0.70)	- (−0.08)	0.20 (0.05)
30/F08	0.03	0.02	7 (7)	0.02 (0.02)	−0.02 (−0.02)	- (−0.95)	- (−0.03)	0.11 (0.001)
46/F15	0.29	0.05	8 (8)	0.09 (0.09)	0.09 (0.08)	- (0.65)	- (1.5)	0.12 (0.08)
46/F16	0.34	0.06	8 (8)	0.12 (0.15)	−0.11 (−0.14)	0.72 (-)	0.76 (-)	0.04 (0.95)
49/F17	0.21	0.06	8 (8)	0.02 (0.04)	0.00 (−0.02)	0.70 (-)	0.42 (-)	0.05 (0.54)
49/F18	0.25	0.07	6 (6)	0.10 (0.13)	−0.09 (−0.13)	- (-)	- (-)	0.60 (0.20)
49/F20	0.20	0.09	4 (4)	0.05 (0.01)	0.04 (0.00)	- (-)	- (-)	0.41 (0.32)
51/F19	0.24	0.08	6 (6)	0.07 (0.08)	−0.07 (−0.08)	0.84 (-)	0.56 (-)	0.04 (0.19)
51/F20	0.20	0.10	6 (6)	0.10 (0.09)	−0.10 (−0.09)	- (-)	- (-)	0.17 (0.51)
AACES-1 mean‡	0.26 (0.29)	0.07 (0.05)	7 (8)	0.07 (0.09)	−0.06 (−0.08)	0.75 (0.65)	0.58 (1.5)	0.04 (0.08)
254/F09	0.33	0.07	9 (9)	0.18 (0.14)	−0.16 (−0.11)	- (-)	- (-)	0.17 (0.74)
256/F07	0.36	0.10	8 (9)	0.12 (0.19)	−0.10 (−0.18)	- (−0.73)	- (−0.47)	0.12 (0.04)
264/F13	0.30	0.07	8 (8)	0.16 (0.19)	−0.14 (−0.16)	- (-)	- (-)	0.59 (0.47)
265/F15	0.25	0.06	7 (7)	0.16 (0.18)	0.01 (0.03)	- (-)	- (-)	0.32 (0.34)
267/F09	0.21	0.07	9 (9)	0.16 (0.15)	−0.15 (−0.15)	- (-)	- (-)	0.90 (0.86)
AACES-2 mean‡	0.36	0.10	- (9)	- (0.19)	- (−0.18)	- (−0.73)	- (−0.47)	>0.10 (0.04)

† R and slope values are reported if p-value<0.10.

‡ the mean values computed for AACES-1 and AACES-2 include only statistically significant (p-value<0.10) results and discard extensive dry days DoY 28-30.

algorithm). An atmospheric correction at 40-km resolution is sufficient and provides even better disaggregation results that applying an atmospheric correction at 5-km resolution.

F. Vegetation Cover

The impact of vegetation cover on DisPATCh output during AACES-1 is analyzed by comparing the disaggregation results obtained in the Zone A+B+C and Zone A only mode. Quantitative comparison between Zone A+B+C and Zone A only modes is provided in Tables IV and V in terms of root mean square difference, mean difference, correlation coefficient, and slope of the linear regression between disaggregated SMOS soil moisture and aggregated *in situ* measurements. It is apparent that statistical results are generally better in the Zone A only than in the Zone A+B+C mode for both LST and RAD modes. In the RAD mode for instance, the mean correlation coefficient is increased from 0.75 in the Zone A+B+C mode (Table IV) to 0.89 in the Zone A only mode (Table V). Also the mean slope is closer to 1 as it switches from 0.58 in the Zone A+B+C mode (Table IV) to 0.91 in the Zone A only mode (Table V). Consequently, results are consistent with the hourglass approach in Fig. 3 that predicts a lower sensitivity of MODIS-derived soil temperature to soil moisture in Zone B and C, Zone A having the highest potential for estimating soil moisture variability from MODIS temperature.

On DoY 256, the negative correlation appearing in Zone A+B+C mode (Table IV) is not significant in Zone A only mode (Table V), suggesting that the contradictory result obtained on DoY 256 is probably an artifact due to the small sample size.

Note that one drawback of the Zone A only mode is the larger amount of data gaps in the soil moisture images. Therefore, the use of both modes is a compromise between application coverage and accuracy in the disaggregation output.

G. Distinguishing Between SMOS and DisPATCh Errors

By solving the extent mismatch between 40-km resolution remote sensing observation and localized *in situ* measurements, DisPATCh could be used as a tool to help improve the validation strategies of SMOS data in low-vegetated semi-arid regions. It also would reduce the coverage requirements identified by [41] for airborne validation campaigns. However, such a validation approach requires separating the different error sources that may be attributed to SMOS soil moisture and to DisPATCh. One solution is to estimate the errors attributed to DisPATCh and then deduce the errors attributed to SMOS soil moisture. To estimate the errors that are associated with the disaggregation

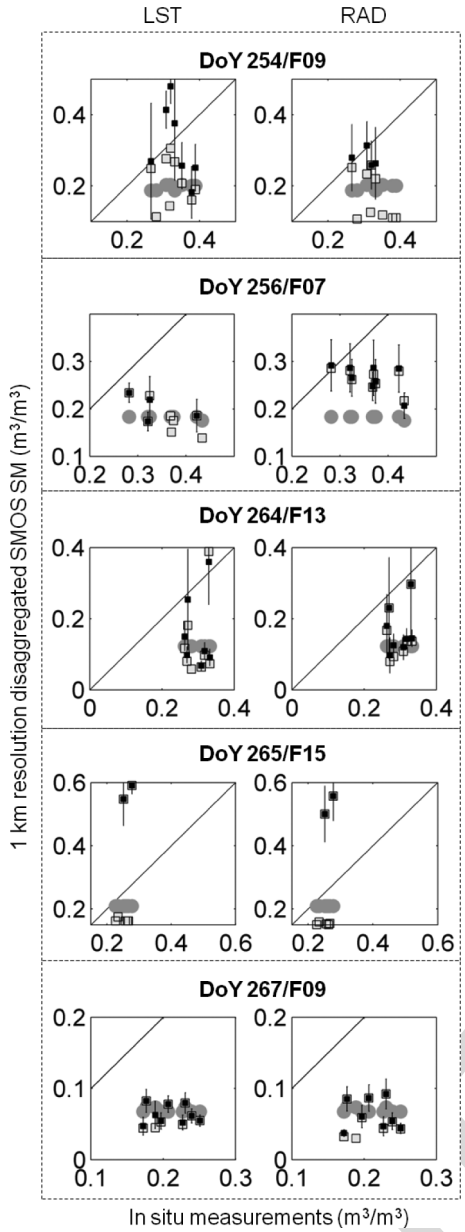

Fig. 9. Scatterplots of 1-km resolution disaggregated SMOS soil moisture versus 1-km resolution aggregated *in situ* measurements for each of the five date-farm data sets during AACES-2. The filled circles correspond to disaggregation with no 1-km information, empty squares to Zone A+B+C mode and black squares to Zone A only mode. For the Zone A only mode, the uncertainty in disaggregated soil moisture is represented by vertical errorbars.

methodology, it is suggested to analyze the spatial correlation between 1-km disaggregated SMOS soil moisture and *in situ* measurements. If the correlation is significant, then the disaggregation product is likely to be sufficiently accurate for validating SMOS data.

Note that the errors in DisPATCh are in part coupled with the errors in SMOS soil moisture, particularly because SMOS is an input to DisPATCh. However, any uncertainties in SMOS soil moisture should not impact the disaggregation results at a distance shorter than the SMOS data sampling length (15 km). This is the reason why such a validation strategy should be conducted with ground measurements made within a distance radius of 15 km.

In this study case, five date-farm units including DoY 46/F15, DoY 46/F16, DoY 49/F17, DoY 49/F18, and DoY 49/F20 indicate a significant correlation between disaggregated SMOS soil moisture and *in situ* measurements. For these units, the root mean square error in disaggregated SMOS soil moisture is mainly explained by a bias in disaggregated soil moisture (see Table IV). However, no conclusion can be drawn from these data because: 1) the bias is sometimes positive (DoY 46/F15, DoY 49/F20), and sometimes negative (DoY 46/F16, DoY 49/F17, DoY 49/F18); and 2) the comparison is made only once for each farm, which does not allow analyzing the temporal behavior. Such a validation approach could be undertaken in the near future using the OzNet (http://www.oznet.org.au/, [42]) soil moisture monitoring network, providing continuous measurements at 68 sites within the Murrumbidgee catchment area.

H. Subpixel Variability and Assimilation Perspectives

DisPATCh is successively run in LST or RAD mode and in Zone A+B+C or Zone A only mode during AACES-1. Fig. 10 plots for each case the estimated uncertainty in disaggregated soil moisture (computed as the standard deviation of the disaggregation output ensemble) against the subpixel variability of 1-km resolution *in situ* measurements (computed as the standard deviation of the *in situ* measurements made within 1-km pixels). The data corresponding to DoY 51 are plotted separately because of the time gap between HDAS/SMOS (DoY 51) and MODIS (DoY 54) collection time. It is interesting to observe that the estimated uncertainty in disaggregated soil moisture is closely related to the observed subpixel variability of *in situ* measurements. Hence, $\sigma_{\mathrm{SM,1\ km}}$ could be used as a proxy for representing the soil moisture variability at scales finer than 1-km resolution. Concerning the data on DoY 51, the linear regression is clearly off the 1:1 line. This is consistent with a decrease of the spatial variability in soil moisture during a dry down period [43]. In particular, the spatial variability in soil moisture is expected to be lower on DoY 54 than on DoY 51.

The correlation between the estimated uncertainty in disaggregated soil moisture and the subpixel soil moisture variability makes an additional link between DisPATCh output and assimilation schemes into hydrological models. A number of optimal assimilation methodologies have been developed to combine model predictions with remote sensing observations. However, any so-called optimal assimilation technique stops being optimal if the uncertainty in remotely sensed data is unknown or estimated with a large uncertainty. In the perspective of assimilating disaggregated SMOS data into land surface models, one should keep in mind that the error information on observable variables is as crucial as the observations themselves, e.g., [44].

V. Summary and Conclusion

DisPATCh is an algorithm dedicated to the disaggregation of soil moisture observations using high-resolution soil temperature data. It converts soil temperature fields into soil moisture fields given a semi-empirical soil evaporative efficiency model

TABLE V
DISPATCH IS RUN IN THE ZONE A ONLY MODE, AND STATISTICAL RESULTS ARE LISTED IN TERMS OF ROOT MEAN SQUARE DIFFERENCE (RMSD), MEAN DIFFERENCE (BIAS), CORRELATION COEFFICIENT (R), AND SLOPE OF THE LINEAR REGRESSION BETWEEN 1-km RESOLUTION DISAGGREGATED SMOS SOIL MOISTURE AND 1-km AGGREGATED *IN SITU* MEASUREMENTS. THE RESULTS OBTAINED USING THE RADIANCE-DERIVED LAND SURFACE TEMPERATURE DATA (RAD MODE) AND USING THE OFFICIAL MODIS LAND SURFACE TEMPERATURE DATA (LST MODE IN PARENTHESIS) ARE COMPARED. THE MEAN AND STANDARD DEVIATION OF GROUND MEASUREMENTS ($\langle SM_{HDAS} \rangle$ AND σ_{HDAS}), THE NUMBER OF CONSIDERED 1-km PIXELS AND STATISTICAL SIGNIFICANCE (P-VALUE) ARE ALSO LISTED FOR EACH DATE-FARM UNIT

DoY/Farm	$\langle SM_{HDAS} \rangle$ (m^3/m^3)	σ_{HDAS} (m^3/m^3)	Number of 1 km pixels	RMSD* (m^3/m^3)	Bias* (m^3/m^3)	R† (-)	Slope† (-)	p-value (-)
28/F05	0.04	0.02	7 (7)	0.04 (0.04)	−0.04 (−0.04)	- (-)	- (-)	0.72 (0.80)
30/F07	0.02	0.03	8 (8)	0.02 (0.02)	−0.02 (−0.02)	- (−0.70)	- (−0.08)	0.20 (0.05)
30/F08	0.03	0.02	7 (7)	0.02 (0.02)	−0.02 (−0.02)	- (−0.95)	- (−0.03)	0.11 (0.001)
46/F15	0.29	0.05	8 (8)	0.09 (0.09)	0.09 (0.08)	- (0.66)	- (1.4)	0.13 (0.07)
46/F16	0.34	0.06	3 (2)	0.07 (0.14)	−0.06 (−0.12)	- (-)	- (-)	0.96 (-)
49/F17	0.21	0.06	8 (8)	0.02 (0.04)	0.02 (−0.02)	0.79 (-)	0.71 (-)	0.02 (0.64)
49/F18	0.25	0.07	1 (0)	- (-)	- (-)	- (-)	- (-)	0.20 (0.20)
49/F20	0.20	0.09	4 (4)	0.05 (0.02)	0.05 (0.01)	0.98 (0.92)	1.1 (0.42)	0.02 (0.08)
51/F19	0.24	0.08	0 (1)	- (-)	- (-)	- (-)	- (-)	0.19 (0.19)
51/F20	0.20	0.10	6 (6)	0.09 (0.09)	−0.09 (−0.09)	- (-)	- (-)	0.70 (0.45)
AACES-1 mean‡	0.21 (0.25)	0.08 (0.07)	6 (6)	0.04 (0.06)	0.04 (0.05)	0.89 (0.79)	0.91 (0.91)	0.02 (0.08)
254/F09	0.33	0.07	4 (7)	0.05 (0.12)	−0.03 (−0.02)	- (-)	- (-)	0.70 (0.30)
256/F07	0.36	0.10	8 (4)	0.12 (0.15)	−0.10 (−0.13)	- (-)	- (-)	0.13 (0.43)
264/F13	0.30	0.07	8 (7)	0.14 (0.17)	−0.13 (−0.14)	- (-)	- (-)	0.64 (0.86)
265/F15	0.25	0.06	2 (2)	0.26 (0.30)	0.26 (0.30)	- (-)	- (-)	- (-)
267/F09	0.21	0.07	8 (9)	0.15 (0.15)	−0.15 (−0.15)	- (-)	- (-)	0.77 (0.85)
AACES-2 mean‡	-	-	- (-)	- (-)	- (-)	- (-)	- (-)	>0.10 (>0.10)

* RMSD and bias values are computed if the number of 1 km pixels>1.

† R and slope values are reported if p-value<0.10.

‡ the mean values computed for AACES-1 and AACES-2 include only statistically significant (p-value<0.10) results and discard extensive dry days DoY 28-30.

and a first-order Taylor series expansion around the field-mean soil moisture. In this study, the disaggregation approach is applied to 40-km resolution version-4 SMOS level-2 soil moisture using 1-km resolution MODIS data. The objective is to test DisPATCh under different surface and atmospheric conditions using the very intensive ground measurements collected in southeastern Australia during the 2010 summer and winter AACES campaigns. Those measurements are aggregated at the downscaling resolution (1 km) and subsequently compared to the disaggregated SMOS soil moisture. Over the study area, climatic (evaporative demand), meteorologic (presence of clouds), and vegetation (cover and water status) conditions are strong constraints on disaggregation results. The quality of disaggregation products varies greatly according to season: while the correlation coefficient between disaggregated and *in situ* soil moisture is 0.7 during the summer AACES, it is about zero during the winter AACES, consistent with a weaker coupling between evaporation and surface moisture in temperate than in semi-arid climate. Moreover, vegetation cover prevents the soil temperature to be retrieved from thermal infrared data and the vegetation water stress may increase the remotely sensed land surface temperature independent of near-surface soil moisture. By separating the 1-km pixels where MODIS temperature is mainly controlled by soil evaporation, from those where MODIS temperature is controlled by both soil evaporation and vegetation transpiration, the correlation coefficient between disaggregated and *in situ* soil moisture is increased from 0.70 to 0.85 during the summer AACES campaign. Also, cloud cover totally obscures the surface during rain events, and on clear sky days, the water vapor in the atmosphere significantly affects the quality of land surface temperature data. It is found that the 5-km resolution atmospheric correction of the official MODIS temperature data has significant impact on DisPATCh output. An alternative atmospheric correction at 40-km resolution increases the correlation coefficient between disaggregated and *in situ* soil moisture from 0.72 to 0.82 during the summer AACES.

The above limitations must be kept in mind when using DisPATCh as a tool for validating SMOS soil moisture. Over semi-arid areas, disaggregation can solve the extent mismatch between the 40-km resolution SMOS data and localized *in situ* measurements. However, the validation of SMOS using DisPATCh requires separation of the errors associated with SMOS data and the errors associated with DisPATCh. As SMOS data are an input to DisPATCh, the errors in DisPATCh are also linked to the uncertainty in SMOS soil moisture. Nevertheless, one way to identify the error sources specifically attributed to DisPATCh is to analyze the spatial correlation between

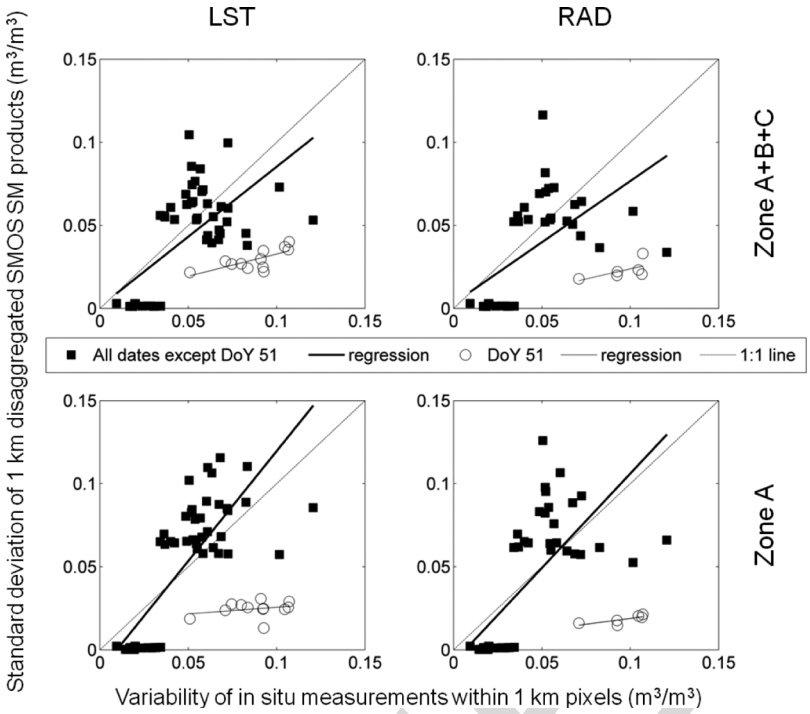

Fig. 10. Estimated uncertainty in disaggregated soil moisture ($\sigma_{\mathrm{SM}}, 1\ \mathrm{km}$) versus subpixel variability of 1 km resolution *in situ* measurements for DisPATCh run in LST or RAD mode and Zone A+B+C or Zone A only mode.

disaggregated SMOS data and the *in situ* measurements made at a distance larger than the downscaling resolution (1 km with MODIS data) and smaller than the SMOS data sampling length (15 km).

Based on the results obtained using the AACES *in situ* measurements, several improvements of DisPATCh can be suggested:

- Use of the MODIS land surface temperature quality index to select the SMOS pixels with the highest MODIS data quality.
- Correcting the MODIS land surface temperature for topography and illumination effects [45]. Within a 40-km SMOS resolution pixel, the elevation range may be very significant and thus induce a variability in land surface temperature that is not attributed to surface soil moisture.
- Use of ancillary air temperature data to constrain the estimation of end-members. The unstressed vegetation temperature $\mathbf{T_{v,min}}$ could be set to the air temperature instead of the minimum MODIS land surface temperature. This would make the estimation of $\mathbf{T_{v,min}}$ less dependent on the representativeness of the surface conditions met within the SMOS pixel [24].
- Accounting for the dependency of soil evaporative efficiency to potential evaporation, by replacing the model in [26] with the model in [38].
- Estimating an optimal downscaling resolution for each season: as the sensitivity of soil evaporative efficiency to soil moisture is lower in the winter months than in the summer months, aggregating DisPATCh output may improve the quality of disaggregation products at the expense of spatial resolution [17].

A robust disaggregation methodology of SMOS soil moisture at 1-km resolution, which would provide both disaggregated soil moisture and its uncertainty at 1-km resolution is a crucial step toward the application of SMOS data to hydrological studies.

REFERENCES

[1] E. G. Njoku and L. Li, "Retrieval of land surface parameters using passive microwave measurements at 6–18 GHz," *IEEE Trans. Geosci. Remote Sens.*, vol. 37, no. 1, pp. 79–93, Jan. 1999.

[2] C. S. Draper, J. P. Walker, P. J. Steinle, R. A. M. D. Jeu, and T. R. H. Holmes, "An evaluation of AMSR-E derived soil moisture over Australia," *Remote Sens. Environ.*, vol. 113, no. 4, pp. 703–710, Apr. 2009. doi:10.1016/j.rse.2008.11.011.

[3] C. Kummerow, W. S. Olson, and L. Giglio, "A simplified scheme for obtaining precipitation and vertical hydrometeor profiles from passive microwave sensors," *IEEE Trans. Geosci. Remote Sens.*, vol. 34, no. 5, pp. 1213–1232, Sep. 1996.

[4] M. Grecu and E. N. Anagnostou, "Overland precipitation estimation from TRMM passive microwave observations," *J. Appl. Meteor.*, vol. 40, no. 8, pp. 1367–1380, Aug. 2001.

[5] T. J. Jackson, M. H. Cosh, R. Bindlish, P. J. Starks, D. D. Bosch, M. Seyfried, D. C. Goodrich, M. S. Moran, and J. Du, "Validation of advanced microwave scanning radiometer soil moisture products," *IEEE Trans. Geosci. Remote Sens.*, vol. 48, no. 12, pp. 4256–4272, Dec. 2010. doi:10.1109/TGRS.2010.2051035.

[6] Y. H. Kerr, P. Waldteufel, J.-P. Wigneron, S. Delwart, F. Cabot, J. Boutin, M. J. Escorihuela, J. Font, N. Reul, C. Gruhier, S. E. Juglea, M. R. Drinkwater, A. Hahne, M. Martin-Neira, and S. Mecklenburg, "The SMOS mission: New tool for monitoring key elements of the global water cycle," *Proc. IEEE*, vol. 98, no. 5, pp. 666–687, May 2010. doi:10.1109/JPROC.2010.2043032.

[7] P. Matos, A. Gutiérrez, and F. Moreira, *SMOS L1 Processor Discrete Global Grids Document*, vol. SMOS-DMS-TN-5200. Lisboa, Portugal: DEIMOS Engenharia, 2004, V1.4.

[8] S. Bircher, J. E. Balling, N. Skou, and Y. Kerr, "SMOS validation by means of an airborne campaign in the Skjern river catchment, Western Denmark," *IEEE Trans. Geosci. Remote Sens.*, 2011, to be published. AQ1

[9] C. Gruhier, P. de Rosnay, S. Hasenauer, T. Holmes, R. de Jeu, Y. Kerr, E. Mougin, E. Njoku, F. Timouk, W. Wagner, and M. Zribi

(2010, Jan.). Soil moisture active and passive microwave products: Intercomparison and evaluation over a Sahelian site. *Hydrol. Earth Syst. Sci.* [Online]. *14(1)*, pp. 141–156. Available: www.hydrol-earth-syst-sci.net/14/141/2010/

[10] J.-C. Calvet, N. Fritz, F. Froissard, D. Suquia, A. Petitpa, and B. Piguet, "In situ soil moisture observations for the CAL/VAL of SMOS: The SMOSMANIA network," in *Proc. IGARSS*, Barcelona, Spain, 2007, pp. 1196–1199.

[11] S. Peischl, J. P. Walker, M. Allahmoradi, D. Barrett, R. Gurney, Y. Kerr, E. Kim, J. Le Marshall, C. Rüdiger, D. Ryu, and N. Ye, "Towards validation of SMOS using airborne and ground data over the Murrumbidgee catchment," in *Proc. MODSIM*, Cairns, Australia, 2009, pp. 3733–3739.

[12] M. H. Cosh, T. J. Jackson, S. M. Moran, and R. Bindlish, "Temporal persistence and stability of surface soil moisture in a semi-arid watershed," *Remote Sens. Environ.*, vol. 112, no. 2, pp. 304–313, Feb. 2008. doi:10.1016/j.rse.2007.07.001.

[13] P. de Rosnay, C. Gruhier, F. Timouk, F. Baup, E. Mougin, P. Hiernaux, L. Kergoat, and V. Le Dantec, "Multi-scale soil moisture measurements at the Gourma meso-scale site in Mali," *J. Hydrol.*, vol. 375, no. 1/2, pp. 241–252, Aug. 2009. doi:10.1016/j.jhydrol.2009.01.015.

[14] N. S. Chauhan, S. Miller, and P. Ardanuy, "Spaceborne soil moisture estimation at high resolution: A microwave-optical/IR synergistic approach," *Int. J. Remote Sens.*, vol. 24, no. 22, pp. 4599–4622, Nov. 2003.

[15] M. Piles, A. Camps, M. Vall-llossera, I. Corbella, R. Panciera, C. Rüdiger, Y. H. Kerr, and J. P. Walker, "Downscaling SMOS-derived soil moisture using MODIS visible/infrared data," *IEEE Trans. Geosci. Remote Sens.*, vol. 49, no. 9, pp. 3156–3166, Sep. 2011.

[16] O. Merlin, A. Al Bitar, J. P. Walker, and Y. Kerr, "An improved algorithm for disaggregating microwave-derived soil moisture based on red, near-infrared and thermal-infrared data," *Remote Sens. Environ.*, vol. 114, no. 10, pp. 2305–2316, Oct. 2010. doi:10.1016/j.rse.2010.05.007.

[17] O. Merlin, A. Al Bitar, J. P. Walker, and Y. Kerr, "A sequential model for disaggregating near-surface soil moisture observations using multi-resolution thermal sensors," *Remote Sens. Environ.*, vol. 113, no. 10, pp. 2275–2284, Oct. 2009. doi:10.1016/j.rse.2009.06.012.

[18] O. Merlin, J. Walker, R. Panciera, R. Young, J. Kalma, and E. Kim, "Soil moisture measurement in heterogeneous terrain," in *Proc. MODSIM—International Congress Modelling Simulation Modelling Simulation Society Australia New Zealand*, Dec. 2007, pp. 2604–2610.

[19] Y. H. Kerr, P. Waldteufel, P. Richaume, P. Ferrazzoli, and J.-P. Wigneron, *SMOS Level 2 Processor Soil Moisture Algorithm Theoretical Basis Document (ATBD)*, vol. SO-TN-ESL-SM-GS-0001. Toulouse, France: CESBIO, May 2011, V3.f.

[20] Y. H. Kerr, P. Waldteufel, P. Richaume, J. P. Wigneron, P. Ferrazzoli, A. Mahmoodi, A. Al Bitar, F. Cabot, C. Gruhier, D. Leroux, A. Mialon, and S. Delwart, "The SMOS soil moisture retrieval algorithm," *IEEE Trans. Geosci. Remote Sens.*, 2011.

[21] O. Merlin, C. Rüdiger, P. Richaume, A. Al Bitar, A. Mialon, J. P. Walker, and Y. Kerr, "Disaggregation as a top-down approach for evaluating 40 km resolution SMOS data using point-scale measurements: Application to AACES-1," in *Proc. SPIE, Remote Sens. Agriculture, Ecosystems, Hydrol. XII*, Toulouse, France, 2010, pp. 782 40I-1–782 40I-8.

[22] K. Nishida, R. R. Nemani, J. M. Glassy, and S. W. Running, "Development of an evapotranspiration index from Aqua/MODIS for monitoring surface moisture status," *IEEE Trans. Geosci. Remote Sens.*, vol. 41, no. 2, pp. 493–501, Feb. 2003.

[23] G. Gutman and A. Ignatov, "The derivation of the green vegetation fraction from NOAA/AVHRR data for use in numerical weather prediction models," *Int. J. Remote Sens.*, vol. 19, pp. 1533–1543, 1998.

[24] O. Merlin, B. Duchemin, O. Hagolle, F. Jacob, B. Coudert, G. Chehbouni, G. Dedieu, J. Garatuza, and Y. Kerr, "Disaggregation of MODIS surface temperature over an agricultural area using a time series of Formosat-2 images," *Remote Sens. Environ.*, vol. 114, no. 11, pp. 2500–2512, Nov. 2010. doi:10.1016/j.rse.2010.05.025.

[25] A. C. T. Pinheiro, J. Descloitres, J. L. Privette, J. Susskind, L. Iredell, and J. Schmaltz, "Near-real time retrievals of land surface temperature within the MODIS rapid response system," *Remote Sens. Environ.*, vol. 106, no. 3, pp. 326–336, Feb. 2007. doi:10.1016/j.rse.2006.09.006.

[26] J. Noilhan and S. Planton, "A simple parameterization of land surface processes for meteorological models," *Monthly Weather Rev.*, vol. 117, no. 3, pp. 536–549, 1989.

[27] O. Merlin, J. P. Walker, A. Chehbouni, and Y. Kerr, "Towards deterministic downscaling of SMOS soil moisture using MODIS derived soil evaporative efficiency," *Remote Sens. Environ.*, vol. 112, no. 10, pp. 3935–3946, Oct. 2008. doi:10.1016/j.rse.2008.06.012.

[28] M. S. Moran, T. R. Clarke, Y. Inoue, and A. Vidal, "Estimating crop water deficit using the relation between surface-air temperature and spectral vegetation index," *Remote Sens. Environ.*, vol. 49, no. 3, pp. 246–263, 1994.

[29] T. N. Carlson, R. R. Gillies, and E. M. Perry, "A method to make use of thermal infrared temperature and NDVI measurements to infer soil water content and fractional vegetation cover," *Remote Sens. Rev.*, vol. 52, pp. 45–49, 1994.

[30] O. Merlin, G. Chehbouni, J. P. Walker, R. Panciera, and Y. Kerr, "A simple method to disaggregate passive microwave based soil moisture," *IEEE Trans. Geosci. Remote Sens.—SMOS Special Issue*, vol. 46, no. 3, pp. 786–796, Mar. 2008. doi:10.1109/TGRS.2007.914807.

[31] W. P. Kustas and J. M. Norman, "Evaluation of soil and vegetation heat flux predictions using a simple two-source model with radiometric temperatures for partial canopy cover," *Agricultural Forest Meteorol.*, vol. 94, no. 1, pp. 13–29, 1999.

[32] M. C. Anderson, J. M. Norman, G. R. Diak, W. P. Kustas, and J. R. Mecikalski, "A two-source time-integrated model for estimating surface fluxes using thermal infrared remote sensing," *Remote Sens. Environ.*, vol. 60, no. 2, pp. 195–216, May 1997.

[33] O. Merlin and G. Chehbouni, "Different approaches in estimating heat flux using dual angle observations of radiative surface temperature," *Int. J. Remote Sens.*, vol. 25, no. 1, pp. 275–289, 2004.

[34] T. J. Lee and R. A. Pielke, "Estimating the soil surface specific humidity," *J. Appl. Meteorol.*, vol. 31, no. 5, pp. 480–484, 1992.

[35] T. S. Komatsu, "Towards a robust phenomenological expression of evaporation efficiency for unsaturated soil surfaces," *J. Appl. Meteorol.*, vol. 42, no. 9, pp. 1330–1334, Sep. 2003.

[36] O. Merlin, J. P. Walker, J. D. Kalma, E. J. Kim, J. Hacker, R. Panciera, R. Young, G. Summerell, J. Hornbuckle, M. Hafeez, and T. J. Jackson, "The NAFE'06 data set: Towards soil moisture retrieval at intermediate resolution," *Adv. Water Resour.*, vol. 31, pp. 1444–1455, 2008. doi:10.1016/j.advwatres.2008.01.018.

[37] Z. Wan and J. Dozier, "A generalized split-window algorithm for retrieving land-surface temperature from space," *IEEE Trans. Geosci. Remote Sens.*, vol. 34, no. 4, pp. 892–905, Jul. 1996.

[38] O. Merlin, A. Al Bitar, V. Rivalland, P. Béziat, E. Ceschia, and G. Dedieu, "An analytical model of evaporation efficiency for unsaturated soil surfaces with an arbitrary thickness," *J. Appl. Meteorol. Climatol.*, vol. 50, no. 2, pp. 457–471, Feb. 2011. doi:10.1175/2010JAMC2418.1.

[39] N. Agam, W. P. Kustas, M. C. Anderson, F. Li, and C. M. U. Neale, "A vegetation index based technique for spatial sharpening of thermal imagery," *Remote Sens. Environ.*, vol. 107, no. 4, pp. 545–558, 2007.

[40] E. E. Small and S. A. Kurc, "Tight coupling between soil moisture and the surface radiation budget in semiarid environments: Implications for land-atmosphere interactions," *Water Resour. Res.*, vol. 39, no. 10, p. 1278, Oct. 2003. doi:10.1029/2002WR001297.

[41] C. Rüdiger, J. P. Walker, and Y. H. Kerr, "On the airborne spatial coverage requirement for microwave satellite validation," *IEEE Geosci. Remote Sens. Lett.*, vol. 8, no. 4, pp. 824–828, Jul. 2011.

[42] R. Young, J. Walker, N. Yeoh, A. Smith, K. Ellett, O. Merlin, and A. Western, *Soil Moisture and Meteorological Observations from the Murrumbidgee Catchment*. Melbourne, Australia: Dept. Civil Environ. Eng., Univ. Melbourne, 2008.

[43] A. J. Teuling, R. Uijlenhoet, R. Hurkmans, O. Merlin, R. Panciera, J. Walker, and P. A. Troch, "Dry-end surface soil moisture variability during NAFE'06," *Geophys. Res. Lett.*, vol. 34, no. L17 402, Sep. 2007.

[44] W. T. Crow and E. F. Wood, "The assimilation of remotely sensed soil brightness temperature imagery into a land surface model using Ensemble Kalman filtering: A case study based on ESTAR measurements during SGP97," *Adv. Water Resour.*, vol. 26, pp. 137–149, 2003.

[45] Q. K. Hassan, C. P.-A. Bourque, F.-R. Meng, and R. M. Cox, "A wetness index using terrain-corrected surface temperature and normalized difference vegetation index derived from standard MODIS products: An evaluation of its use in a humid forest-dominated region of eastern Canada," *Sensors*, vol. 7, no. 10, pp. 2028–2048, 2007.

Olivier Merlin, photograph and biography not available at the time of publication.

Christoph Rüdiger, photograph and biography not available at the time of publication.

Ahmad Al Bitar, photograph and biography not available at the time of publication.

Philippe Richaume, photograph and biography not available at the time of publication.

Jeffrey P. Walker, photograph and biography not available at the time of publication.

Yann H. Kerr, photograph and biography not available at the time of publication.

AUTHOR QUERIES

AUTHOR PLEASE ANSWER ALL QUERIES

Please be aware that the authors are required to pay overlength page charges ($200 per page) if the paper is longer than 6 pages. If you cannot pay any or all of these charges please let us know.

AQ1 = Please provide publication update in Ref. [8].
AQ2 = Please provide volume. issue number, page range and month of publication in [20].

END OF ALL QUERIES